Expression and purification of HGXPRT from *Plasmodium falciparum* and characterisation of its interaction with an effector chalcone

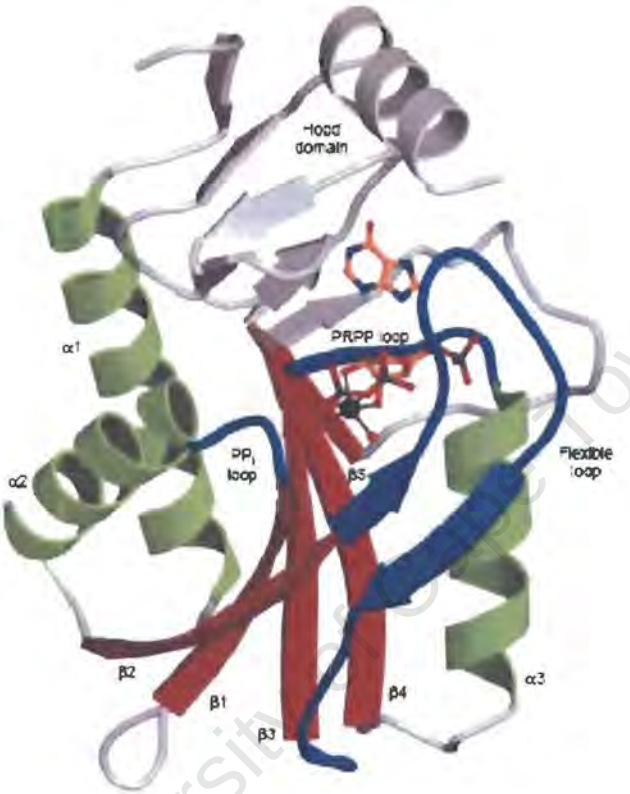

Sinha and Smith, 2001

Naadia van der Bergh
VBRNAA001

SUBMITTED TO THE UNIVERSITY OF CAPE TOWN
In fulfilment of the requirements for the degree
***Magister Scientiae* (Medicine) in Chemical Pathology**

Faculty of Health Sciences
November 2008

Supervisor: Professor David B. McIntosh
Division of Chemical Pathology

DECLARATION

I, NAADIA VAN DER BERGH, hereby declare that the work on which this dissertation is based is my original work (except where acknowledgements indicate otherwise) and neither the whole work nor any part of it has been, is being, or is to be submitted for another degree in this or any other university.

I empower the university to reproduce for the purpose of research either the whole or any portion of the contents in any manner whatsoever.[1]

SIGNATURE.....

DATE.....24 NOVEMBER 2008.....

[1] The financial assistance of the National Research Foundation (NRF) towards this research is hereby acknowledged. Opinions expressed and conclusions arrived at, are those of the author and are not necessarily to be attributed to the NRF.

ABSTRACT

Malaria is endemic in 107 countries and causes 500 million clinical disease episodes annually. The disease in humans is caused by four protozoan species of the genus *Plasmodium*, the most virulent form being *P. falciparum*. The emergence of drug-resistant strains of the parasite has necessitated finding new drug targets and drugs.
P. falciparum is unable to synthesise purines *de novo* and relies on an enzyme, hypoxanthine guanine xanthine phosphoribosyltransferase, HGXPRT, to salvage purine bases from host erythrocytes to fulfill its purine requirements. The enzyme is a member of the phosphoribosyltransferase family of proteins and catalyses the Mg^{2+}-dependent conversion of hypoxanthine, guanine or xanthine and α-D-5-phosphoribosyl 1-pyrophosphate to purine nucleotides and inorganic pyrophosphate. HGXPRT is a recognised drug target in *P. falciparum*.

Previous work in our laboratory established methodology for cloning and expressing malarial HGXPRT (*Pf*HGXPRT) in *E. coli*, and its purification both untagged and with a his-tag. The enzyme is inactive as isolated but may be activated by incubation with partial substrates. A family of chalcones, of which 4′-iodo-chalcone is the parent compound, has been discovered that interacts with *Pf*HGXPRT in unusual ways; they accelerate Mg^{2+}-dependent catalytic activity, are potent inhibitors of Ca^{2+}-dependent catalytic activity, and can replace partial substrates in converting the isolated enzyme from an inactive to active form.

The aim of this study was to express and purify *Pf*HGXPRT and to explore three techniques, namely gel filtration HPLC, photolabelling, and Isothermal Titration Calorimetry (ITC) for ultimately characterising the interaction of the effector chalcones with the protein.

His-tagged as well as the non his-tagged enzyme was expressed and purified by Ni-affinity chromatography and anion-exchange + Reactive Red-120 affinity chromatography,

respectively. The his-tagged enzyme was finally ~95% pure as judged visually by SDS-PAGE, and up to 6 mg protein could be obtained from 1 L culture. The non his-tagged enzyme was ~90 % pure, with yields of up to 16 mg protein/ L culture. Both forms of the protein were inactive as isolated but could be activated by incubation with partial substrates to specific activities of up to 2 and 3 μmolGMP/min/mg.

Gel filtration HPLC was explored as a possible method for measuring the oligomeric state of *Pf*HGXPRT under various conditions, with an ultimate view of determining the effect of chalcone binding. The active form of the enzyme is a tetramer – the dimer is inactive. Two forms of the enzyme could readily be separated by the technique, an early and late eluting form, which were tentatively ascribed to the tetramer and dimer. The proportion of each is sensitive to ionic strength, with the tetramer and dimer predominating at low and high NaCl respectively (half maximal effect at 50 mM). The equilibrium is very sensitive to the concentrations of $CaCl_2$ and $MgCl_2$ (half-maximal effects at 1 mM), respectively. Preincubation of the protein in 1 M NaCl suggested rapid interconversion between oligomeric forms. Activation of the enzyme did not alter the salt concentration dependence of its quarternary structure suggesting the process does not involve stabilisation of the active tetrameric form over the inactive dimer.

The light-sensitive ATP analogue, [γ-^{32}P]TNP-8N_3-ATP, was developed in our laboratory as a specific photoaffinity probe of the active site of sarcoplasmic reticulum Ca^{2+}-ATPase. In this study we explore its use as a photolabel of the active site of *Pf*HGXPRT. [γ-^{32}P]TNP-8N_3-ATP covalently derivatises the enzyme to the extent of 0.01 to 0.1 mol probe/ mol protein, which is similar to levels achieved with Ca^{2+}-ATPase, depending on pH and and protein activation. 4′-iodo-chalcone had no effect on labeling of the protein, compatible with it binding to an allosteric site outside of the active site.

Isothermal titration calorimetry was investigated as a technique for measuring 4′-iodo-chalcone binding to *Pf*HGXPRT. However, very small or negligible heats of titration were produced due to either the chalcone not binding under the conditions used or because no heat is produced or taken up on binding due to a balance of exothermic and endothermic factors.

Overall, gel filtration HPLC appears to be a useful technique for determining the quarternary state of the protein under a variety of conditions, and [γ-^{32}P]TNP-8N_3-ATP may be developed further as a photolabel of the active site. ITC cannot be used to measure chalcone binding.

ACKNOWLEDGEMENTS

I am eternally grateful to my supervisor, Professor David B. McIntosh, for teaching by example, patience, inspiration, an open-door policy, a great (dry) sense of humour and sharing knowledge with me.

Mr. Dave G. Woolley, for help with so many aspects of my project.

I also wish to thank:

My parents, for constant support.
My sister, Shireen, for words of encouragement, being my friend and for providing transport to the lab after midnight.
Jackson Marakalala, for our friendship and company in the laboratory when sleeping was a further option.
Dr. Boniface Mbewe, for help with the protein purification protocol.
The University of Cape Town and the National Research Foundation for funding this project.

ABBREVIATIONS

AMPS	Ammonium persulphate
cDNA	Complementary DNA
Ca^{2+}-ATPase	Calcium adenosine triphosphatase
CHES	2-(*N*-cyclohexylamino)ethanesulphonic acid
DE-52	Diethyl aminoethyl cellulose
dH_2O	Distilled water
DMSO	Dimethylsulphoxide
DNA	Deoxyribonucleic acid
DNaseI	Deoxyribonulease I
DTT	Dithiothreitol
E. coli	*Escherichia coli*
EDTA	Ethylenediaminetetra-acetic acid
EGTA	Ethylene glycol-bis(β-aminoethylether)N,N,N′,N′-tetraacetic acid
EPPS	N-[2-Hydroxyethyl]piperazine-N′-[3-propanesulphonic acid]
GMP	Guanosine 5′-monophosphate
HEPES	N-2-hydroxyethylpiperazine-N′-2-ethanesulphonic acid
HGXPRT	Hypoxanthine-guanine-xanthine phosphoribosyltransferase
IPTG	Isopropyl-ß-D-thiogalactopyranoside
MES	2-[N-morpholino]ethane sulphonic acid
MOPS	3-(*N*-morpholino)-propanesulphonic acid
$NaPP_i$	Sodium pyrophosphate
NappiLB	Luria-Bertani medium enriched with sodium phosphate
PBS	Phosphate buffered saline
***Pf*HGXPRT**	*Plasmodium falciparum* hypoxanthine guanine xanthine phosphoribosyltransferase
PMSF	Phenylmethyl sulphonylfluoride
PP_i	Inorganic pyrophosphate

Ppt	Precipitate
PRPP	α-D-5-phosphoribosyl-1-pyrophosphate
RR-120	Reactive Red-120 agarose
rpm	Revolutions per minute
SDS-PAGE	Sodium dodecyl sulphate polyacrylamide gel electrophoresis
SR	Sarcoplasmic reticulum
TEMED	*N,N,N′,N′*-tetramethylenediamine
TMAH	Tetramethylammonium hydroxide
TNPATP	2′,4′,6′-trinitrophenyl adenosine triphosphate
[γ-^{32}P]TNP-8N$_3$-ATP	[γ-^{32}P]2′,3′-0-(2,4,6-trinitrophenyl)-8-azido-adenosine triphosphate

List of Tables and Figures

Tables

Figures

Contents

CHAPTER 1: Introduction

1.1 The global malaria burden

Malaria (*It.* "bad air") is the most lethal of the parasitic diseases affecting humans. In 2007, an estimated 2.37 billion people were living in areas at risk of malaria transmission (Guerra *et al*, 2008) whilst an estimated 500 million cases and 1 million deaths are reported annually (WHO Malaria Fact Sheet N° 19, 2007). The African continent carries the bulk of the burden of the disease, with 90% of deaths due to malaria occurring in the Sub-Saharan region. Primarily, pregnant women and children below five years of age are affected. Globally, malaria is prevalent in tropical and subtropical regions (see figure 1.1).

The disease is caused by four species of the genus *Plasmodium*, i.e. *P. malariae* (malaria tertiana), *P. ovale* (malaria quartana), *P. vivax* (malaria tertiana), and *P. falciparum* (malaria tropica). The latter causes the most virulent form of the disease in humans. The intermediate host and vector of the unicellular protozoan parasite is the female *Anopheles gambiae* mosquito, which transmits infectious stages (sporozoites) to humans upon feeding.

In 1998, prompted by resurgence in the protozoal disease, the World Health Organisation initiated the Roll Back Malaria (RBM) Campaign (WHO Malaria Report, 2003; Nabarro and Tayler, 1998). The aims of this initiative were to halve the number of deaths due to malaria by 2010 and to halve this number again by 2015. These goals were to be achieved by "sustained delivery and use of the most effective prevention and treatment for those affected most by malaria by promoting increased investment in health systems and incorporation of malaria control into all relevant multisector activities".
However, the campaign has failed in its attempts. In 2004, more people were dying due to malaria than when the campaign was initiated in 1998 (Yamey, 2004). Two major drawbacks may be implicated in this event, i.e. the emergence and spread of drug-resistant parasites and the development of insecticide-resistance by the mosquito vector. There now exists a need for the development of

new, cost-effective antimalarials as these compounds are important intervention tools.

Malaria is associated with poverty and in a continent with already fragile economies and poor health services, the disease is an impediment to development and in highly endemic countries, the disease causes a 1.3% loss of economic growth annually (WHO Malaria Fact Sheet N° 19, 2007).

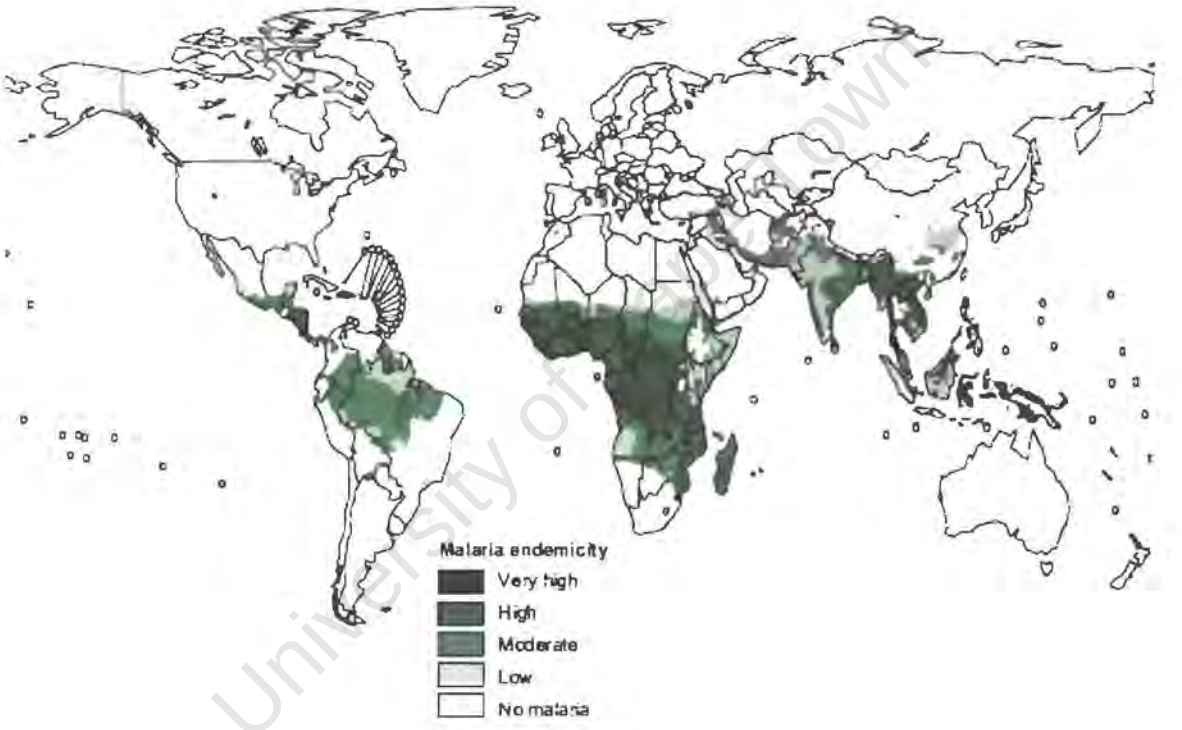

Figure 1.1. Global distribution of malaria in 2003 (WHO World Malaria Report, 2005).

1.2 Life cycle of *Plasmodium falciparum* and pathogenesis of disease

Plasmodium is transmitted to the human host by an arthropod vector, the female *Anopheles gambiae* mosquito. The parasite has a complex life cycle consisting of intra- and extracellular stages in the mosquito and human hosts (see figure 2).

The life cycle of *Plasmodium* may be divided into three stages, i.e. the mosquito, liver and blood stages. Transmission of sporozoites (from the salivary glands of the mosquito) occurs when an infected mosquito takes a bloodmeal from the human host. Once in the bloodstream, the parasite migrates to the liver where it invades haepatic parenchymal cells. Here, they mature into schizonts by a process called exoerythrocytic schizogony. Within two weeks, the cells rupture and merozoites are released into the circulation. Invasion of the red blood cells by merozoites initiates the asexual blood stage which is responsible for the symptoms of fever and chills associated with the disease.

Inside the erythrocytes, the merozoites mature into ring-shaped trophozoites and schizonts (intraerythrocytic schizogony). Upon maturation, the red blood cells rupture and the parasites are released back into the circulation. Some merozoites produce the sexual stages, male and female gametocytes. The gametocytes are taken up by the mosquito vector upon feeding and this initiates the sexual reproduction stage. Inside the mosquito's gut, male and female gametes fuse to produce zygotes, which develop into oocysts. These give rise to sporozoites which migrate to the salivary glands and are transmitted to the human host upon feeding to initiate a new cycle.

The severity of disease is determined by the immune status and age of the patient, the parasite species, as well as social and geographic factors. Symptoms of the disease are associated exclusively with the asexual blood stage and range from fever to fatal cerebral malaria (for review, see Miller *et al*, 2002).

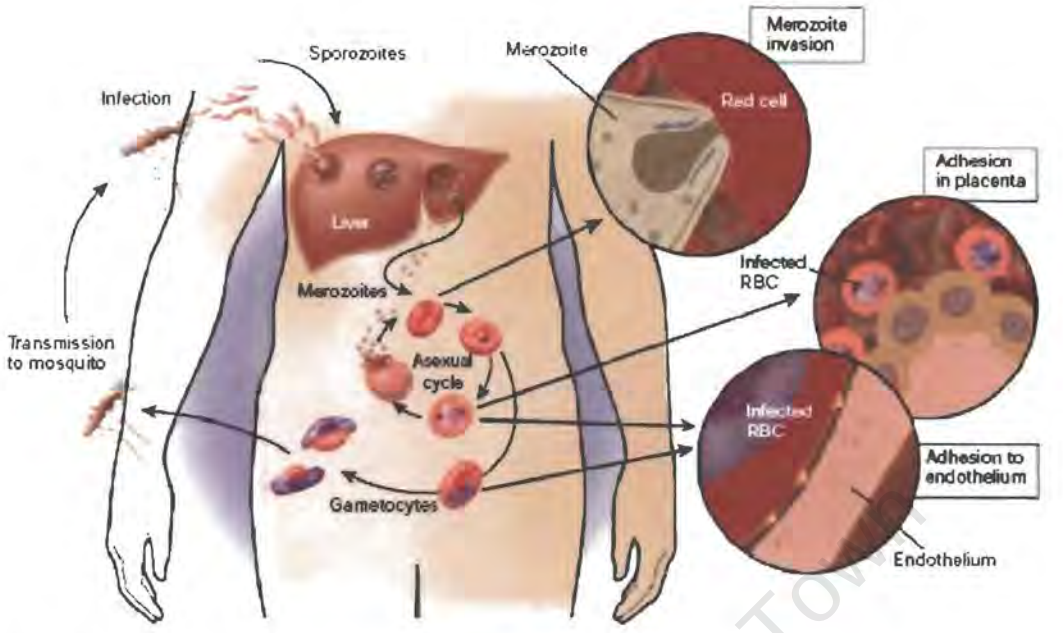

Figure 1.2. Parasite life cycle (from Miller *et al*, 2002).

Disease is initiated by the asexual replication of parasites in the red blood cells. Fever and anaemia are key features of disease, resulting from the rupture of erythrocytic schizonts. This is generally accompanied by headache, vomiting and muscle pains. In falciparum malaria, convulsions and coma are common complications possibly caused by the adhesion of red blood cells to cerebral capillaries. Sequestration of infected erythrocytes was associated with upregulation of intercellular adhesion molecule 1 (ICAM-1) which is mediated by the nuclear transcription factor NF-κB (Tripathi *et al*, 2006). Interestingly, Liu *et al* (2007) recently found that a group of flavonoids known as chalcones (see Section 1.5) had inhibitory effects on NF-κB.

1.3 Antimalarial Chemotherapy

Disease prevention is currently afforded by chemoprophylaxis and by avoiding contact with the vector. A limited number of drugs are available for treatment of the disease. Currently, the WHO recommends artemisinin combination therapy (ACT) as the treatment of choice for malaria as increasing resistance to chloroquine and the antifolates continues to impede efforts to prevent disease transmission.

1.3.1 Currently available drugs and their biological targets

1.3.1.1 Quinine and its derivatives

During the intraerythrocytic stage, malaria parasites digest host haemoglobin to produce haematin which is incorporated into malaria pigment (haemozoin). Quinoline antimalarials have been shown to reduce the rate of production of haemozoin (Egan and Ncokazi, 2005).
Quinine remains, along with the artemisinins, the drug of choice in high-transmission areas (Dondorp and Day, 2007). Interestingly, a recent study comparing the efficacy of parenteral quinine and artemisinin derivatives showed the artemisinins were not more effective than quinine in treating severe malaria in children (PrayGod *et al*, 2008).

Chloroquine, a 4-aminoquinoline derivative of quinine, was the drug of choice for chemophoprophylaxis and treatment of uncomplicated malaria since it was first synthesised in the 1930s.
The compound has since been used in the treatment of non-severe disease as well as for chemoprophylaxis, however, the efficacy of this drug has been compromised by the development of drug-resistance in both *P. falciparum* and *P. vivax*. Mutations in pfcrt, a gene located on chromosome 7, has been linked to chloroquine resistance in *P. falciparum*. The gene encodes a transmembrane protein, *Pf*CRT which is located in the digestive vacuole at the site of chloroquine

action (Fidock *et al*, 2000). Other quinine derivatives are clinically valuable. These include amodiaquine, used in combination with the artemisinins (see Section 1.3.1.4) and mefloquine, which is extensively used as prophylaxis and to treat chloroquine resistant malaria (Freedman, 2008).

1.3.1.2 The Antifolates

This group of compounds consists of the sulphones (e.g. sulphadoxine and dapsone) as well as combinations of inhibitors of enzymes of folate biosynthesis (e.g. proguanil and pyrimethamine). The antifolates are used in combinations to provide a synergistic effect, as parasite resistance develops rapidly in monotherapy. Two classes of antifolates are currently used: inhibitors of dihydropteroate synthase (DHPS) and inhibitors of dihydrofolate reductase (DHFR) (reviewed in Nzila, 2006).

Parasite resistance to the antifolates has been linked to mutations in the dihydrofolate reductase-thymidylate synthase gene (Cowman *et al*, 1988), i.e.Thr-108 or Ser-108 to Asn-108 confers resistance to pyrimethamine (Peterson *et al*, 1988) whilst mutations in the dihydropteroate synthase gene confers resistance to the sulphonamides (Triglia *et al*, 1997).

1.3.1.3 Antibiotics

The malarial parasite possesses a plastid-like organelle, an apicoplast, which is the site of fatty acid biosynthesis, DNA replication and transcription, isoprenoid biosynthesis, amino acid synthesis, and haem biosynthesis (for review, see Ralph *et al*, 2001). McConkey *et al* (1997) demonstrated the importance of the organelle in protein synthesis by inhibition of parasite growth using thiostrepton, a specific inhibitor of protein synthesis in this organelle. Triclosan (Surolia and Surolia, 2001) as well as thiolactomycin (Waller *et al*, 2003) were shown to inhibit growth of intraerythrocytic parasites through inhibition of fatty acid biosynthetic pathways, also located here. Another antibacterial agent, tetracycline, is used in

combination with quinine in areas where the latter shows reduced efficacy to reduce fever and clear parasites (Watt *et al*, 1992). Dahl *et al* (2007) showed that treatment of chloroquine-resistant parasites with doxycycline, widely used for malaria prophylaxis, resulted in progeny unable to complete asexual development due to abnormal apicoplast function.

1.3.1.4 Artemisinins

The development of parasite resistance to former first-line antimalarials (e.g. chloroquine and sulphadoxine-pyrimethamine) led to the recommendation of artemisinin-based combination therapies (ACTs) as preferred first-line drugs by the WHO in 2005 (Eckland and Fidock, 2008). These compounds are extracted from the annual shrub, *Artemesia annua*. *Qinghaosu* (artemisinin), a traditional Chinese medicine, was found to have antimalarial properties in 1971. However, it was only after in vitro, animal and human trials that the compound was revealed to the rest of the world. Since then, a number of derivatives of artemisinin have been synthesised, including dihydroartemisinin (DHA) and its derivatives, artemether, artemotil and artesunate.

The compound has a stable, 15-carbon peroxide structure (see figure 1.3).

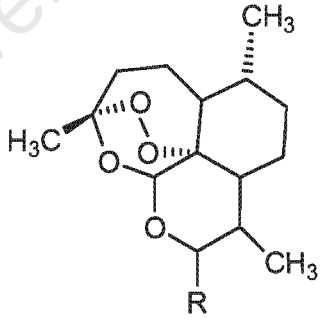

1. R: = O
2. R: = βO-CH_3
3. R: = βO- C_2H_5
4. R: = α$CO(CH_2)_2COO$

Figure 1.3. Chemical structures of artemisinin and its derivatives. 1, artemisinin; **2**, artemether; **3**, artemotil (arteether); **4**, artesunate.

Artemisinins are toxic to the asexual and sexual stages of parasite development (ter Kuile *et al*, 1993) and although the details of the mechanism of action are unknown, it is thought to act by the formation of free radicals (Krungkrai and Yuthavong, 1987). This broad specificity and potency makes it possible to kill most sensitive parasites with a single administration and, furthermore, this class of drugs has the potential to reduce transmission of the parasite through its ability to inhibit the formation of gametocytes (Price *et al*, 1996). Eckstein-Ludwig *et al* (2003) showed that artemisinins effect antiplasmodial activity by inhibiting the SERCA (sarcoendoplasmic reticulum calcium adenosine triphosphatase) enzyme, PfATP6.

These drugs have short half-lives and so are administered in combinations to reduce the probability of the development of a mutant resistant to the co-drug (White, 2008), e.g. artesunate-pyronaridine, artesunate-mefloquine, artesunate-amodiaquine and artemether-lumefantrine. At present, the artemisinins are our last resort for the treatment of malaria. A major obstacle in delivering these drugs to vulnerable populations is the cost involved in the synthesis of artemisinin derivatives. Recently, the Artemisinin Project was initiated (Hale *et al,* 2007), aiming to reduce these costs by producing semi-synthetic derivatives using a fermentation process.

1.4 The PRT family of proteins

The phosphoribosyltransferase family of proteins consists of enzymes of the nucleotide biosynthetic and salvage pathways. The proteins are found in various organisms and differ mainly with regard to substrate specificity. To date, more than 40 crystal structures of PRTs have been solved. Figure 1.4 shows the PRT fold in a crystal structure of HGPRT from *Trypanosoma cruzi*. The common core is shaded in green and consists of a parallel ß sheet situated between α helices. A hood domain is formed by residues of the N terminus together with a larger section at the C-terminus.

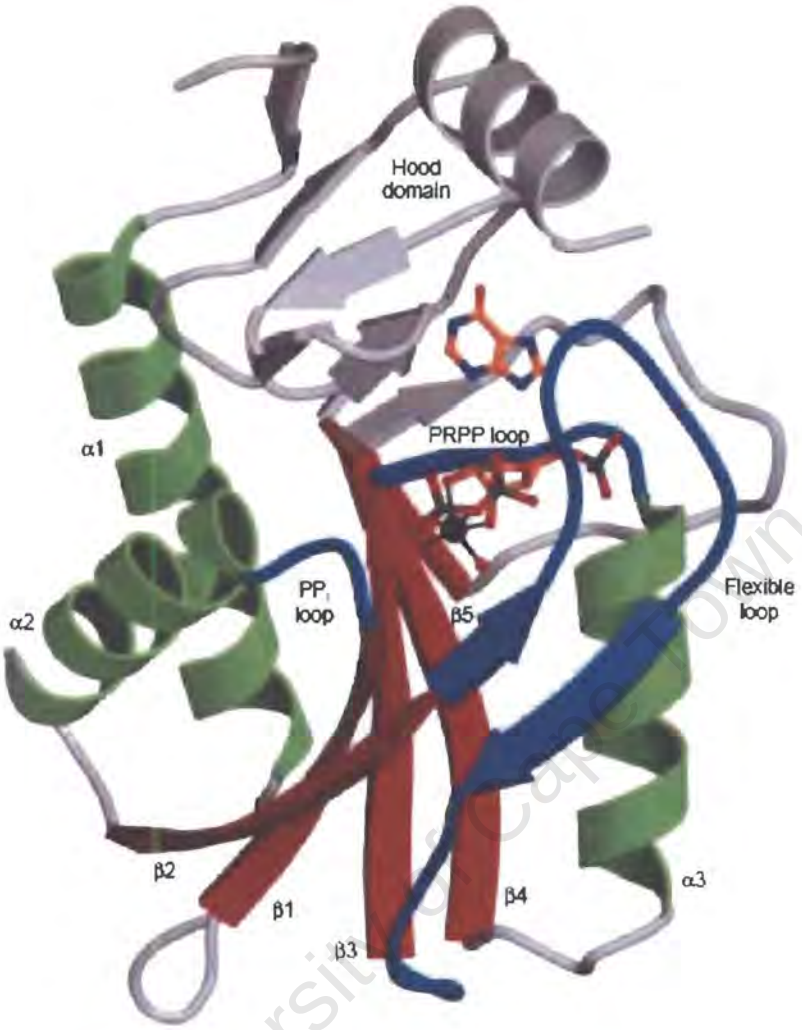

Figure 1.4. The PRT protein family common fold. The structure represents HGPRT from *Trypanosoma cruzi* in complex with hypoxanthine (purine base), PRPP and Mg^{2+}. The dark blue region represents the conserved Mg·PRPP binding loops, the core domain is represented by green α helices and red β sheets, and the light blue structure is the hood domain. The black sphere is Mg^{2+}, carbon atoms are orange, oxygen atoms are red, nitrogen atoms are blue, and phosphorus is coloured green. The figure was taken directly from Sinha and Smith (2001).

The conserved PRPP-binding site consists of a PP_i loop, a flexible loop and a PRPP loop. The amino acid residues of these loops are not conserved across members of the family although they are highly conserved for each class of PRT.

The high conservation within a class is illustrated in Figure 1.5, where the sequences of five HGPRTs are compared. The polypeptides range in size from ~21 kDa to ~26 kDa (Free *et al*, 1990; Vasanthakumar *et al*, 1994, Shahabuddin and Scaife, 1990; Vasanthakumar *et al*, 1994; Allen and Ullman, 1994; Chin and Wang, 1994).

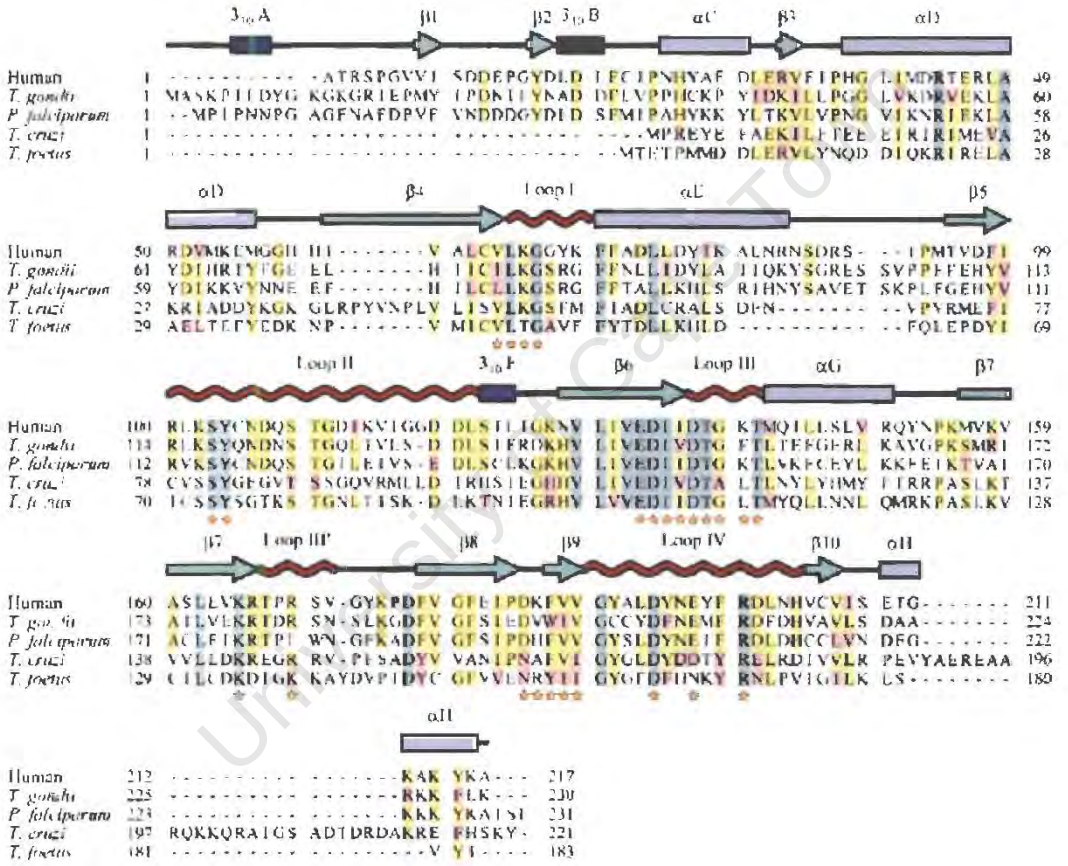

Figure 1.5. Amino acid sequence alignment of human, *Toxoplasma gondii*, *Plasmodium falciparum*, *Trypanosoma cruzi* and *Tritrichomonas foetus* HGPRTs. Figure taken, with permission, from Héroux *et al*, 1999a. Gold stars below the sequence indicate active site residues. Conserved residues are shaded green and those that are conservatively substituted are yellow. Secondary structures are indicated above the sequence.

1.4.1 HGPRT structure and catalytic mechanism

HGPRTs catalyse the conversion of purine bases (hypoxanthine, guanine and xanthine) and phosphoribosyl pyrophosphate (PRPP) into the respective mononucleotides and pyrophosphate (see figure 1.6).

Kinetic studies of HGPRT were initially conducted using mainly the human homologue. Henderson *et al* (1968) showed that the forward reaction catalysed by human HGPRT is ordered and involves the formation of ternary complexes of the enzyme, with PRPP binding first (Henderson *et al*, 1968, Giacomello and Salerno, 1978) followed by hypoxanthine (Xu *et al*, 1997). Subsequent product release was shown to be ordered, i.e. PP_i is released first followed by the nucleotide.

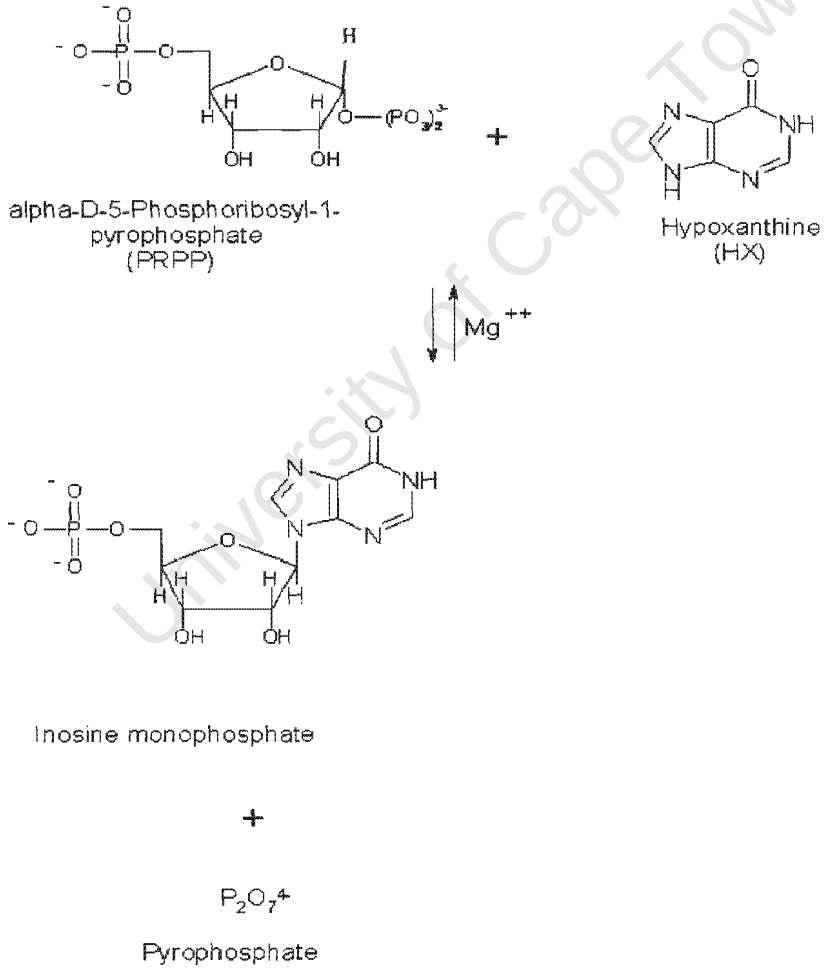

Figure 1.6. Reaction catalysed by HGXPRT. Here, hypoxanthine (purine base) is converted to its related 6-oxopurine mononucleotide, inosine 5′-monophosphate (IMP). Product formation occurs by linkage of the base to the ribose ring of PRPP with concomitant release of PPi.

The first crystal structure of an HGPRT was that of the human enzyme with bound GMP (Eads *et al*, 1994), followed by the structure of the free enzyme detailing the conformational changes necessary for catalysis (Keough *et al*, 2005). The crystal structure of a chimera of human and *P. falciparum* was recently published (Gayathri *et al*, 2008) and it is hoped that the structure would provide useful information for designing selective inhibitors against the malarial enzyme.

Several crystal structures of HGPRTs from other organisms have since been published. *T. gondii* (Schumacher *et al*, 1996) and *T. cruzi* (Focia *et al*, 1998) structures were published in short succession. HGPRT from *T. gondii* was further crystallised with GMP and IMP, respectively (Héroux *et al*, 1999*a*) and later with XMP, PP_i and two Mg^{2+} ions (Héroux *et al*, 1999*b*). Based on these structures, Héroux *et al* (1999*b*) proposed the first detailed structure-based description of HGPRT catalysis shown in figure 1.7 (A-F)[1].

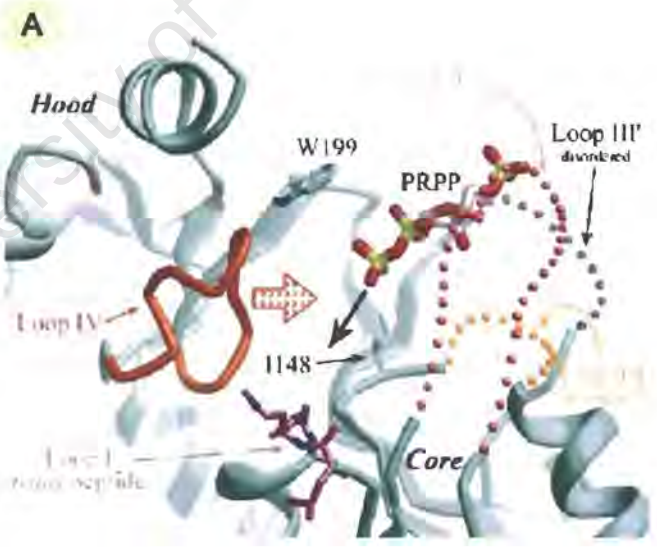

PRPP is entering the active site of the **apoenzyme**. Here, loops II, III, III' and the purine-binding site (Ile148, Trp199) are open. Loop IV closes once PRPP is fully bound.

[1] Figures reproduced from Héroux *et al* (1999*b*) with permission from Dr. A Héroux.

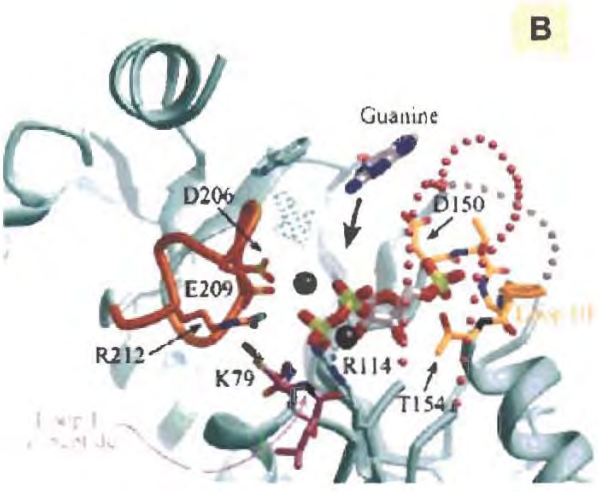

The **PRPP complex**. PRPP and Mg^{2+} are bound and the hood closes onto the core domain. The pyrophosphate group is held in position by the two Mg^{2+} ions, prepared for phosphoribosyl transfer. Guanine is shown entering the active site, following which the purine-binding clamp will close.

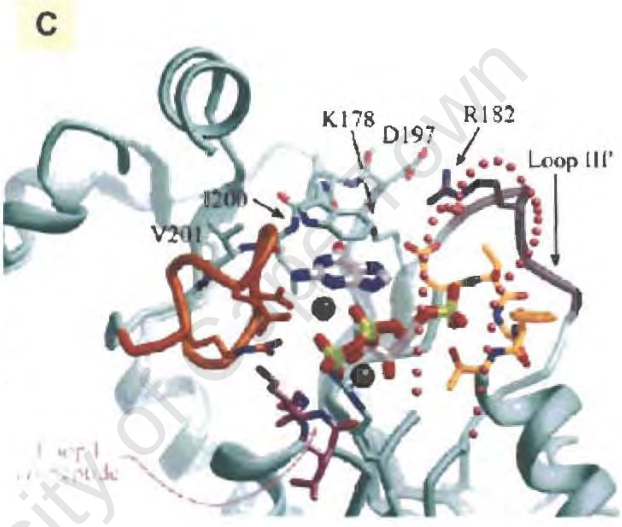

The **bisubstrate complex**. Loop III is ordered by the binding of the 5'-phosphate group (of PRPP) and the purine-binding clamp is closed around the base. Loop III' is now able to approach the active site and closure of loop II allows phosphoribosyl transfer.

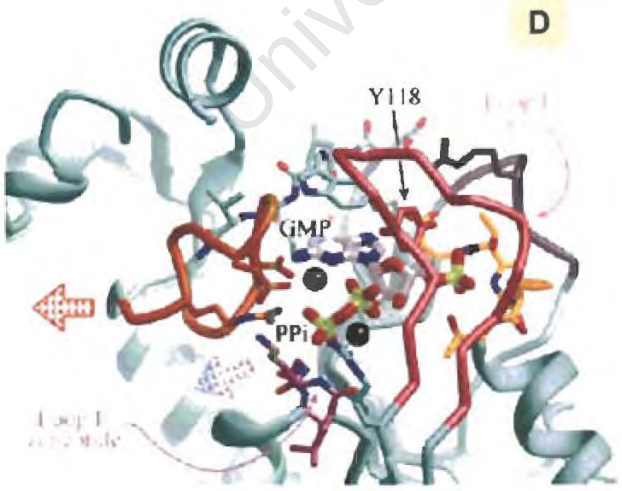

The **biproduct complex**. Loop II is closed, placing Tyr118 in position to hydrogen-bond to the 5'-phosphate group. The opening of loops I and IV will now allow PP_i to be expelled.

The **nucleotide complex**. Here, PP_i is shown leaving the active site and loop II has reopened. Loop III' and the hood will now open as the departure of PP_i destabilises the interactions linking the core and hood in the lower active site. This event allows the nucleotide to leave the active site.

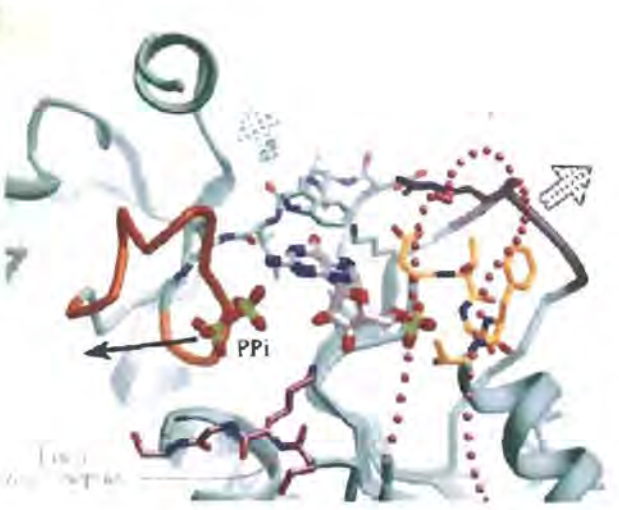

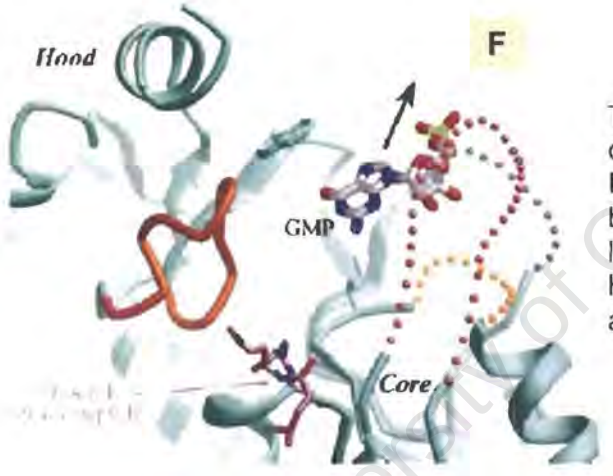

The **apoenzyme**. The sequential opening of the hood domain, loop III', and finally loop III, is followed by the release of GMP in the rate-limiting step of the catalysis. HGPRT now returns to the apoenzyme state.

Figure 1.7. Structure-based description of HGPRT catalysis. Green ribbons represent the enzyme. The hood and core domains are, as indicated in **A**, at the upper left and lower right corners, respectively. The active site loops are coloured as follows: I, lavender; II, pink; III, gold; III', grey and IV, orange.

The human (Shi *et al*, 1999*a*) and malarial (Shi *et al*, 1999*b*) enzymes were crystallised with transition state inhibitors (immucillinGP and immucillinHP, respectively, see figure 1.8). The equilibrium inhibition constants for these transition state analogues have been shown to be lower than for the enzyme substrates (i.e. tighter binding) and the compounds could serve as leads for related

compounds with greater specificity for protozoal HGPRTs over the human form (Li *et al*, 1999). Chemical structures of these inhibitors are shown in figure 1.8.

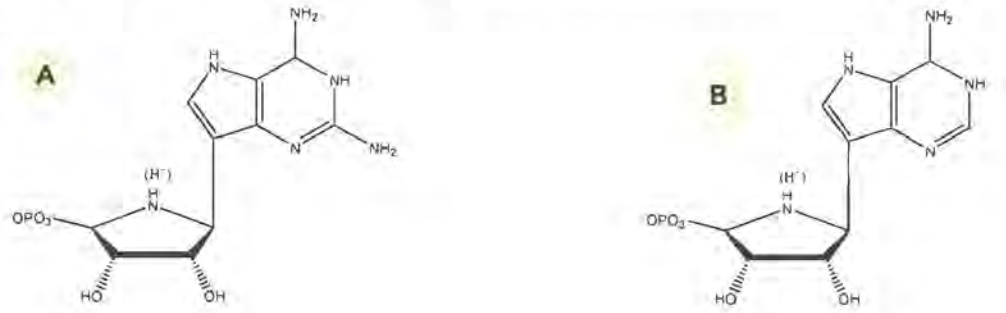

Figure 1.8. Transition state inhibitors of humHGPRT and *Pf*HGPRT, immucillinGP **(A)** and immucillinHP **(B)** (Shi *et al*, 1999*a*; Shi *et al*, 1999*b*)

1.4.2 *Plasmodium falciparum* HGXPRT[2]

*Pf*HGXPRT was initially purified from *P. falciparum* grown in culture and was shown to be highly unstable and have very low activity (Queen *et al*, 1988) compared to the human homologue. Recombinant protein expressed in *E. coli* (Shahabuddin and Scaife, 1990; Keough *et al*, 1999; Phehane, 2002; Mbewe *et al*, 2007) is inactive as isolated in a highly purified form but may be activated by prolonged incubation with partial substrates, i.e. hypoxanthine + PRPP (no added Mg^{2+}) or MgPRPP, so that an active form of the enzyme is stabilised without inducing turnover (Keough *et al*, 1999; Phehane, 2002). However, the enzyme rapidly inactives during enzyme assay under standard conditions (Phehane, 2002).

The enzyme consists of 231 amino acids and has a molecular mass of 26 232 Da. Ultracentrifugation studies showed that *Pf*HGXPRT is tetrameric at low salt concentrations and dimeric at high salt concentrations (Keough *et al*, 1999). Although the *Pf*HGXPRT is 44% homologous to the human enzyme (Shi *et al*, 1999*b*), it has broader substrate specificity, i.e. the protozoal enzyme is able to use hypoxanthine (Webster *et al*, 1984; Asahi *et al*, 1996), guanine and xanthine as

[2] HGXPRT differentiates the *P. falciparum* phosphoribosyltransferase from the human homologue (HGPRT) which is unable to utilise xanthine as a substrate.

substrates whereas the human homologue is unable to utilise the latter (Queen *et al*, 1988).

Only one crystal structure of *Pf*HGXPRT exists, that of the enzyme in complex with a transition-state analogue inhibitor, as mentioned above (Shi *et al*, 1999*a*). The difficulty in obtaining crystals in the absence of such tight binding compounds may be attributed to the intrinsic instability of the enzyme and the fact that the isolated enzyme is inactive (Keough *et al*, 1999). The 2.0 Å structure of *Pf*HGXPRT with immucillinHP revealed a tetramer, with each subunit consisting of six α-helices and eleven β-strands (see figure 1.9). Within each subunit (monomer) there is a core domain (residues 46 - 194) and a hood domain (residues 1 – 45 and 193 – 231).

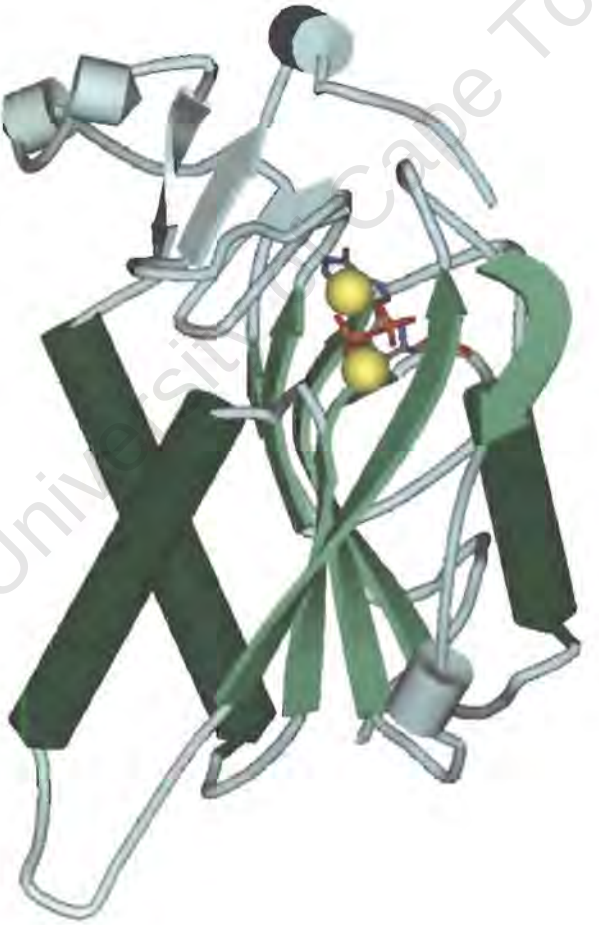

Figure 1.9. Subunit of *P. falciparum* HGXPRT. The monomer is complexed with the transition state analogue inhibitor, immucillinHP (stick representation), pyrophosphate (stick) and two Mg^{2+} (yellow spheres).

ImmucillinHP, two Mg^{2+}, and PP_i were bound at each of the four active sites of the tetramer (see figure 1.10) with β4′ and β5 folded over the catalytic site. Although the human and malarial homologues differ in substrate specificity, the structures of the enzymes with bound immucillins show that amino acid residues in contact with the inhibitors are conserved and the active site complexes show marked similarity.

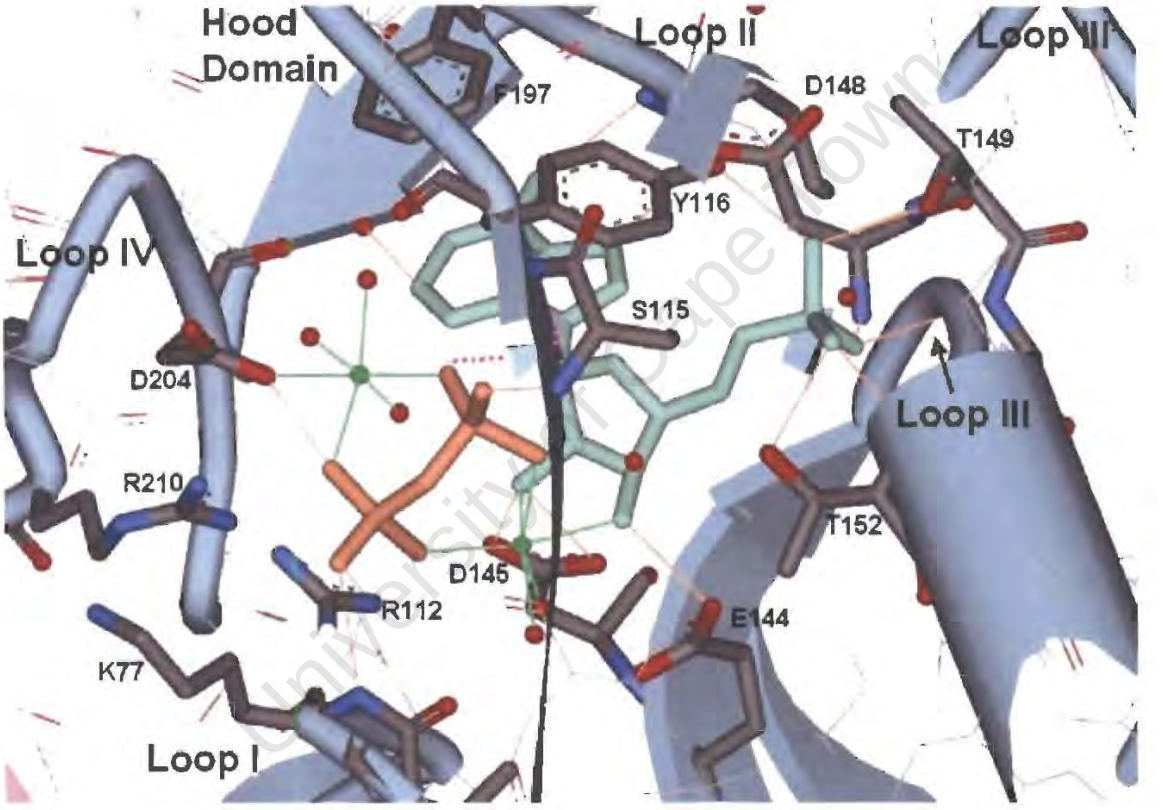

Figure 1.10. ImmucillinHP (light blue), PP_i (pink), and two Mg^{2+} (green spheres) bound at the active site of *P. falciparum* HGXPRT in a mimic of the closed transition state. Red spheres are water molecules. Key residues ligating the bound substrates/pseudosubstrates are indicated.

1.5 Flavonoids

The number of flavonoids that have been isolated from plants exceeds 4000 and these compounds can be classified into six groups (see figure 1.11). A wide range of functions of the flavonoids have been established. In plants, the compounds

have been found to protect against damage by ultraviolet radiation (Rao and Ormrod, 1995), microbial invasion (Grayer and Harborne, 1994; Grayer *et al*, 1992), and guard against being devoured by herbivores (for review see Harborne and Williams, 2000).

Humans consume significant quantities of various flavonoids in their diet and reportedly, these secondary plant metabolites exhibit anti-inflammatory (Wang *et al*, 1999*b*), antioxidant (Tournaire *et al*, 1993; Miyase *et al*, 1999a; Miyase *et al*,1999*b*), and antitumor activity (Alias *et al*, 1995; Saeki *et al*, 2000, Achanta *et al*, 2006).

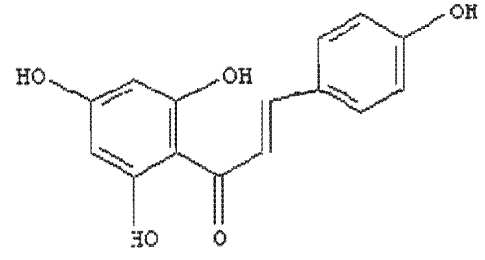

Chalcones

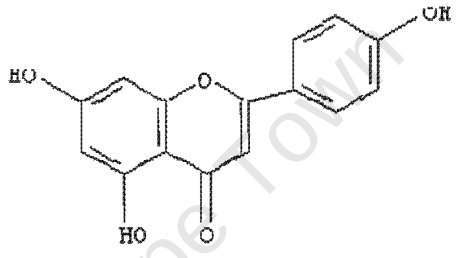

Flavones

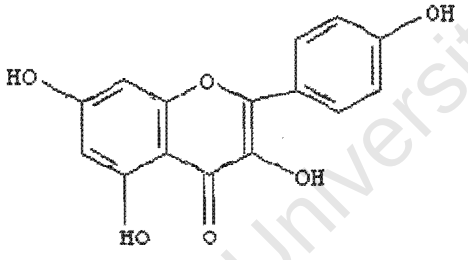

Flavonols

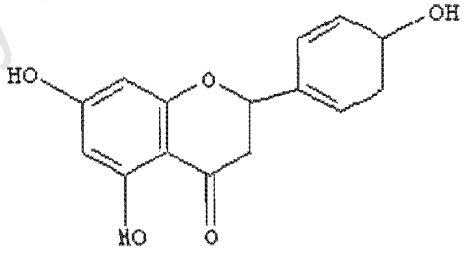

Flavanones

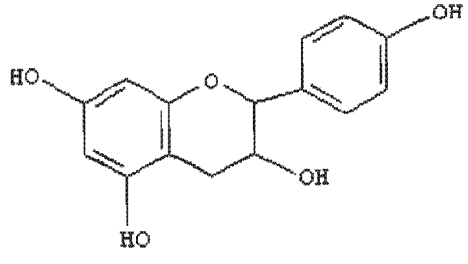

Anthocyanins

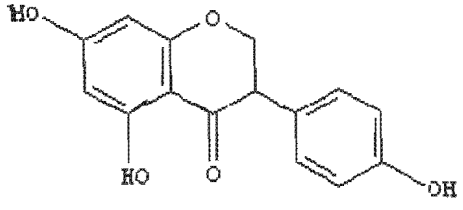

Isoflavonoids

Figure 1.11. Classification of the flavonoids.

1.5.1 Interaction of chalcones with *Pf*HGXPRT

Previous work in our laboratory involved the screening of a library of 38 flavonoids for inhibition of *Pf*HGXPRT activity. None of the compounds displayed inhibitory effects under the assay conditions in Mg^{2+}. However, a chalcone (4′-iodo-2′,4′,6′-trihydroxychalcone, figure 1.12) was found to accelerate catalytic turnover approximately 5-fold (Phehane, 2002). Interestingly, the chalcone had no effects on the human and *Toxoplasma gondii* homologues.

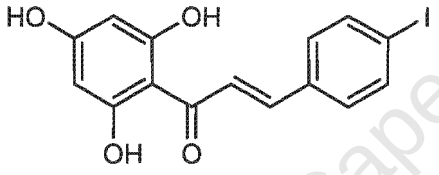

Figure 1.12. Chemical structure of 4′-iodo-2′,4′,6′,-trihydroxychalcone (4′-iodo-chalcone).

Further work in the laboratory showed that, when substituting Mg^{2+} with Ca^{2+} in the activity assay of *Pf*HGXPRT, the chalcone became a potent inhibitor of enzyme activity (Mbewe, 2005). The inhibition was non-competitive with respect to PRPP, suggesting the inhibitor binds to an allosteric site.

Nine analogues of the chalcone were synthesised and two of these were also shown to accelerate catalytic turnover of the *Pf*HGXPRT in the presence of Mg^{2+} and inhibit activity in the presence of Ca^{2+} (Mbewe, 2005).

In a further development, 4′-iodo-chalcone could replace partial substrates in converting the isolated inactive protein into the active form (Mbewe, 2007). While PRPP needs hypoxanthine or Mg^{2+} to effect the conversion, chalcone alone was able to perform this.

Thus, this group of chalcones displayed remarkable and unique effects specifically on *Pf*HGXPRT: converting the purified enzyme from an inactive to active form, accelerating catalytic activity in Mg^{2+}, and becoming potent inhibitors in Ca^{2+}. This is the first time an accelerator of catalytic activity has been found for any of the proteins in the PRT family as far as we are aware.

The mechanisms of these effects are unknown, but one possibility that we explored was whether the chalcones influenced the quarternary state of the protein, perhaps stabilizing the active tetrametic form, which is prevalent at low salt concentrations. This necessitated the development of a method for assaying the quarternary state and first investigating the salt concentration effect.

It is hoped that knowledge of the interaction of the chalcones with *Pf*HGXPRT would reveal an effector site for drug targeting.

1.6 Aims of the study

The first objective of the project was to prepare highly purified, active *Pf*HGXPRT following the procedure developed by Phehane (2002) using a pET vector with his-tag facility, expression in *E. coli*, and purification by Ni-affinity chromatography.

We hoped to use gel filtration HPLC to analyse the oligomeric state of *Pf*HGXPRT and analyse the tetramer ↔ dimer equilibrium at various salt concentrations, and explore the effects of $MgCl_2$ and $CaCl_2$. A basic understanding of the inherent instability of *Pf*HGXPRT could provide insights into the diverse effects of chalcone binding.

Next, the usefulness of a photoprobe, TNP-$8N_3$-ATP, in labelling of the active site of *Pf*HGXPRT would be determined. A probe that specifically derivatised the active site would be very useful for providing additional information on the site of binding of effector chalcones, i.e. do they compete with the active site probe.

Finally, we wanted to explore the possibility of using Isothermal Titration Calorimetry (ITC) to directly measure chalcone binding to *Pf*HGXPRT. ITC potentially can provide binding affinities (K_d values) and binding stoichiometry, as well as yielding the thermodynamic parameters like change in free energy, change in enthalpy, and change in entropy, which provide insights into the nature of the binding.

For the purposes of this study, the following definitions pertain to *Pf*HGXPRT:

*Isolated Pf*HGXPRT refers to protein obtained after purification and dialysis which is inactive but capable of being activated.

*Active Pf*HGXPRT refers to protein activated by overnight incubation at 0°C with partial substrates, which displays catalytic activity in the standard assay.

*Inactive Pf*HGXPRT refers to protein which is incapable of being activated.

CHAPTER 2: Materials and Methods

2.1 Materials

Reagents, and suppliers, used in this study are listed below.

Reagent	Supplier
Acrylamide	Bio-Rad
Amicon® stirred ultrafiltration cell (Model 8010)	Millipore
Ampicillin	Boehringer-Mannheim
AMPS	Bio-Rad
β-mercaptoethanol	Riedel-De Haen AG Seelze-Hannover
Bio-Rad reagent	Bio-Rad
Bromophenol blue	Sigma
DNase I	Roche
DE-52 resin	Whatman
DMSO	Merck
DTT	Sigma
E. coli BL21(DE3)pLysS cells	Novagen
EDTA	BDH
EGTA	Sigma
EPPS	Sigma
Glycerol	Merck
Guanine	Aldrich
Hypoxanthine	Sigma
Imidazole	Fluka
IPTG	Merck
KCl	Merck
MES	Sigma

$MgCl_2$	Merck
$MgSO_4$	Merck
MOPS	Sigma
MS Phosphor Screens	Perkin Elmer™
MW-GF-200 Kit	Sigma
NaCl	Merck
$NaH_2PO_4 \cdot H_2O$	Merck
$Na_2HPO_4 \cdot 2H_2O$	Merck
NaN_3	Unilab
$NaPP_i$	Sigma
Ni-CAM™ HC Resin	Sigma
^{32}P (10 mCi)	Amersham
PMSF	Sigma
Precision Plus Protein™ Standards	Bio-Rad
PRPP	Sigma
Reactive Red-120 resin	Sigma
Sephadex™ G-25	Amersham
SDS	Bio-Rad
SDS-PAGE Molecular Weight Standards (Low Range)	Bio-Rad
TMAH	Fluka
Tris	Merck
Tryptone powder	Merck
Yeast Extract	Merck

2.2 Methods

For the purposes of this study, *Pf*HGXPRT was expressed from two vectors, i.e. pET15b and pET17b. The different vectors provide proteins with distinct purification requirements. Expression from pET17b yields *Pf*HGXPRT which is purified by ion-exchange and dye-ligand affinity chromatography (in tandem) whilst expression from pET15b provides a his-tagged protein which is purified by nickel-affinity chromatography.

2.2.1 Methods in transformation, expression, purification and activation of his-tagged *Pf*HGXPRT

Malarial HGXPRT cloned into the expression vector pET15b was a gift from Drs D. Borhani and G. Vasanthakumar, Southern Research Institute, Birmingham, Alabama. *Pf*HGXPRT/pET15b was transformed into *E. coli* BL21(DE3)pLys*S* cells and expression was induced with IPTG. The protein was purified by nickel affinity chromatography.

Transformation of *Pf*HGXPRT

Cloning of the gene for malarial HGXPRT into pET15b (with his-tag facility) was performed in our laboratory by V.N. Phehane (2002). Plasmid extracts stored at -20°C were used to transform the expression strain, *E. coli* BL(21)DE3pLys*S*. A 100µl aliquot of competent *E. coli* BL21(DE3)pLys*S* cells was thawed on ice and 10 ng of *Pf*HGXPRT/pET15b was added. Cells were incubated on ice for 30 min, heat-shocked at 42°C for 50 s and then incubated on ice for a further 2 min. An aliquot (900 µl) of sterile SOC medium (2% w/v tryptone, 0.5% w/v yeast extract, 8.6 mM NaCl, 2.5 mM KCl and 20 mM $MgSO_4$) was added, followed by incubation at 37°C and rotating at 200 rpm for 1 h.
Cells were then cultured on Luria plates containing 100 µg/ml ampicillin and

34 µg/ml chloramphenicol. Selected colonies were cultured in LB medium supplemented with ampicillin (100 µg/ml), chloramphenicol (34 µg/ml) and 10 mM sodium phosphate at 37°C overnight until an OD_{600} 0.4 – 0.6 was attained. Glycerol stocks of the cultures were stored at -81°C.

Expression of his-tagged *Pf*HGXPRT

The glycerol stocks were cultivated on a larger scale in a litre of LB medium supplemented with antibiotics and sodium phosphate as described above. Protein expression was induced with 0.4 mM IPTG at 37°C in an orbital shaker at 200 rpm and expression was monitored by taking 1 ml aliquots before and after induction. Based on the findings of Studier (2005), it was later decided to induce protein expression at 25°C. The aliquots were centrifuged at 9000 rpm for 5 min and cell pellets were resuspended in water and mixed with an equal volume of 2x SDS-PAGE solubilisation buffer (125 mM Tris-Cl, pH 6.8, 10% v/v glycerol, 4% w/v SDS, 300 mM β-mercaptoethanol, 0.1 mg bromophenol blue). The samples were thoroughly mixed by vortexing, heated at 95°C for 5 min and a 20µl aliquot of each sample was loaded onto a 14% polyacrylamide gel for analysis according to the method of Laemmli (1970). Initially, low levels of expression were encountered and it was decided to induce at room temperature (see Results). Cells were collected by centrifugation at 8 000 rpm for 10 min at 4°C. Cell pellets were washed with sterile 1X PBS and stored at -81°C overnight.

Purification by nickel-affinity chromatography

First described in 1975 (Porath *et al*, 1975), metal-affinity chromatography is used for purification of peptides, nucleic acids and proteins (Lindner *et al*, 1992) and is also useful for the separation of cells.

In nickel-affinity chromatography, proteins containing a histidine tail bind immobilised nickel ions (electron acceptor) via the imidazole group (electron

donor) on the side chain. Bound proteins may then be eluted competitively by using another electron-donating group (Winzerling *et al*, 1992).

Cell pellets were thawed on ice and resuspended in filtered, ice-cold 5 mM imidazole, 20 mM Tris-Cl, pH 7.9, 500 mM NaCl, 1 mM PMSF, and incubated on ice for 1 h. Resuspended cells were then frozen in liquid nitrogen and thawed in water at room temperature. This freeze-thaw process was repeated twice. $MgCl_2$ (10 mM) and DNaseI (20 µg/ml) were added, followed by incubation at room temperature for 20 min. The lysate was centrifuged at 21 000 rpm for 20 min at 4°C and the supernatant was filtered (0.45 µm filter, Millex®) before loading onto the nickel affinity resin column. Further purification was conducted at 4°C.

The column was equilibrated with 5 mM imidazole, 20 mM Tris-Cl, pH 7.9, 500 mM NaCl, 1 mM PMSF and washed with equilibration buffer followed by equilibration buffer containing 30 mM imidazole. Attempts to obtain increasingly pure protein included variation in the concentration of imidazole in the column wash buffer (see Results). In the final purification step, the target protein was eluted in equilibration buffer containing 1 M imidazole. The eluate was then passed through a Sephadex™ G-25 column equilibrated with 25 mM Tris-Cl, pH 8.0, 1 mM DTT, 1 mM PMSF in order to remove imidazole. The protein was eluted with 3.5 ml of equilibration buffer. Fractions were collected at various stages during the purification and analysed on 14% SDS-PAGE according to the method of Laemmli (1970)[3].

Protein concentration determination

Protein concentration was determined using the Bio-Rad ® protein determination assay according to the manufacturer's instructions.

[3] For the duration of the study, 20 µl aliquots of all samples taken during expression and purification experiments were used for analysis by SDS-PAGE.

Activation

It has previously been shown that *Pf*HGXPRT was inactive as isolated and required incubation with substrates to obtain measurable activity (Keough *et al*, 1999). This was achieved by the addition of 1 mM PRPP and 10 mM $MgCl_2$ or 1mM PRPP and 60 µM hypoxanthine, followed by incubation at 4°C on ice for 16 h. Initial experiments included glycerol and EDTA in the incubation mixture. Standard enzyme activity assays were performed as described by Keough *et al* (1987) using an Agilent 8453 Chemstation spectrophotometer. The assays were conducted at room temperature in 100 mM Tris-Cl, pH 8.5, 110 mM $MgCl_2$, 60 µM purine base and 1 mM PRPP. The reaction was initiated by the addition of an aliquot of purified enzyme (generally 5-20 µg/ml). The increase in absorbance for conversion of guanine to its nucleotide (GMP) was measured at 257.5 nm. The difference extinction coefficient at pH 8.5 is 5 817 for guanine and the initial rate was automatically calculated over 15s by the instrument.

2.2.2 Methods in expression, purification and activation of *Pf*HGXPRT without a his-tag

Mbewe (2005) had cloned the gene for malarial HGPRT, obtained as a his-tagged insert in pET15b, into pET17b (without his-tag). Competent *E. coli* BL21(DE3)pLys*S* cells were transformed with recombinant pET17b and glycerol stocks of the transformed cells were used in the present study.

Protein expression

E. coli BL21(DE3)pLys*S* cells containing the recombinant pET17b vector were cultivated in LB medium supplemented with ampicillin (100 µg/ml), chloramphenicol (34 µg/ml) and 10 mM sodium phosphate at 37°C overnight until

an OD_{600} 0.4 – 0.6 was attained. Recombinant protein expression was then induced by the addition of 0.4 mM IPTG. Expression was monitored by taking 1 ml aliquots before and after induction and aliquots were analysed by SDS-PAGE according to the method of Laemmli (1970) as described above. Cells were collected by centrifugation at 8 000 rpm for 10 min at 4 °C and cell pellets were stored at -81°C overnight.

HGXPRT Purification

Malarial HGXPRT was purified by anion-exchange chromatography (using DEAE resin, figure 2.1) and Reactive Red-120 (figure 2.2, type 3000-CL in 0.5 M NaCl, 0.02% thimerosal) affinity chromatography (Mbewe *et al*, 2007). The malarial protein is peculiar as, unlike most proteins, it fails to bind to an anion exchange resin (under the conditions used). Reactive Red-120 is commonly used to purify nucleotide binding proteins. The two columns were used in tandem: the flow-through of the anion-exchange resin was allowed to drip onto the reactive red-120 column, the columns separated, and the protein of interest eluted with sodium pyrophosphate. All purification procedures were performed at 4 °C. In ion-exchange chromatography, proteins are separated from other components in a solution by taking advantage of the fact that different proteins carry specific net charges at different pH values (Doonan and Cutler, 2004; Marshall and Inglis, 1986; Scopes, 1994; Selkirk, 2004). Two types of ion-exchange chromatography are distinguished: anion- and cation-exchange chromatography (Horton *et al*, 2002; Marshall and Inglis, 1986; Scopes, 1994; Selkirk, 2004; Voet and Voet, 1995). In anion-exchange chromatography, the column matrix carries a net positive charge whilst in cation-exchange chromatography, the matrix bears a net negative charge. Therefore, anion-exchangers bind negatively-charged proteins and cation exchangers positively charged proteins (Horton *et al*, 2002; Voet and Voet, 1995). Matrix-bound proteins may be eluted by an increasing salt gradient (Horton *et al*, 2002; Marshall and Inglis, 1986; Selkirk, 2004; Voet and Voet, 1995) or by altering the pH. Those proteins with low affinity (low charge) would

elute sooner than those with a high affinity (high charge) for the column (Horton *et al*, 2002; Marshall and Inglis, 1986; Voet and Voet, 1995).

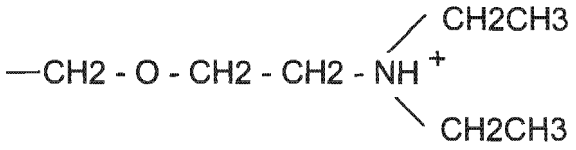

Figure 2.1. Chemical structure of diethyl aminoethyl (DEAE).

The development of a technique for separation of proteins by affinity chromatography was based on the knowledge that enzymes bind substrates and inhibitors in a reversible manner (Cuatrecasas *et al*, 1968), i.e. many proteins are able to bind certain molecules in a noncovalent way. Purification by affinity chromatography entails the passage of the protein of interest through a column consisting of a porous gel matrix (preferably containing many hydroxyl groups) to which a ligand has been covalently attached. Commonly used ligands include antibodies specific for the target protein or molecules known to interact with the protein *in vivo*. The latter could be any of a number of molecules, including other proteins, cofactors, nucleotides and amino acids (Denizli and Pişkin, 2001).
In this technique, a protein solution is passed through the column and, hopefully, only the target protein binds to its immobilised ligand while other proteins flow through the inert matrix (Cuatrecasas *et al*, 1968, Horton et al, 2002; Voet and Voet, 1995) and, therefore, the major advantage of affinity chromatography lies in its ability to purify even a small amount of a target protein from a mixture of proteins because of the high degree of specificity afforded by the ligand (Cutler, 2004). The ligand-bound protein may then be eluted by changing conditions, for example by altering the pH, temperature or salt concentration of the elution buffer (Denizli and Pişkin, 2001; Horton *et al*, 2002; Voet and Voet, 1995). These are

meant to destabilise the protein-ligand interaction but care needs to be taken that the protein of interest is not denatured (Voet and Voet, 1995). In some cases, the protein may also be eluted from the column by the addition of a solution containing a higher concentration of the ligand than that bound to the matrix of the column, such that the competitive effect displaces the protein from the resin. (Horton *et al*, 2002).

Dye-ligand affinity chromatography involves the use of synthetic dyes covalently attached to agarose as ligands for the purification of macromolecules. These dyes are composed of a chromophore (often laced with sulphonic acid groups) and a reactive group (which permits covalent attachment to the agarose). The chromophore is designed to mimic enzyme substrates. For example, Reactive Red-120 (figure 2.2) contains a chromophore that resembles nucleotides and therefore often binds nucleotide-binding proteins. The dye-agarose resins are especially useful as they are commercially available and inexpensive, and are more attractive than other ligands such as antibodies and nucleotides which are costly and tend to be difficult to immobilise.

Figure 2.2. Chemical structure of Reactive Red-120. The molecule reacts with the agarose via the chloro groups (green) in order to immobilise the resin. The S of the negatively-charged sulphonate groups is shown in orange/yellow.

Cell pellets obtained as described before were thawed on ice and then resuspended in 50 mM Tris-Cl, pH 8.0, 25 mM NaCl, 2 mM EDTA, 1 mM PMSF and 1 mM DTT in a volume that was 1/10 of the cell culture. Resuspended cells were frozen

in liquid nitrogen and thawed in water at room temperature. The viscous cell paste was then treated with DNaseI (20 µg/ml) in the presence of 10 mM $MgCl_2$ for 20 min at room temperature followed by centrifugation at 21 000 rpm for 20 min at 4°C to yield a crude pellet and supernatant.

Anion-exchange chromatography was performed using a column (5 x 3 cm) equilibrated with buffer containing 750 mM Tris-Cl, pH 8.0, 1 mM DTT and 1 mM PMSF. The resin was then washed with 10 ml lysis buffer (50 mM Tris-Cl, pH 8.0, 25 mM NaCl, 2 mM EDTA, 1 mM PMSF and 1 mM DTT) before loading the supernatant. The reactive red-120 resin (3 x 2 cm) was washed with dH_2O and the anion-exchange column flow-through was allowed to pass through this column. The target protein was eluted from the affinity resin in ~7 ml of 50 mM $NaPP_i$, 50 mM Tris-Cl, pH 8.9, 1 mM DTT and 1 mM PMSF. Fractions collected during these steps were analysed on 14% SDS-PAGE according to the method of Laemmli (1970).

Protein concentration determination

Protein concentration was determined using the Bio-Rad ® protein determination assay according to the manufacturer's instructions.

Activation of *Pf*HGXPRT

As mentioned above, it has previously been shown that *Pf*HGXPRT is inactive as isolated and requires incubation with partial substrates to obtain measurable activity. Following elution of *Pf*HGXPRT from the Reactive Red-120 column, protein-containing fractions were dialysed against 10 mM MOPS, pH 7.0, overnight at 4°C. Aliquots of the dialysate were incubated with partial substrates (i.e. either lacking Mg^{2+} or one of the substrates in order to prevent turnover). This was achieved by the addition of 1 mM PRPP and 60 µM hypoxanthine followed by incubation at 4°C on ice for 16 h.

Enzyme activity assays were performed as described above (Keough *et al,* 1987).

2.2.3 Gel filtration chromatography

Gel filtration (also called size-exclusion) chromatography is used for the partitioning (or fractionation) of molecules on the basis of their size. In addition to the separation of molecules, size exclusion chromatography may also be used to determine the molecular mass for a given molecule (Voet and Voet, 1995; Waterfield, 1986). The matrix used in this type of chromatography consists of beads with pores of different dimensions. When a solution of proteins of different molecular masses is passed through such a column, the pores are differentially penetrated by the proteins in the solution. Proteins too large to penetrate the pores would flow through the column whereas smaller proteins would diffuse into the pores of the resin. Those proteins able to enter the pores would have different molecular masses, with the smallest of the proteins taking up most of the internal space.

Gel filtration may be carried out under high pressure in a technique called high-performance liquid chromatography (HPLC) by using equipment able to withstand high pressures (Horton *et al*, 2002; Scopes, 1994; Waterfield, 1986), as was performed in the present study. In order to calibrate the column used in this technique, a mixture of proteins of known molecular weight (standard proteins) is applied to the column. The volume excluded from the internal space of the pores is called the void volume (V_o) and this is usually measured by using a high-molecular weight protein or dextran. The volume included within the internal space of the resin is termed the total volume (V_i), and is measured by the volume required to elute the protein or compound with a low molecular mass. Any other protein in the mixture would have a required retention volume (V_r) located between the values of V_o and V_i (Cutler, 2004; Scopes, 1994; Voet and Voet, 1995; Waterfield, 1986).

In order to obtain a calibration (standard) curve, the values of V_r for the standard proteins are plotted against the logarithms of their molecular masses (figure 2.3), respectively, yielding a linear relationship (Cutler, 2004; Scopes, 1994; Voet and Voet, 1995; Waterfield, 1986).

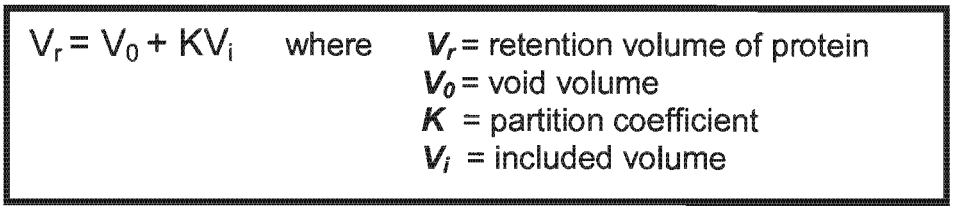

Figure 2.3. Equation for determining the retention volume for a protein on gel filtration HPLC. The void volume is the volume of the mobile phase between the beads of the stationary phase. The partition coefficient reflects the extent to which a protein can penetrate the stationary phase and the included volume is the volume of the mobile phase within the porous beads. The retention volume of a protein allows for the calculation of its molecular mass from the calibration curve constructed by plotting the logarithm of the molecular weights of the standards against their respective retention volumes.

Gel filtration on HPLC is a technique normally used during the final stages of protein purification, but also as a tool for the analysis of interactions between proteins (oligomeric structure), and protein folding (Cutler, 2004; Scopes, 1994; Voet and Voet, 1995; Waterfield, 1986).

The column used in the present study (TosoHaas TSKgel G3000SW, 7.5 mm × 30 cm) was calibrated using the MW-GF-200 Kit. Molecular weight standards used are indicated in table 2.1. Blue Dextran was used as the void volume marker (V_o) whilst tyrosine was used as the included volume marker (V_i). The mixture of standard proteins was injected directly onto the HPLC column and separated in 0.01 M MOPS.TMAH buffer, pH 7.0, and 20, 100, or 400 mM NaCl, over 15 min. The flow rate was 1 ml/min. The elution profile obtained was used to construct the calibration curve in figure 3.14.

Table 2.1. Molecular weight standards used in TSKgel G3000SW calibration.

Standard	Molecular weight (MW)
Blue Dextran (V_o)	2 000 000
Alcohol dehydrogenase	150 000
Albumin (Bovine serum)	67 000
Ovalbumin	44 000
Carbonic anhydrase	29 000
Cytochrome c	11 700
Tyrosine (V_i)	185

It has been shown that the quarternary structure of *Pf*HGXPRT is sensitive to ionic strength (Keough *et al*, 1999) and in the present study gel filtration was used to analyse protein oligomerisation under varying salt conditions.

Sodium, calcium and magnesium concentration dependences were analysed at the various concentrations shown in Table 2.2.

Table 2.2. Ionic strengths used in *Pf*HGXPRT oligomerisation analysis by gel filtration HPLC.

Salt	**Concentration** (mM)
NaCl	20 – 400
$CaCl_2$	0.2 - 100
$MgCl_2$	0.2 - 100

For analysis, 30 µl aliquots of the protein (1.3 mg/ml) were injected onto the column. The mobile phase was 10 mM MOPS·TMAH, pH 7.0, containing the various salts at the concentrations indicated in Table 2.2.

The effects of protein dilution as well as preincubation of *Pf*HGXPRT in 1 M NaCl at room temperature were also analysed. An aliquot of the protein was

diluted ten-fold with running buffer and injected onto the column in running buffer containing either 20 or 50 mM NaCl.

The effect of enzyme activation was determined by incubation with the substrates hypoxanthine (60 μM) and PRPP (1 mM) at 4°C on ice for 16 h. An aliquot of the active enzyme was injected onto the HPLC column in running buffer containing 20 to 100 mM NaCl.

2.2.4 Photolabelling

Photoaffinity labelling is a technique which allows the covalent derivatisation of a protein by a ligand through the use of a light-sensitive moiety attached to the ligand (Singh *et al*, 1962). Irradiation of the protein-ligand complex converts the ligand into a highly reactive carbene or nitrene which immediately reacts with nucleophiles like tyrosine or lysine side chains in its proximity (McIntosh *et al*, 1996; reviewed in Kotzyba-Hibert *et al*, 1995 and Dormán and Prestwich, 2000). If the light-sensitive ligand is radiolabeled, the extent of derivatisation can be measured by scintillation counting or radioimaging of gels. The binding of other ligands, for example substrates, can be conveniently measured through their competitive effect on the photolabeling, if they bind to the same site.
8-N_3 nucleotides have been extensively used to derivatise proteins with nucleotide-binding sites. TNP derivatives of nucleotides were developed as fluorescent probes of nucleotide binding sites. The TNP moiety often makes the nucleotide bind very much tighter than for example ATP itself. TNP-8N_3-ATP (figure 2.4) was first synthesised in our laboratory as a tight-binding, light-sensitive, fluorescent probe of ATP binding sites (Seebregts and McIntosh, 1989).

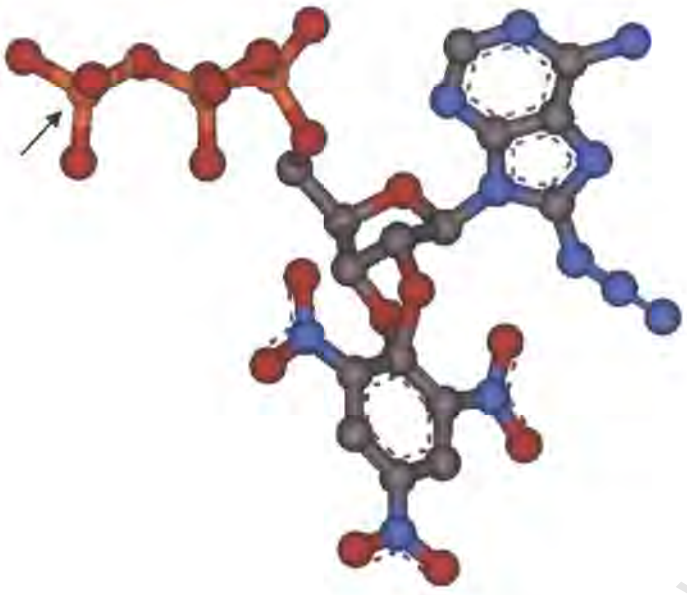

Figure 2.4. Chemical structure of TNP-8N_3-ATP. The ^{32}P atom in [γ-^{32}P]TNP-8N_3-ATP is indicated by the black arrow. [γ-^{32}P]TNP-8N_3-ATP, a light-sensitive ATP analogue was used to covalently derivatise *Pf*HGXPRT .

In the present study, we explored the use of the radioactive photolabel [γ-^{32}P]TNP-8N_3-ATP (figure 2.4) as a possible probe of the active site of *Pf*HGXPRT. Even though the TNP nucleotide is different and larger compared to the enzyme substrates and products, the structures of the homologous apoenzyme from *Toxoplasma gondii* and human show that the active site is wide open – all the loops that fold over the bound substrates are well apart – and it is certainly conceivable that TNP-8N_3-ATP, with the tail of the phosphate chain extending out of the site (see later). In a previous study (Murungi, 2007), the use of [γ-^{32}P]TNP-8N_3-ITP was found to be reasonably effective as a photoprobe of *Pf*HGXPRT ($K_{0.5}$ in the low micromolar range), however the synthesis of this probe starts with [γ-^{32}P]TNP-8N_3-ATP and requires further chemical steps. It would be much simpler if we could use [γ-^{32}P]TNP-8N_3-ATP instead of [γ-^{32}P]TNP-8N_3-ITP.

Ultimately, once it is established that the photoprobe labels the active site, we would like to study the effect of introducing 4'-iodo-chalcone, and determining whether it binds at the active site (competitive) or elsewhere (allosteric site).

2.2.4.1 Synthesis of [γ-^{32}P]TNP-8N_3-ATP and photolabelling methodology

[γ-^{32}P]TNP-8N_3-ATP was synthesised in our laboratory according to methods previously described by Seebregts and McIntosh (1989) and McIntosh *et al* (1996). The probe is routinely synthesised in our laboratory for measuring ATP binding to mutants of sarcoplasmic reticulum Ca^{2+}-ATPase. Very briefly, the synthesis consists of enzymatically introducing [^{32}P]P_i into 8-azido-ATP, then introducing the TNP moiety by reaction with trinitrobenzenesulphonic acid.

The methodology for photolabelling is described in Seebregts and McIntosh (1989). The irradiation mixture, containing the photolabel and protein, was prepared in a volume of 75 µl. The mixtures were irradiated at room temperature in a quartz micro cuvette, between two toluene filters (only light above 290 nm allowed through), and approximately 8 cm from a 150 W Xenon lamp (Applied Photophysics) with a front facing reflector located behind the cuvette. The filters were produced by filling two standard quartz cuvettes (1 cm path length) with toluene. Irradiation time was 1.5 min. Following irradiation, cuvettes containing the samples were kept on ice. Samples were transferred to 1.5 ml Eppendorf tubes and 8 µl solubilisation buffer (1.2 % SDS, 3.6 % ß-mercaptoethanol and bromophenol blue) was then added. The samples were analysed by 7% (Ca^{2+}-ATPase) or 12% (*Pf*HGXPRT) acrylamide SDS-PAGE gels, according to the method of Laemmli (1970). The gels were run for 3-4 h at 45 mA and were then dried by heating and vacuum.

Reference spots of known volume and [γ-^{32}P]TNP-8N_3-ATP concentration were placed alongside the bands on the gel, i.e. spots contained 1 µl of 10 µM [γ-^{32}P]TNP-8N_3-ATP, in order to quantify the extent of derivatisation (see below). The dried gel was then placed on a MS Phosphor Screen in a film cassette, within

a lead-lined box, for approximately 24 h. Storage in a lead-lined box protects the gel from background cosmic radiation which otherwise produces interference on the phosphor screen after extended periods. Subsequently, the screen was scanned on a Cyclone™ Storage Phosphor Screen (Packard Bioscience) to measure radioactivity. Visible bands were quantified using OptiQuant software.

MW of Ca^{2+} -ATPase = 110000 g/mol >> 0.11 mg/nmol ≡ 9 nmol/mg
Assume 5 nmol/mg if ATPase consists of ~70% of total protein
[Protein]: 0.002 g/ml ≡ 10 nM ≡ 0.01 nmol/ml
0.05 ml onto gel ∴ 0.01 x 0.05 = 0.0005 nmol protein loaded onto gel

. **a** dlu in gel band
b dlu in mean background
c dlu in 1µl spot (mean of 3) (54580 for this expt)

1µl 1 µM [γ-^{32}P]TNP-8N_3-ATP ≡ 0.001 nmol
c dlu / 0.001 nmol TNP-8N_3-ATP
∴ **c** x 1000 dlu / nmol TNP-8N_3-ATP
nmol probe in gel band = (**a** – **b**) / **c** x 1000 nmol
mol probe bound / mol protein = (**a** – **b**) / (**c** x 1000 x 0.0005) mol / mol
e.g. for 3 µM TNP >> (1297 – 212) / 54580 x 1000 x 0.0005) mol / mol
= 0.040 mol TNP-8N_3-ATP / mol ATPase

Figure 2.5. Calculation of the moles of probe bound per mole of protein using SR Ca^{2+}-ATPase as an example

2.2.4.2 Photolabelling of sarcoplasmic reticulum Ca^{2+}-ATPase and ATP inhibition

TNP-8N_3-ATP and the radiolabelled derivative, [γ-^{32}P]TNP-8N_3-ATP, has been used extensively to characterise nucleotide interactions with Ca^{2+}-ATPase in our laboratory. The probe specifically derivatises Lys^{492} in the ATP binding site with high efficiency (McIntosh *et al* 1992) and is a useful model system for demonstrating the usefulness of the technique and for comparing to the results obtained with those for *Pf*HGXPRT.

Ca^{2+}-ATPase in sarcoplasmic reticulum vesicles was obtained from rabbit skeletal muscle and is prepared routinely in our laboratory according to the method of Champeil *et al* (1985) as modified by McIntosh *et al* (1992). Very briefly, rabbit back skeletal muscle is homogenised and the microsomal fraction isolated by differential centrifugation. The preparation is finally resuspended in 5 mM HEPES/0.3 M sucrose, pH 7.4 and stored at -81 °C.

The concentration dependence of derivastisation by [γ-^{32}P]TNP-8N_3-ATP was performed in 25 mM EPPS·TMAH, pH 8.5, 2 mM EDTA, 20% (v/v) glycerol, 0.002 mg/ml SR ATPase, and 0.001 to 10 µM [γ-^{32}P]TNP-8N_3-ATP. ATP inhibition of the photolabelling was in 25 mM EPPS·TMAH, pH 8.5, 2 mM EDTA, 20% (v/v) glycerol, 0.002 mg/ml SR ATPase, 0.3 µM [γ-^{32}P]TNP-8N_3-ATP and 0-3 mM ATP.

The moles of [γ-^{32}P]TNP-8N_3-ATP bound per mole of SR Ca^{2+}-ATPase was calculated as illustrated in figure 2.5

The photolabelling technique allows determination of K_d for ATP binding. In order to achieve this the $K_{0.5}$ for [γ-^{32}P]TNP-8N_3-ATP derivatisation needs to be obtained. A certain photoprobe concentration is then used (we generally use 2-3 x $K_{0.5}$, as this means that the majority (60-75%) of the protein is derivatised) and the $K_{0.5}$ for ATP inhibition is obtained, and then these values are used to derive a true K_d for ATP binding.

The equations needed for fitting the curves and calculation of the true K_d are described in McIntosh *et al* (1996), and are as follows:

After quantification of the radioactivity using OptiQuant software, the [γ-^{32}P]TNP-8N_3-ATP concentration dependence data were fitted using the following equation:

$$Y = V_{max}\cdot[S]/(K_{0.5(TNP)} + [S]) + m\cdot[S] \quad \text{Eq. 2.1}$$

Where Y = relative dlu, Y_{max} = relative maximal dlu, [*S*] = ligand concentration and $K_{0.5(TNP)}$ = the concentration of the photolabel at which half-maximal derivatisation occurs.

The ATP concentration dependence data of inhibition of [γ-^{32}P]TNP-8N_3-ATP photolabelling was fitted using the equation

$$Y = [E] \cdot K_{0.5(ATP)} / \{K_{0.5(ATP)} + [ATP]\} \quad \text{Eq. 2.2}$$

where Y= mol probe/mol enzyme, [*E*] = concentration of enzyme and $K_{0.5(ATP)}$ = concentration of ATP at half-maximal inhibition.

Using Eq. 2.2, the $K_{0.5(ATP)}$ was calculated. Substituting this value into the equation

$$K_{d(ATP)} = K_{0.5(ATP)} / \{1 + ([TNP\text{-}8N_3\text{-}ATP] / K_{0.5(TNP)})\} \quad \text{Eq. 2.3}$$

provided the "true" dissociation constant for ATP binding.

2.2.4.3 Photolabelling of *Pf*HGXPRT

Photolabelling of the malarial enzyme was performed in media and at protein concentrations described in the figure legends in the Results section.

2.2.5 Isothermal Titration Calorimetry

Isothermal titration calorimetry (ITC) is used to characterise binding interactions as well as the kinetics of enzyme-catalysed reactions. Chemical reactions are accompanied by changes in heat and this is directly related to the rate at which a reaction occurs. In protein science, thermodynamic parameters provide useful information pertaining to protein structure and function.

In a typical experiment, the heat produced or taken up during a reaction between two components may be measured by the stepwise addition of one reactant (in the syringe) to the other (in the cell, see figure 2.7). These reactions include protein-protein (Chung *et a*l, 1999), protein-ligand (Singh and Kishore, 2008), DNA-protein (Chen *et al*, 2008), protein-carbohydrate (Gopalakrishnapai *et al*, 2006) as well antigen-antibody binding (Raman *et al*, 1995). ITC data may be used to determine binding constants (K_B), stoichiometry (n) and the thermodynamic parameters enthalpy (ΔH), entropy (ΔS), and free energy (ΔG) provided the initial concentrations of the reactants are known (reviewed in Ladbury and Chowdry, 1996).

Each ITC experiment needs careful planning so that the change in heat is measurable for each injection and, secondly, the change should vary for successive injections in order to produce a curved thermogram (see figure 2.7). The curvature of the thermogram is dependent on the concentrations of the macromolecule and ligand and the equilibrium constant (K_{eq}). A useful reference source for experimental design and data analysis can be found in Freyer and Lewis (2008).

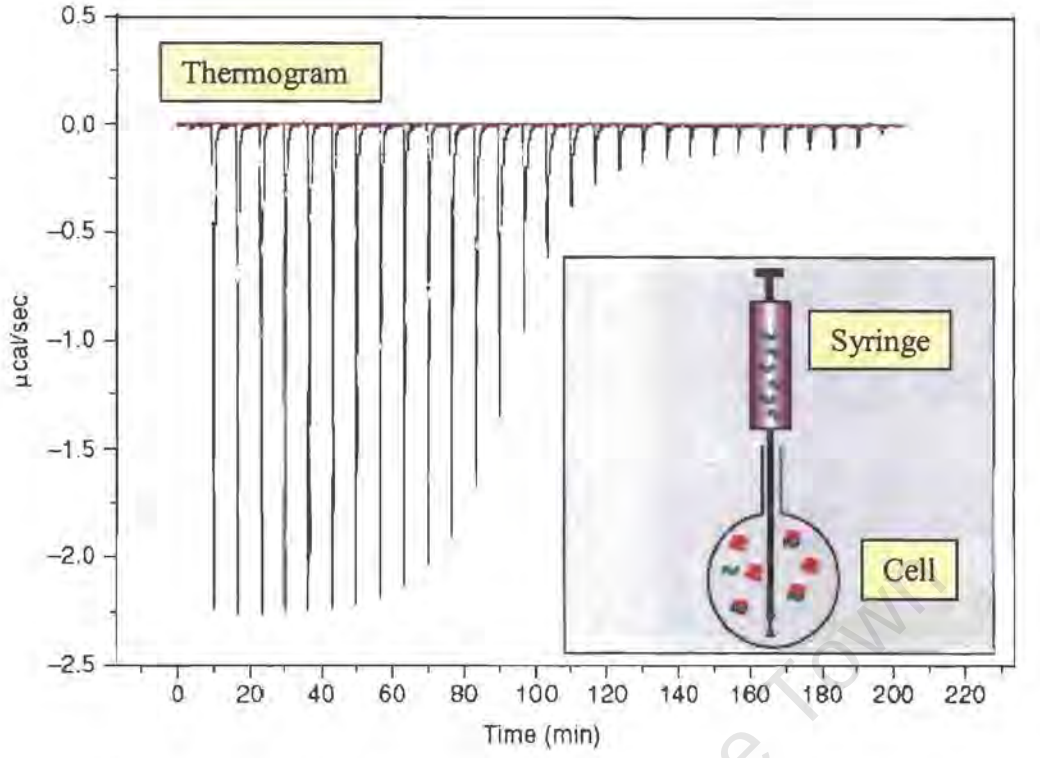

Figure 2.6. Model ITC raw data for an exothermic reaction. The inset shows an ITC reaction cell (containing the protein – red blobs) and injection syringe (containing the ligand - green blobs) which stirs the contents of the cell to ensure homogeneity. The titration is effected by timed injections of a fixed volume of the ligand into the cell thereby producing characteristic "heats of injection" (main thermogram). The heat produced is initially maximal as the binding sites are largely empty, then as the sites available become less the amount of heat produced diminishes, until saturation, where the heat produced is the result of dilution of the protein only and these tail end values should be subtracted from the earlier data prior to analysis. The area under each peak is the heat associated with each timed injection needed to maintain the temperature between the reference and reaction cells. The figure was taken directly from Leavitt and Freire (2001).

All ITC experiments in the present study were carried out using a VP-ITC microcalorimeter (Microcal, Inc.) with a cell volume of 200-300 µl and a total volume delivered from the syringe of 35-40 µl. The experiments were conducted at 25°C, the cell stirred at 500 rpm, and the intervals between injections 180 s. Solutions were stirred and degassed prior to use (under vacuum) to avoid bubbles. It is important that the two solutions in the cell and syringe are matched in composition as far as possible, e.g. pH, buffer and salt concentrations.

Three types of experiments were performed, namely, a model experiment involving titration of $CaCl_2$ into a solution of EDTA, measurement of the heat evolved from a dilution of DMSO in water, and thirdly titration of 4′-iodo-chalcone into a solution of *Pf*HGXPRT. The second was necessarily because the stock concentrated solutions of the chalcone had to be made up in neat DMSO. In order to minimise the DMSO effect, the solubility of the chalcone at different pH values was determined (see later).

The conditions used for each experiment are provided in the legends to the figures in the Results section. In general though, for the protein titration, the experiments were conducted at alkaline pH, 6-36 μM isolated or activated *Pf*HGXPRT, $MgCl_2$ or $CaCl_2$, without or with PRPP and hypoxanthine, and either 10% DMSO in both cell and syringe or 0.1% DMSO in the syringe only (later experiments). The concentration of chalcone in the syringe was also varied.

ORIGIN™ software purchased with the calorimeter was used to calculate the thermodynamic data.

The general equation used to obtain the change in enthalpy (ΔH) and binding constant (K_a) from the heat produced or taken up for a simple single site/macromolecule situation is as follows:

$$Q = V_o\Delta H[M]_tK_a[L]/ K_a[L] \quad \text{.....Eq. 1.1}$$

Where Q is the heat evolved or taken up on addition of ligand
V_o is the corrected cell volume
$[M]_t$ is the concentration of macromolecule in the cell
[L] is the concentration of the ligand in the cell on each injection

The change in free energy (ΔG) is obtained from $\Delta G = -RTLnK_a$
and the change in entropy (ΔS) is obtained from $\Delta H = \Delta G - T\Delta S$

CHAPTER 3: Results

3.1 Transformation, Expression, Purification and Activation of his-tagged *Pf*HGXPRT

3.1.1 Transformation of *E. coli* with *Pf*HGXPRT/pET15b

The expression strain, *E. coli* BL21(DE3)pLys*S*, was successfully transformed with recombinant pET15b containing the insert encoding *Pf*HGXPRT. Glycerol stocks of these cells were stored at -81°C.

3.1.2 Expression and purification of *Pf*HGXPRT from pET15b

Initial experiments yielded low levels of the target protein and it was decided to prepare a fresh IPTG stock solution and to compare expression levels when using this and a solution that had been frozen at -20°C for approximately three months. However, induction with fresh 0.4 mM IPTG at 37°C produced no significant differences in expression levels (see figure 3.1).

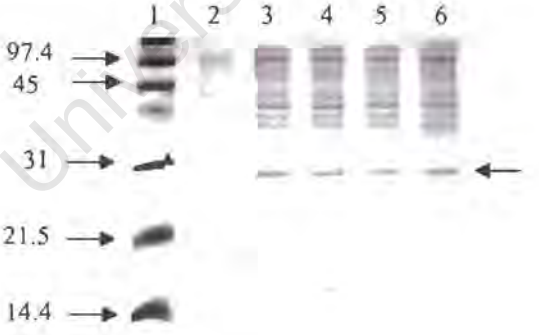

Figure 3.1 SDS-PAGE analysis of his-tagged *Pf*HGXPRT expression at 37°C with frozen and fresh IPTG stock solutions. Aliquots of 1ml culture were taken before and after 3 h induction with 0.4 mM IPTG, solubilised, and 20 µl subjected to SDS-PAGE with 14% acrylamide. **1**, Molecular weight markers (kDa); **2**, Before induction; **3** and **4**, After induction with "old" IPTG stock solution (frozen for 3 months); **5** and **6**, After induction with fresh IPTG. The right hand arrow indicates the position of *Pf*HGXPRT based on molecular weight (~26 kDa).

Nevertheless, despite low expression levels, it was decided to subject the preparation to Ni-chelate chromatography and the results are shown in figure 3.2. The supernatant (lanes 2 and 3) shows the poor expression. The pellet (lane 4) contains negligible amounts of the protein of interest indicating it is not in inclusion bodies. Passage through the Ni-chelate column decreased the amount of *Pf*HGXPRT in the material flowing through (lane 5). Most of the *Pf*HGXPRT was eluted in the first 2 ml of 1 M imidazole (lanes 7 and 8). The preparation is not all that pure mainly because of the low expression levels.

Figure 3.2 Purification of his-tagged *Pf*HGXPRT using nickel-affinity chromatography after induction with 0.4 mM IPTG at 37°C. 1, Molecular weight marker (kDa); **2**, Supernatant before filtration; **3**, Supernatant after filtration; **4**, Crude pellet (resuspended to the same volume as the supernatant) after induction; **5**, Flow-through; **6**, 5 mM imidazole wash fraction (5 ml); **7**, 2 ml 1 M imidazole fraction; **8**, further 2 ml 1 M imidazole. The right hand arrow indicates the position of *Pf*HGXPRT (~26 kDa). Equal volume aliquots were placed in each well.

Studier (2005) found that it is beneficial to induce expression at 25°C rather than 37°C. Also, a recent study by Berwal *et al* (2008) on the expression of lactate dehydrogenase from *P. falciparum* showed that decreasing the temperature of induction was crucial for obtaining better yields of soluble protein when the enzyme was overexpressed in *E. coli*. Induction of *Pf*HGXPRT expression at 25°C showed significantly increased yields (see supernatant, lanes 2 and 3, figure 3.3) and this led to a much purer preparation after Ni-chelate chromatography (lanes 7 and 8). We adopted a temperature of 25°C in future experiments.

Figure 3.3. Purification of his-tagged *Pf*HGXPRT using nickel-affinity chromatography after induction with 0.4 mM IPTG at 25°C. 1, Molecular weight markers (kDa); **2**, Supernatant before filtration; **3**, Supernatant after filtration; **4**, Crude pellet (resuspended to the same volume as the supernatant) after induction; **5**, Flow-through; **6**, 5 mM imidazole wash fraction (5 ml); **7 - 10**, 1 M imidazole fractions (2 ml aliquots) . The arrow on the right indicates the position of *Pf*HGXPRT (~26 kDa). Equal volume aliquots were placed in each well.

We attempted to obtain better purification by increasing the concentrations of imidazole and NaCl in the solutions used to wash the nickel column before elution of the target protein and such an experiment, in which a 60 mM imidazole + 1 M NaCl wash was included, is shown in figure 3.4 [note that normally 500 mM NaCl was included in all buffers]. However, a significant amount of the target protein was eluted with this strategy (lane 7). Hence, we considered that it might be better to revert to the usual 30 mM imidazole and 500 mM NaCl wash but increase the volume.

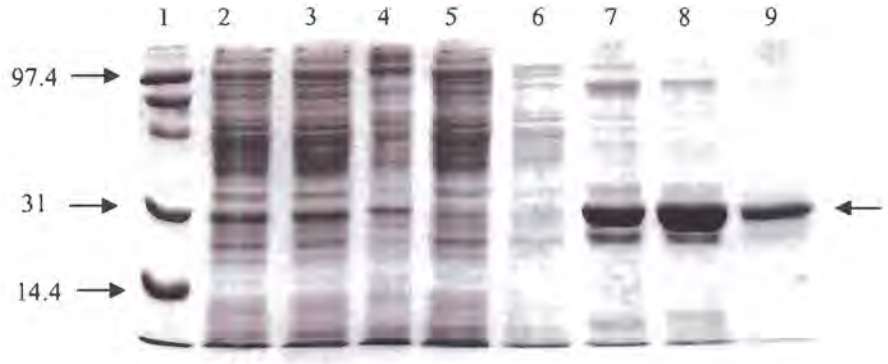

Figure 3.4. Purification of his-tagged *Pf*HGXPRT using higher concentrations of imidazole (60 mM) and NaCl (1 M) in the column wash buffer. 1, Molecular weight markers (kDa); **2**, Supernatant before filtration; **3**, Supernatant after filtration; **4**, Crude pellet after induction; **5**, Flow-through; **6**, 5 mM imidazole wash fraction (5 ml); **7**, 60 mM imidazole wash fraction (5 ml) ; **8**, 1 M imidazole fraction (2ml); **9**, 1 M imidazole fraction (2 ml).

Figure 3.5 shows the results of such an experiment and a very pure preparation of *Pf*HGXPRT was achieved (lane 8 and 9, and these two pooled fractions, lane 10). The final pooled 4 ml had a protein concentration of 1.5 mg/ml (6 mg yield from 1 L culture).

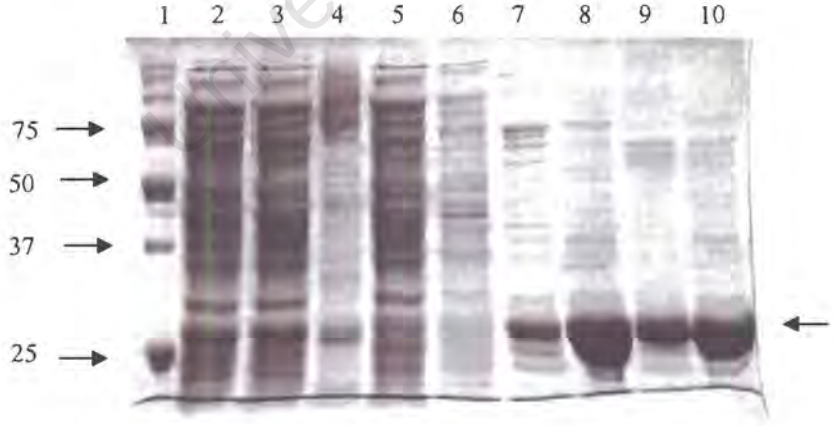

Figure 3.5. Purification of his-tagged *Pf*HGXPRT using nickel-affinity chromatography and larger wash volume. 1 L culture. **1**, Molecular weight markers (kDa); **2**, Supernatant before filtration; **3**, Supernatant after filtration; **4**, Crude pellet after induction; **5**, Flow-through; **6**, 5 mM imidazole wash (10 ml); **7**, 30 mM imidazole wash (10 ml); **8**, 1 M imidazole (2ml); **9**, further 1 M imidazole (2ml); **10**, combined 1 M imidazole fractions (4 ml).

3.1.3 Activation of his-tagged *Pf*HGXPRT

Previous work had found that *Pf*HGXPRT, expressed with a his-tag, was inactive as isolated, but could be activated by incubation with partial substrates (i.e. hypoxanthine + PRPP without Mg^{2+} or MgPRPP alone, conditions which do not result in enzyme turnover) (Phehane, 2002). However we had difficulty in reproducing this and found no measurable activity after several purification experiments. In an effort to obtain active enzyme, and thinking that the high imidazole and salt concentrations may be detrimental, the protein was first dialysed against 25 mM Tris-Cl, pH 8.0, 1 mM DTT and 1 mM PMSF. Unfortunately, the protein precipitated after a ~16 h dialysis. We then tried to change the medium faster by using two PD-10 desalting columns immediately after purification. For this experiment we used the preparation shown in figure 3.5, and the final 4 ml was divided into two portions of 2 ml, and each made up to 2.5 ml (required for optimal PD-10 usage). The PD-10 columns were equilibrated with 25 mM Tris-Cl, pH 8.0, 1 mM DTT and 1 mM PMSF. The flow-throughs were collected and the protein of interest eluted in the same buffer (figure 3.6).

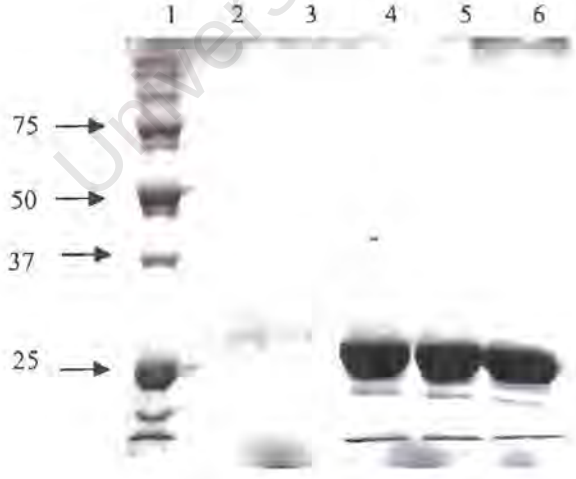

Figure 3.6. Changing buffer medium using PD-10 columns (containing Sephadex™ G-25 resin). **1**, Molecular weight markers (kDa); **2**, Flow-through (column 1); **3**, Flow-through (column 2); **4**, Eluate (column 1); **5**, Eluate (column 2); **6**, Combined eluates (volume 7 ml).

The desalted preparation was then subjected to activation by overnight incubation with MgPRPP, and analysed for activity by our standard procedure (adapted from Keough *et al* (1999)) and found specific activity of 2.86 μmol GMP/min/mg. Other preparations yielded activities of between 2 and 3 μmol GMP/min/mg. These activities were very encouraging and close to the levels obtained by Keough *et al* (1999), and our laboratory previously (Phehane, 2002).

Unfortunately, freezing the enzyme preparations and subsequent thawing always caused the protein to precipitate. We also discovered that even the freshly prepared enzyme without freezing failed to elute from a HPLC gel filtration column (which we wanted to use for separating the quarternary forms of the enzyme). Finally, we found that the his-tagged protein was exceptionally well photolabeled by our photoprobe, TNP-8N_3-ATP, and suspected that this was because the histidines were being labelled. We were thus forced to abandon the his-tagged protein and to consider expressing and purifying the non-his tagged form.

3.2 Expression, Purification and Activation of *Pf*HGXPRT without a his-tag

3.2.1 Expression and Purification of *Pf*HGXPRT from pET17b

Cultures of *E. coli* (1 L) transformed with non his-tagged *Pf*HGXPRT (from glycerol stocks made previously) were induced with IPTG and analysed by SDS-PAGE (figure 3.7). A very large band of induced protein was evident.

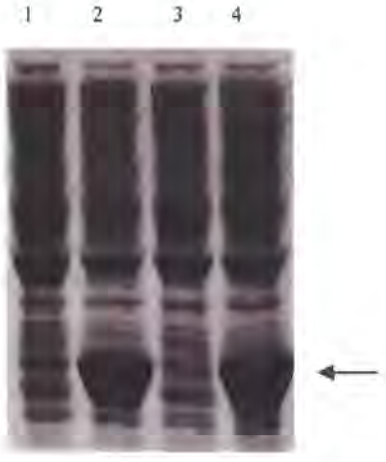

Figure 3.7. Induction of non his-tagged *Pf*HGXPRT. Two cultures of transformed *E. coli* were grown at 37°C overnight and then aliquots were taken before (lanes 1 and 3) and after (lanes 2 and 4) induction with 0.4 mM IPTG and the samples analysed by SDS-PAGE. The right hand arrow indicates the position of *Pf*HGXPRT.

The cells were pelleted, resuspended to 100 ml and lysed. The lysate was then subjected to centrifugation of 21 000 rpm for 20 min, and the pellet resuspended to the same volume as the supernatant. The composition of the supernatant and pellet is shown in figure 3.8 (lanes 2 and 3). Most of the protein of interest appeared in the pellet. The supernatant was processed further according to a purification protocol developed in our laboratory (Mbewe *et al*, 2007), which consisted of tandem columns of anion exchange resin and Reactive Red-120. Under the conditions used, *Pf*HGXPRT does not bind to the anion exchange resin, but most of the contaminating proteins do, and binds to the Reactive Red-120 resin. The material coming straight through both columns is shown in lane 4, and very little protein is evident. A wash of the Reactive Red-120 column alone is shown in lane 5, and a small amount *Pf*HGXPRT appears.

The majority of *Pf*HGXPRT was eluted with sodium pyrophosphate buffer as shown in figure 3.9. A number of contaminating proteins are evident, with some eluting earlier and others later, but it was difficult to select specific fractions with purer protein. It was decided to pool all the fractions to obtain a preparation that

was dialysed against 10 mM MOPS, pH 7.0, 1 mM DTT and 1 mM PMSF, to provide ~10 ml of 1.3 mg *Pf*HGXPRT/ml (yield 13 mg protein).

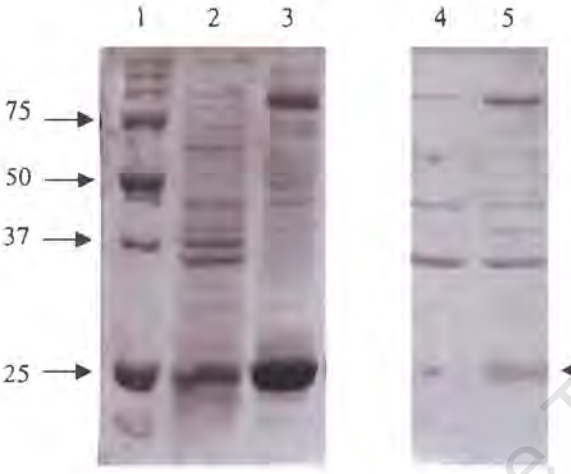

Figure 3.8. Purification of *Pf*HGXPRT using DE-52 anion-exchange and Reactive Red-120 affinity chromatography. 1, Molecular weight markers (kDa); **2**, Crude supernatant after induction (volume 100 ml) ; **3**, Crude pellet after induction (resuspended to the same volume as the supernatant); **4**, Reactive red-120 flow-through (100 ml); **5**, Reactive red-120 wash (5 ml, 200 mM NaCl, 50 mM Tris-Cl, pH 8.00) after separating the two columns. The right hand arrow indicates the position of *Pf*HGXPRT (~26 kDa). Equal volume aliquots were analysed by SDS-PAGE after solubilisation.

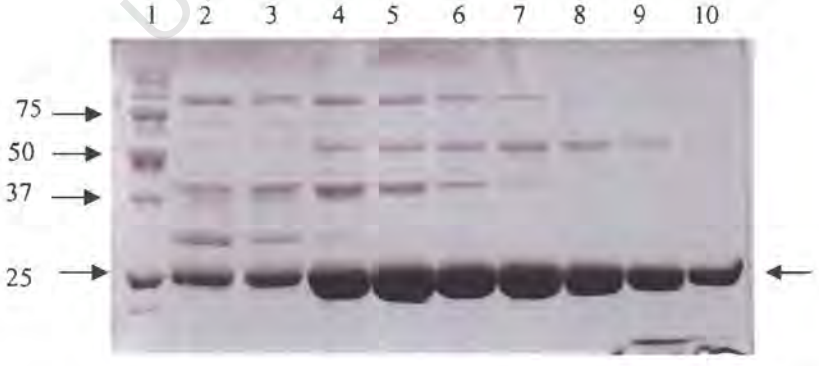

Figure 3.9. Purification of *Pf*HGXPRT continued: Reactive Red-120 elution profile.
1, Molecular weight markers (kDa); **2-10**, Fractions 1-9 (1 ml each, 50 mM NaPPi, 50 mM Tris-Cl, pH 8.9, 1 mM DTT, 1 mM PMSF). The arrow on the right indicates the position of the target protein (~26 kDa).

It was disappointing to see the amount of *Pf*HGXPRT in the crude pellet fraction (figure 3.8), most probably in inclusion bodies and, consequently, induction of protein expression was attempted at 25°C (figure 3.10). The result appeared much better with more *Pf*HGXPRT appearing in the supernatant fraction (compare lanes 2 and 3 in figures 3.8 and 3.10). The elution profile from Reactive Red-120 is shown in figure 3.11, and was very similar to that obtained before.

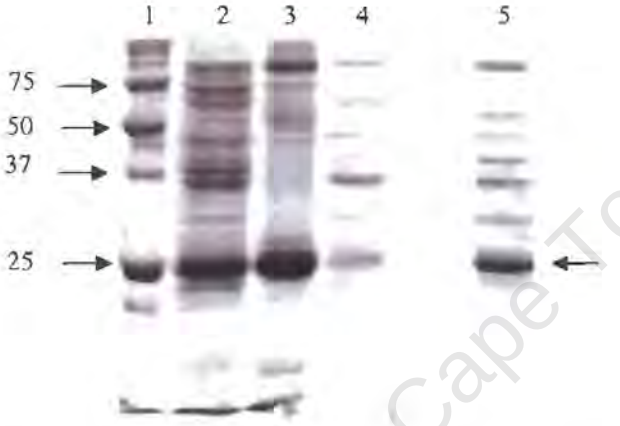

Figure 3.10. Purification of *Pf*HGXPRT after induction at 25°C using DE-52 anion-exchange and Reactive Red-120 affinity chromatography. **1**, Molecular weight markers (kDa); **2**, Crude supernatant after induction; **3**, Crude pellet after induction; **4**, Flow-through from both columns; **5**, Reactive red-120 wash (5ml, 200 mM NaCl, 50 mM Tris-Cl, pH 8.0). The arrow on the right indicates the position of *Pf*HGXPRT (~26 kDa). Equal volume aliquots were analysed by SDS-PAGE after solubilisation.

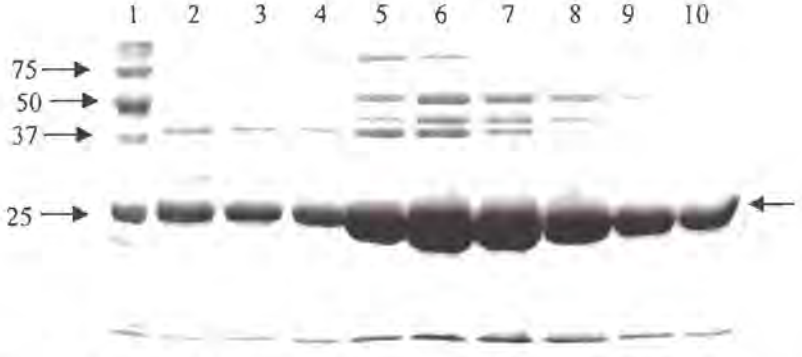

Figure 3.11. Purification of *Pf*HGXPRT continued: Reactive-Red 120 elution profile.
1, Molecular weight markers (kDa); **2-10**, Fractions 1-9 (1 ml each, 50 mM NaPPi, 50 mM Tris-Cl, pH 8.9, 1 mM DTT, 1 mM PMSF).

The 9 fractions from the Reactive Red-120 column were pooled and dialysed against 10 mM MOPS, pH 7.0, 1 mM DTT and 1 mM PMSF. The final yield of *Pf*HGXPRT was higher, ~10 ml of 1.6 mg protein/ml (total 16 mg), though a considerable amount of the enzyme was still lost in the crude pellet fraction.

The dialysate was then concentrated using an Amicon® ultrafiltration cell and the resulting preparation analysed by SDS-PAGE (figure 3.12). The protein concentration was 22.96 mg/ml. The concentrated protein was stored in 10 µl aliquots at -81°C for binding experiments using isothermal titration calorimetry.

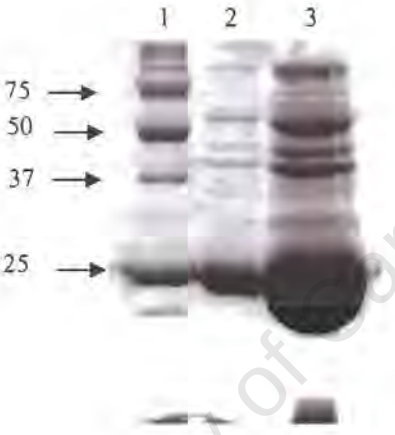

Figure 3.12. Effect of concentrating *Pf*HGXPRT using an Amicon® ultrafiltration cell. **1**, Molecular weight markers (kDa); **2**, *Pf*HGXPRT before concentrating; **3**, *Pf*HGXPRT after concentrating.

3.2.2 Activation of *Pf*HGXPRT expressed without a his-tag

The protein as isolated was inactive but has previously found to be capable of being made active by incubation with partial substrates. It was also found that it was essential to dialyse the non his-tagged protein overnight after Reactive Red-120 chromatography to remove the sodium pyrophosphate (Mbewe, 2005).

Following these procedures produced protein that exhibited activities of up to 2 µmol GMP/min/mg, which is similar to that obtained with the his-tagged enzyme.

3.3 Gel filtration chromatography

3.3.1 Calibration of TosoHaas TSKgel G3000SW column

HPLC gel filtration was used to investigate the oligomerisation of *Pf*HGXPRT under various conditions, but mainly exploring the salt dependence. The TosoHaas TSKgel G3000SW column was calibrated using the molecular weight standards shown in table 2 in a buffer containing 10 mM MOPS·TMAH, pH 7.0, and either 20, 100 or 400 mM NaCl. The separation profiles obtained are shown in figure 3.13.

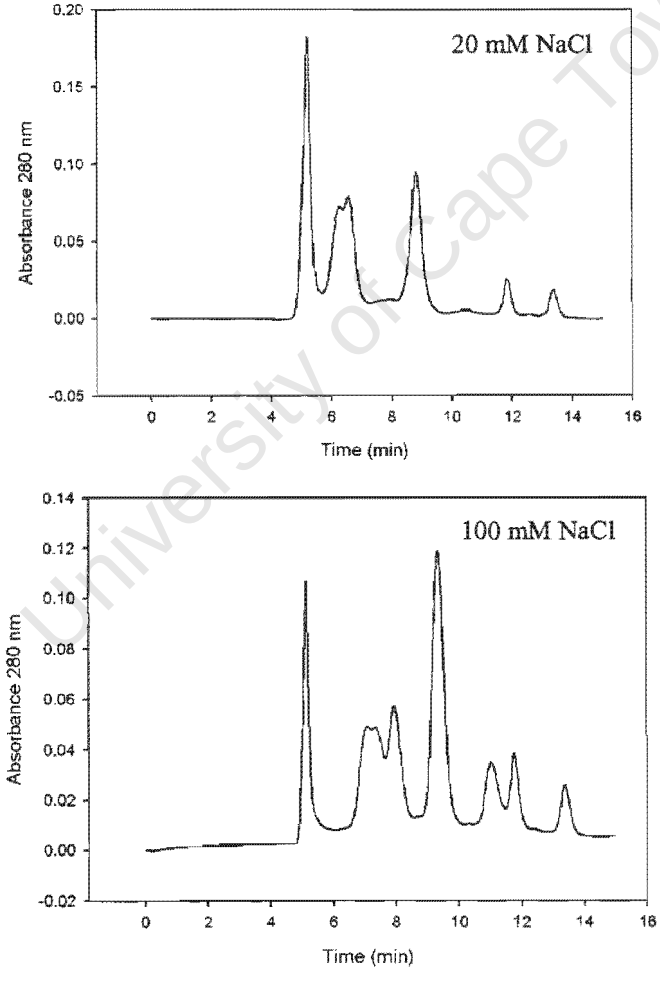

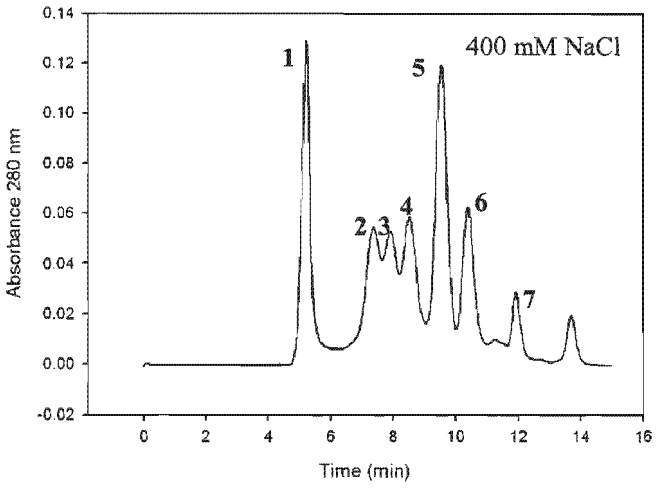

Figure 3.13. Calibration of TosoHaas TSKgel G3000SW gel filtration HPLC column: Profiles of standards at different NaCl concentrations. A mixture of standards was injected onto the column at time zero in 10 mM MOPS·TMAH, pH 7.0, containing 20 (top panel), 100 (middle panel) or 400 mM NaCl. The flow rate was 1 ml/min. Peaks: **1:** Dextran Blue (2×10^6 Da), **2:** Alcohol dehydrogenase (150 000 Da), **3:** Bovine serum albumin (67 000 Da), **4:** Ovalbumin (44 000 Da), **5:** Carbonic anhydrase (29 000 Da), **6:** Cytochrome c (11 700 Da), **7:** Tyrosine (185 Da)

It is apparent that the elution profile is highly sensitive to the ionic strength of the buffer, and some of the standard proteins must be interacting with the column resin. For example, the elution time of cytochrome c is very different at 100 and 400 mM NaCl, and completely fails to elute at 20 mM, and therefore must be binding to the resin at low salt. Ovalbumin (figure 3.13, 4) behaves in an opposite manner, at low salt it elutes earlier, apparently repelled by the resin.

The retention volumes (V_r) for molecular weight standards were calculated according to the equation in figure 2.3. The logarithm of the molecular mass of a standard protein was then plotted against its retention volume in the calibration curve shown in figure 3.14.

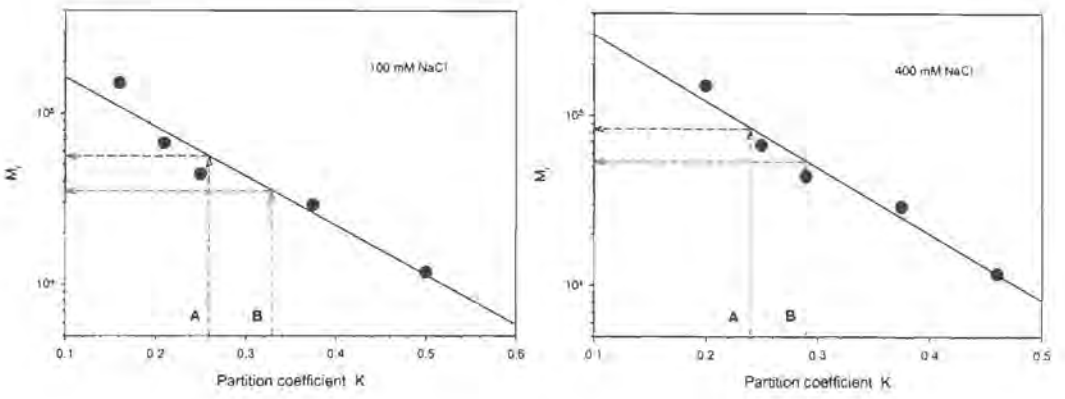

Figure 3.14 Calibration curves for Tosohaas TSKgel G3000SW gel filtration HPLC column. Standard proteins (see Table 2.1) were injected onto the column in 10 mM MOPS·TMAH, pH 7.0, containing either 100 mM (left panel) or 400 mM NaCl (right panel).

3.3.2 NaCl, $CaCl_2$, and $MgCl_2$ concentration dependence of the quarternary structure of *Pf*HGXPRT

The NaCl concentration dependence was determined by injecting aliquots of isolated *Pf*HGXPRT onto the column that had been equilibrated in 10 mM MOPS·TMAH, pH 7.0, containing 20, 50, 100 or 400 mM salt. The elution profiles are shown in figure 3.15. At each of the salt concentrations four peaks are evident. The first two are labelled A and B, and both are the enzyme of interest as proven by collecting the peaks and analysis by SDS-PAGE (not shown), whereas the two peaks eluting later were not *Pf*HGXPRT, and represent low molecular weight contaminants. The proportion of A and B is clearly salt concentration dependent, with a greater amount of the earlier eluting material (apparently higher molecular weight) at low salt and almost entirely the retarded (smaller) form at high salt (the concentration of NaCl for half maximal effect is approximately 50 mM). They are ascribed to different oligomeric forms of *Pf*HGXPRT, and the salt dependence of the equilibrium is compatible with known KCl concentration dependence (tetramer↔dimer equilibrium) described by Keough *et al* (1999), determined by sedimentation centrifugation measurements. According to the standard calibration curves at 100 mM NaCl and 400 mM NaCl (figure 3.14), we obtain apparent molecular weights of the two forms as 58 and 35 kDa, and 85 and

55 kDa at 100 and 400 mM NaCl for the tetramer and dimmer, respectively. At low salt (20 mM) the separation of standard proteins was incomplete and as the column manufacturers recommend a working concentration of 300 mM NaCl, we thought that 400 mM NaCl was more representative of an optimal separation profile. Also, the molecular weights obtained for the tetramer (85 kDa) and dimer (55 kDa) closer to the expected values for the two species.

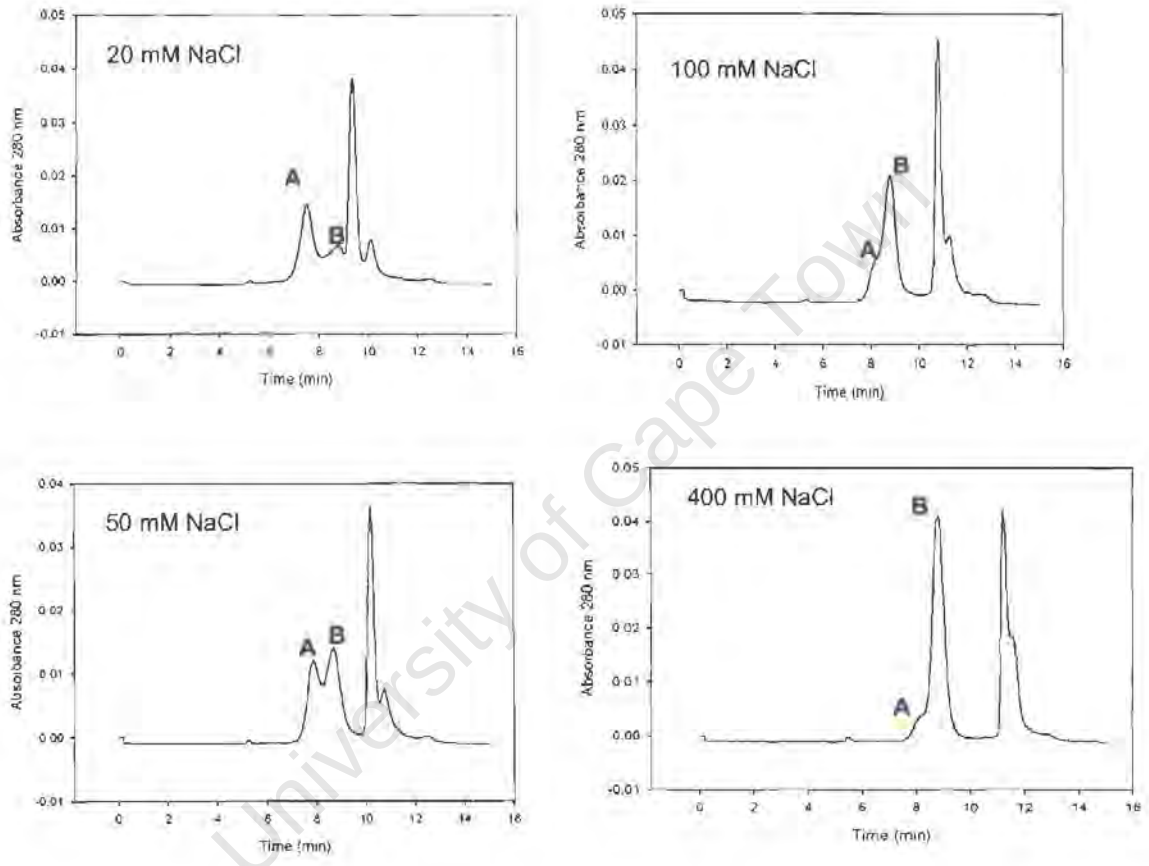

Figure 3.15. HPLC gel filtration elution profiles of *Pf*HGXPRT: NaCl dependence. Aliquots of protein (30µl, 1.3 mg/ml protein) were injected onto a TosoHaas TSKgel G3000SW column at time zero with running buffer of 10 mM MOPS·TMAH, pH 7.0, and the concentrations of NaCl shown. **A** and **B** identify two putative quarternary forms of *Pf*HGXPRT.

The elution profiles obtained for analysis of the $CaCl_2$ concentration dependence are shown in figure 3.16. Again, increasing concentrations of $CaCl_2$ shifted the

equilibrium towards B – the apparently lower molecular weight form - with a half maximal effect at approximately 1 mM.

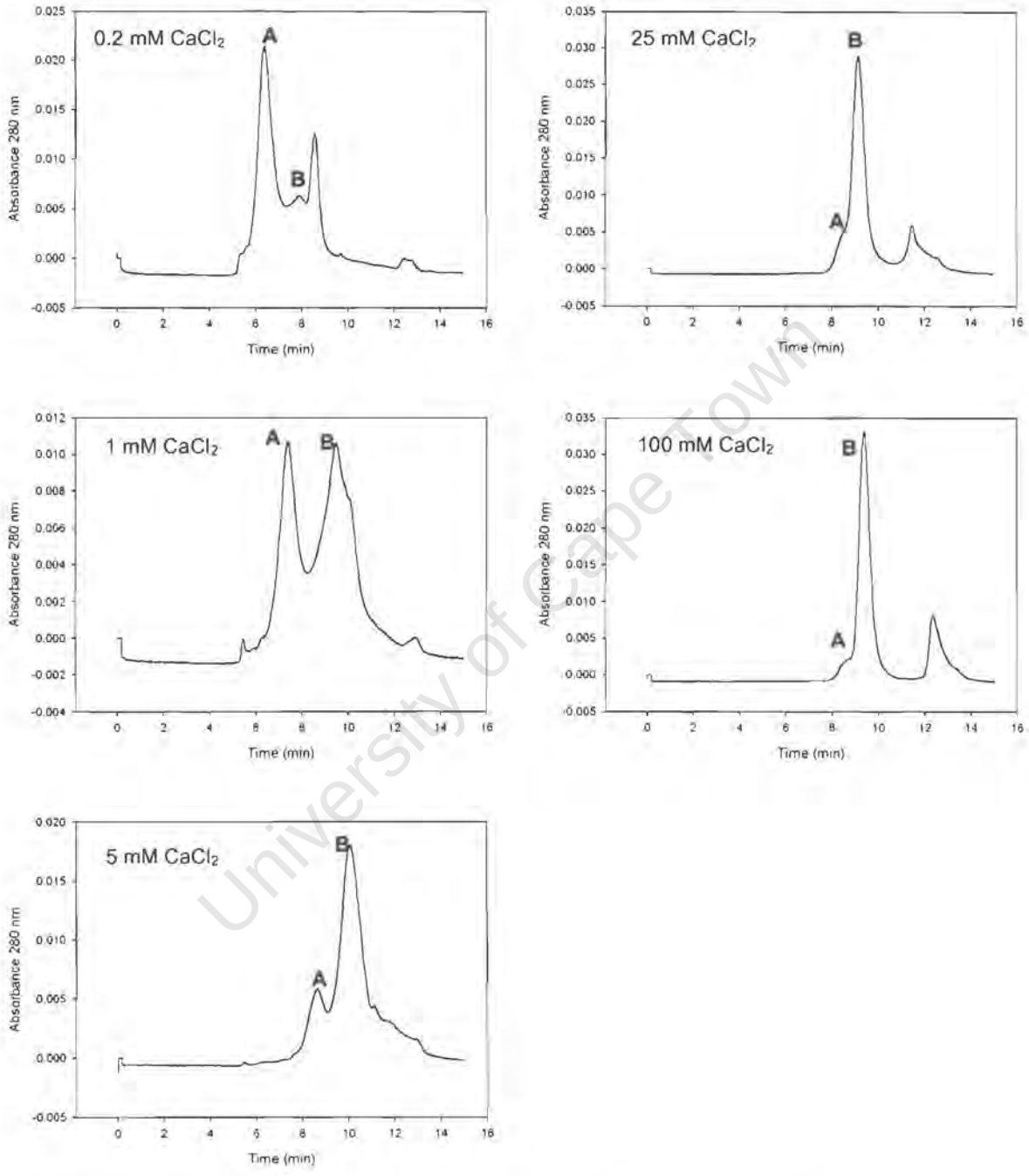

Figure 3.16. HPLC gel filtration elution profiles of *Pf*HGXPRT: $CaCl_2$ concentration dependence. Aliquots of isolated protein (30 µl, 1.3 mg/ml) were injected onto a TosoHaas TSKgel G3000SW column at time zero in 10 mM MOPS·TMAH, pH 7.0, containing the concentrations of $CaCl_2$ shown. **A** and **B** identify two putative quarternary forms of *Pf*HGXPRT.

The $MgCl_2$ concentration dependence was determined similarly and is shown in figure 3.17, and is almost identical to that found for $CaCl_2$.

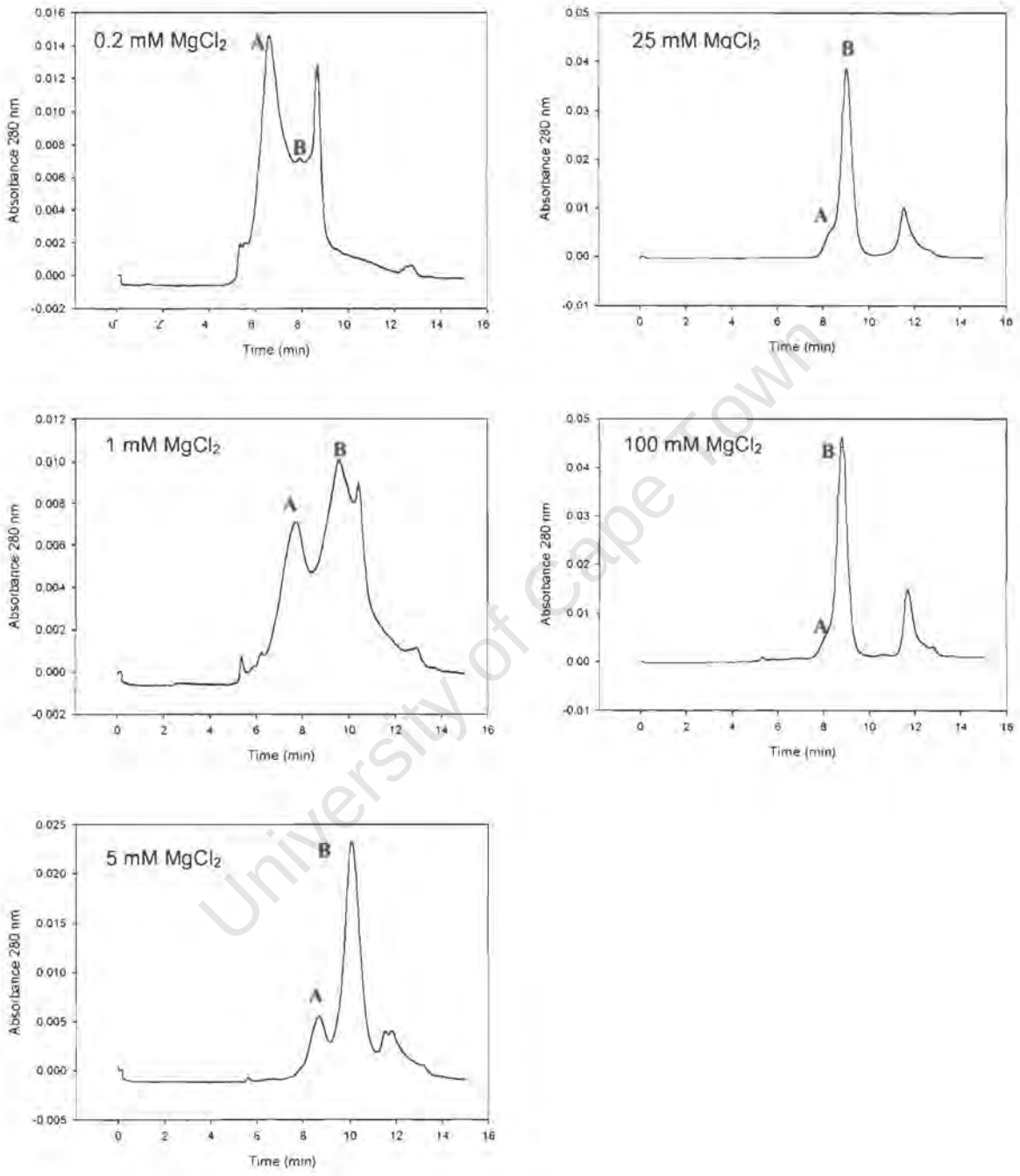

Figure 3.17. HPLC gel filtration elution profiles of *Pf*HGXPRT: $MgCl_2$ concentration dependence. Aliquots of isolated protein (30 µl, 1.3 mg/ml) were injected onto a TosoHaas TSKgel G3000SW column at time zero in 10 mM MOPS·TMAH, pH 7.0, containg the concentrations of $MgCl_2$ shown. **A** and **B** identify two putative quarternary forms of *Pf*HGXPRT.

3.3.3 Preincubation of *Pf*HGXPRT in 1 M NaCl

The above suggest that incubation at high salt converts *Pf*HGXPRT into the later eluting (smaller) form. The effect of preincubation of *Pf*HGXPRT in 1 M NaCl was determined by incubating the protein at room temperature for either 1 or 20 min, and aliquots of the protein then injected onto the column in running buffer containing low salt (20 mM NaCl), and the results are shown in figure 3.18 (note difference in y-scale). It is evident that preincubation at high salt concentration had very little effect on the elution profile, which must mean that the rate of interconversion of the two forms in the equilibrium is very rapid.

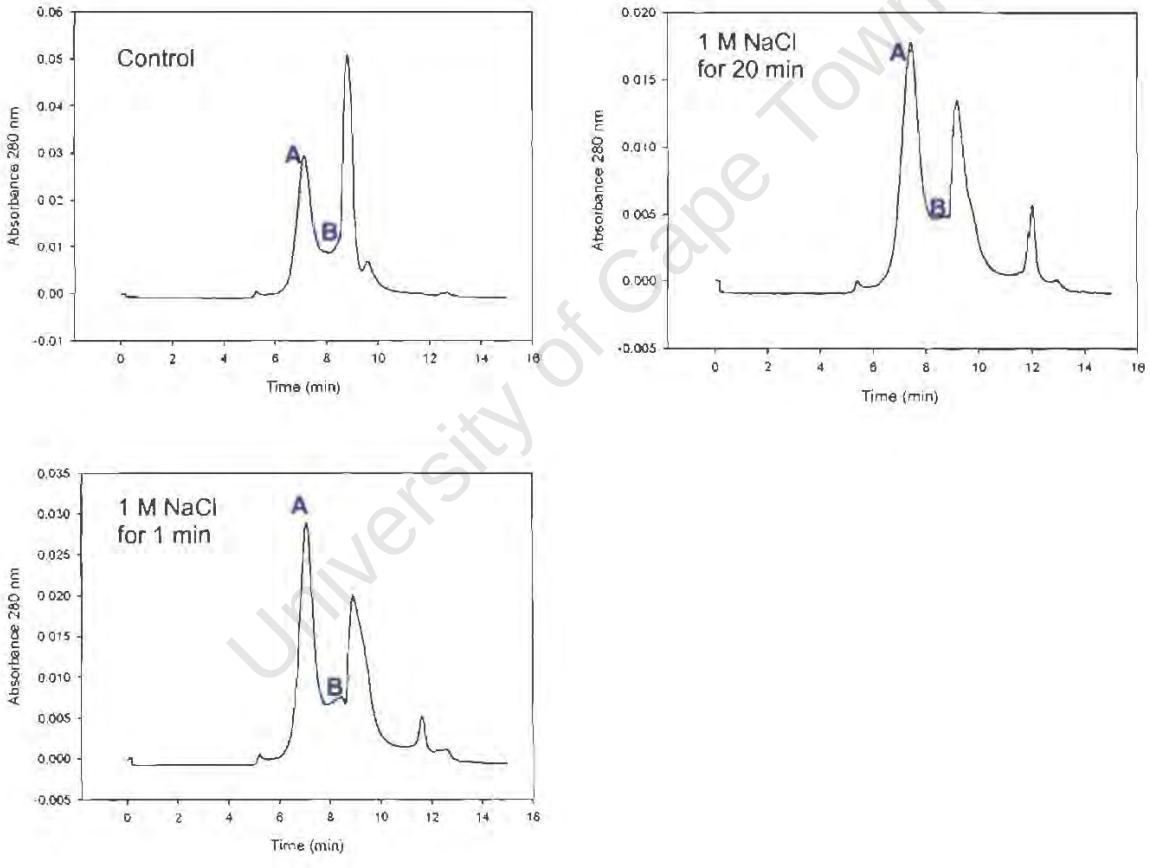

Figure 3.18. HPLC gel filtration elution profiles of *Pf*HGXPRT: Effect of preincubation in 1 M NaCl. Aliquots of isolated protein (30 µl, 1.3 mg/ml, preincubated at room temperature for the times indicated) were injected onto a TosoHaas TSKgel G3000SW column at time zero in 10 mM MOPS·TMAH, pH 7.0, containing 20 mM NaCl. **A** identifies the putative higher molecular weight quarternary form of *Pf*HGXPRT and **B** marks the position when the other smaller form is expected to elute.

3.3.4 *Pf*HGXPRT dilution

The equilibrium between association and dissociation of subunits of an oligomeric protein is necessarily protein concentration dependent. The effect of a 10-fold dilution of *Pf*HGXPRT on the equilibrium is shown in figure 3.19. In these experiments, the oligomeric status was determined initially at low salt (20 mM NaCl) and the undiluted sample showed the expected predominance of the earlier (larger) form. Dilution appeared to have no effect. Further dilutions were beyond the limit of detection by the HPLC. We also checked to see if the salt dependence had been altered by the protein dilution, and the diluted protein was run in 50 mM NaCl. As can be seen in figure 3.19 (right hand side), approximately equal amounts of each form was obtained similar to what had been found before in the NaCl concentration dependence experiments with undiluted protein (see figure 3.15). Because we were at the limits of detection, the experiment was repeated where a larger aliquot was injected, but with a similar result (figure 3.19, lower right hand side). We conclude that the association between subunits is very tight.

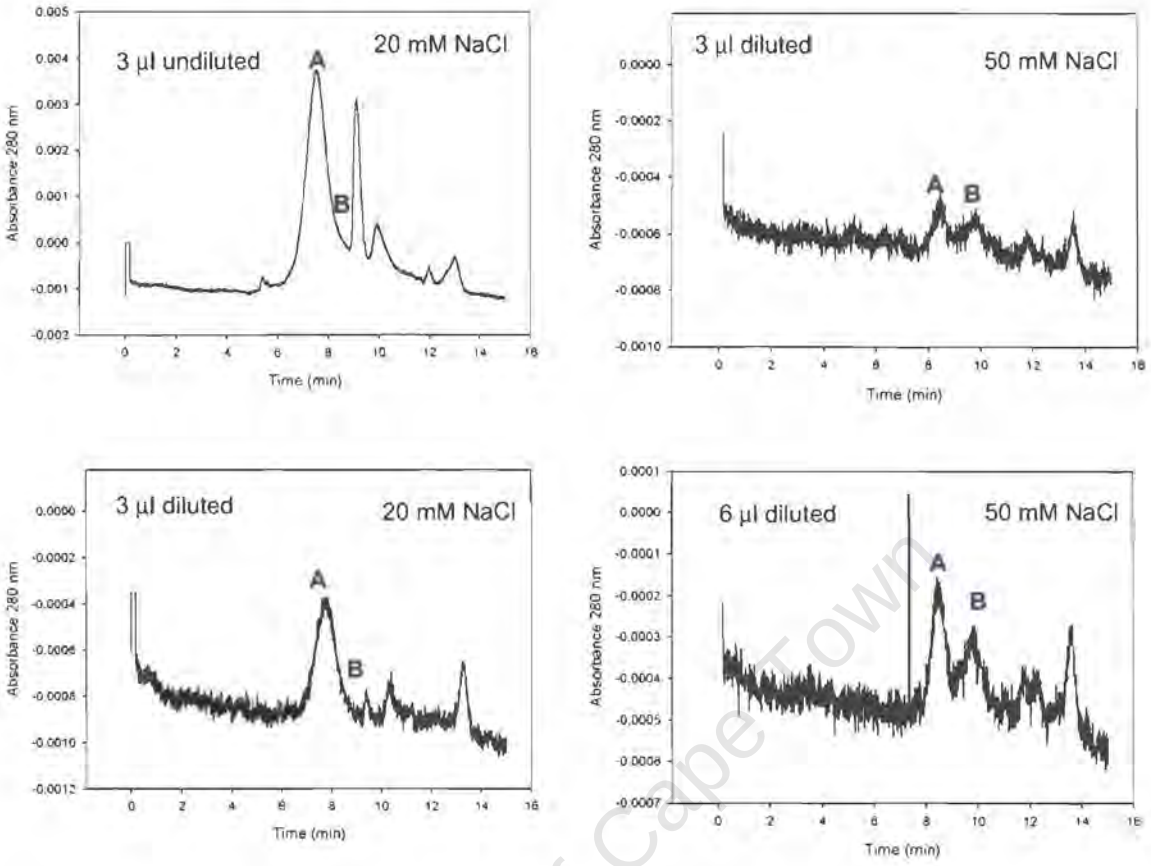

Figure 3.19. HPLC gel filtration elution profiles of *Pf*HGXPRT: Effect of protein dilution. Aliquots of protein (3 or 6 µl, 1.3 or 0.13 mg/ml, i.e. undiluted or diluted with running buffer) were injected onto a TosoHaas TSKgel G3000SW column at time zero with running buffer of 10 mM MOPS·TMAH, pH 7.0, containing either 20 or 50 mM NaCl as indicated. A identifies the putative higher molecular weight quarternary form of *Pf*HGXPRT and B marks either the smaller form or the position where it is expected to elute.

3.3.5 NaCl concentration dependence of activated *Pf*HGXPRT

For analysis of the effect of activation of the protein on its oligomerisation, *Pf*HGXPRT was activated by overnight incubation with 60 µM hypoxanthine and 1 mM PRPP at 0°C. Aliquots of the activated enzyme were then injected onto the column in running buffer containing 20, 100 or 400 mM NaCl. Elution profiles are shown in figure 3.20. Essentially no difference was found between isolated and activated *Pf*HGXPRT (compare the profiles obtained here with those in figure 3.15).

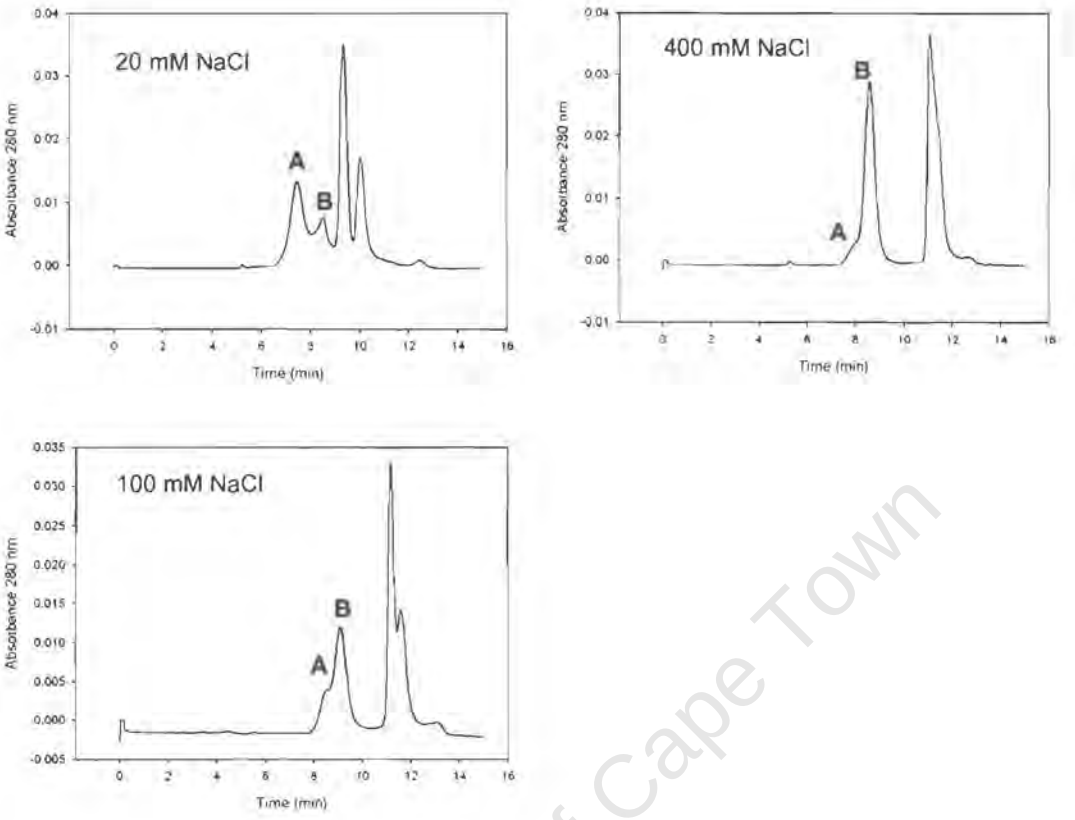

Figure 3.20. HPLC gel filtration elution profiles of activated *Pf*HGXPRT: NaCl concentration dependence. Aliquots of protein (30 µl, 1.3 mg/ml, activated by overnight incubation at 0°C with 60 µM hypoxanthine and 1 mM PRPP) were injected onto a TosoHaas TSKgel G3000SW column at time zero with running buffer of 10 mM MOPS·TMAH, pH 7.0, containing the concentrations of NaCl shown. **A** and **B** identify two putative quarternary forms of *Pf*HGXPRT.

3.4 Photolabelling

A model binding reaction, the photolabelling of sarcoplasmic reticulum Ca^{2+}-ATPase with [γ-^{32}P]TNP-8N_3-ATP, was performed to demonstrate the usefulness of this technique in studying proteins with nucleotide-binding sites. The effect of mutagenesis of specific SR Ca^{2+}-ATPase amino acid residues on ATP binding has been studied extensively in our laboratory (Seebregts and McIntosh, 1989; McIntosh *et al*, 1996) using photolabelling with the N_3-nucleotide. In such experiments, the concentration dependence of labelling of the Ca^{2+}-ATPase is first performed with [γ-^{32}P]TNP-8N_3-ATP and subsequently the ATP concentration dependence of inhibition at a fixed photoprobe concentration is performed. The results we obtained in a medium containing EDTA at pH 8.5 are shown in figure 3.21 and 3.22). Increasing the concentration of [γ-^{32}P]TNP-8N_3-ATP increased the extent of derivatisation in the range 0-2 μM and thereafter it reached a maximum (panel A). A fit of the data yielded a $K_{0.5(TNP)}$ = 0.16 μM, indicating very tight binding. The extent of derivatisation reached 0.04 mol probe/ mol Ca^{2+}-ATPase.

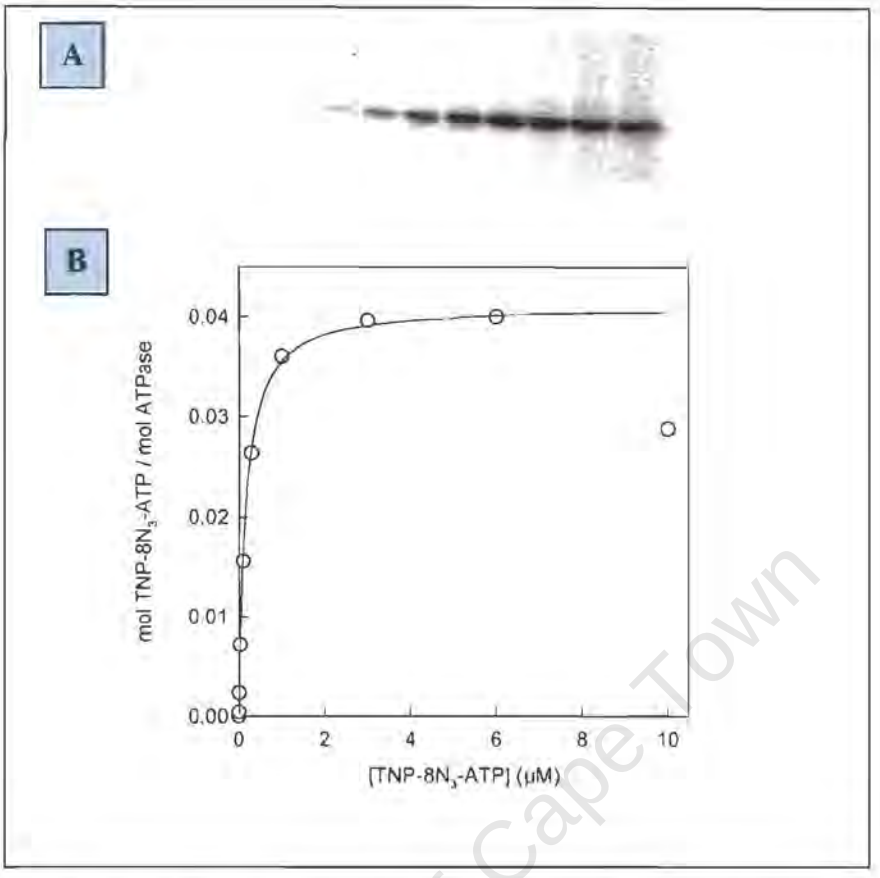

Figure 3.21. [γ-^{32}P]TNP-8N$_3$-ATP concentration dependence of photolabelling of Ca^{2+}-ATPase in SR vesicles. A: Autoradiographs following SDS-PAGE. Photolabelling was performed in 25 mM EPPS·TMAH, pH 8.5, 2 mM EDTA, 20% (v/v) glycerol, 0.002 mg/ml SR and the concentrations of [γ-^{32}P]TNP-8N$_3$-ATP indicated here: **1**, 0.001 μM; **2**, 0.003 μM; **3**, 0.01 μM; **4**, 0.03 μM; **5**, 0.1 μM; **6**, 0.3 μM; **7**, 1 μM; **8**, 3 μM; **9**, 6 μM; **10**, 10 μM.
B: Quantification. The [γ-^{32}P]TNP-8N$_3$-ATP concentration dependence data were fitted using Eq. 2.1, without a linear component. The data point at 10 μM was not included in the fit. Maximum labelling = 0.04 mol/mol; $K_{0.5(TNP)}$ = 0.16 μM.

The concentration dependence of ATP inhibition at 0.3 μM [γ-^{32}P]TNP-8N$_3$-ATP showed that complete inhibition is achieved in the millimolar range, and a fit of the data produced $K_{0.5(ATP)}$ = 57 μM. The true $K_{d(ATP)}$ was derived using eq. 2.3 (Methods section) and produced 20 μM, which is almost identical to that obtained previously with wild type rabbit Ca^{2+}-ATPase produced in COS-1 cells under the same conditions (18 μM, McIntosh *et al*, 1999).

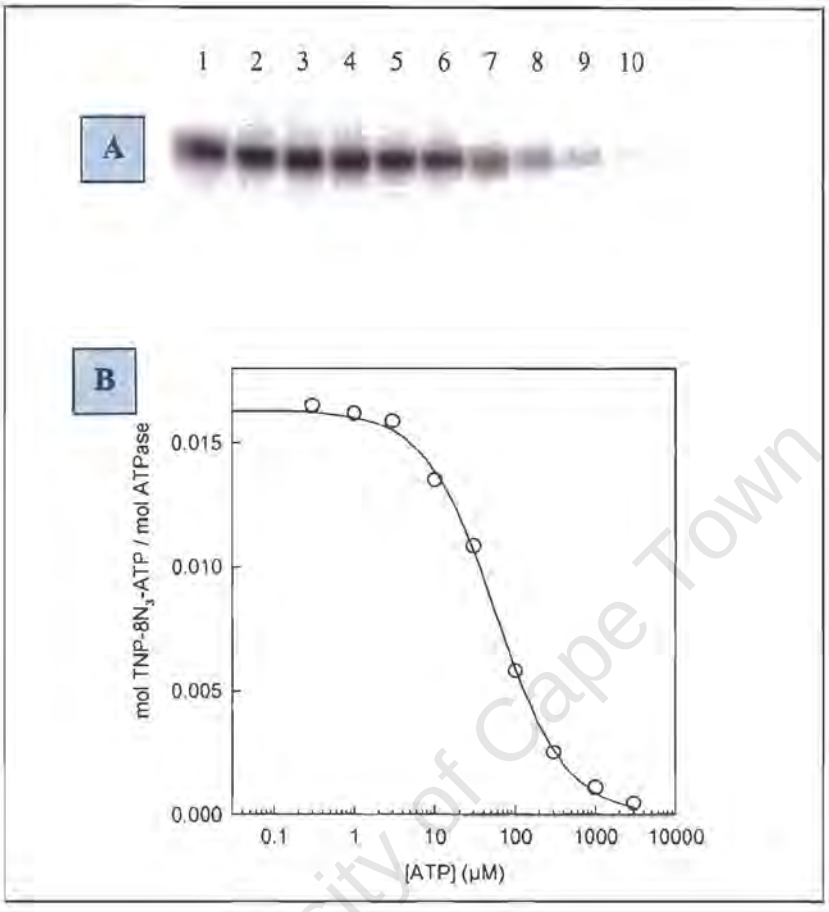

Figure 3.22. ATP inhibition of photolabelling of Ca^{2+}-ATPase in SR vesicles. A: Autoradiographs following SDS-PAGE. Photolabelling was performed in 25 mM EPPS·TMAH, pH 8.5, containing 2 mM EDTA, 20% v/v glycerol, 0.002mg/ml SR, 0.3 μM [γ-^{32}P]TNP-8N_3-ATP, and the concentrations of ATP indicated here: **1**, 0 μM; **2**, 0.3 μM;**3**, 1 μM ;**4**, 3 μM ;**5**, 10 μM ; **6**, 30 μM ; **7**, 100 μM; **8**, 300 μM; **9**, 1000 μM; **10**, 3000 μM. **B: Quantification.** ATP inhibition data were fitted using Eq. 2.2. $K_{0.5(ATP)}$ = 57 μM.

We then attempted to ascertain whether *Pf*HGXPRT could be photolabelled by [γ-^{32}P]TNP-8N_3-ATP and whether it could be used as a probe of the active site, specifically with the view of using it to determine whether 4′-iodo-chalcone bound at the active site or elsewhere.

In preliminary experiments, the pH dependence of the reaction of isolated and active *Pf*HGXPRT with [γ-^{32}P]TNP-8N_3-ATP was examined at pH 6.0, 7.0 and 8.0 in EDTA (A) , $CaCl_2$ (B) and $MgCl_2$ (C) (figure 3.23). The protein was derivatised under all conditions, but differences in the extent of photolabelling and in the concentration dependences were apparent. For example, focusing on the EDTA results (A), the affinity for the photoprobe seems higher at pH 6.0 for the isolated protein, whereas there appears to be a higher affinity at pH 8.0 in the case of active enzyme. There is no dramatic difference between the different divalent cation conditions (between A, B and C), but perhaps the labelling is a bit better in EDTA.

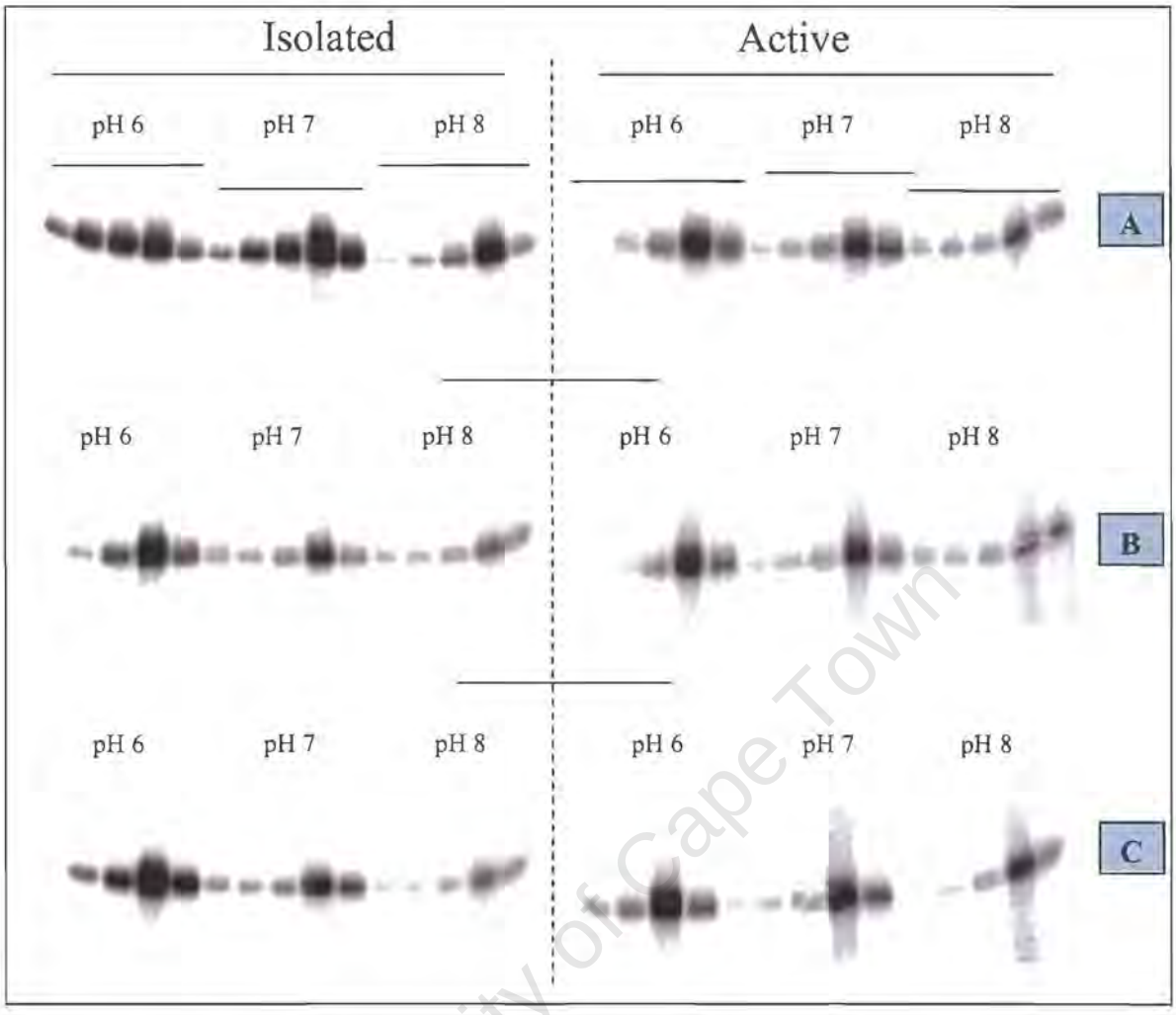

Figure 3.23. Autoradiographs of the pH dependence of photolabelling of isolated (left panel) **and active** (right panel) ***Pf*HGXPRT with [γ-^{32}P]TNP-8N$_3$-ATP at pH 6.0 (25 mM MES·TMAH), 7.0 (25 mM MOPS·TMAH), and 8.0 (EPPS·TMAH) and effect of 4′-iodo-chalcone. A:** In addition to the buffers, the photolabelling medium contained 2 mM EDTA, 20% v/v glycerol, 0.01 mg/ml *Pf*HGXPRT, and either 0.3, 1.0, 3.0, and 30 μM [γ-^{32}P]TNP-8N$_3$-ATP. In the case of the 5th lane at each pH the nucleotide concentration was 3 μM with 10μM chalcone. In **B** and **C,** 1 mM $MgCl_2$ or $CaCl_2$ replaced the EDTA, respectively.

The effect of including 10 μM 4′-iodo-chalcone on the photolabelling at 3 μM [γ-^{32}P]TNP-8N$_3$-ATP is also shown for each of the conditions, and in general, the chalcone had no effect or enhanced labelling. The one exception was with isolated enzyme in EDTA at pH 6.0 where the labelling was less. Overall it appeared that the chalcone did not compete with the photoprobe.

Photolabelling was examined in more detail in EDTA at pH 6.0 (figure 3.24) and pH 8.0 (figure 3.25). An extended concentration dependence revealed that photolabelling of the isolated protein at both pHs resolved into two components, a specific tight phase and a nonspecific linear phase, whereas with the active protein the data was best fitted to a simple single component hyperbolic equation. Thus it appears that there was tighter binding (1.24 and 1.12 μM at pH 6.0 and 8.0 respectively, compared with 12.4 and 6.05 μM at pH 6.0 and 8.0 respectively) to the isolated protein compared with the active species but more nonspecific labelling (linear component) in the former compared with the active form.

The effect of including 1 mM PRPP was examined at 3 μM [γ-^{32}P]TNP-8N_3-ATP, and only at pH 8.0 using the active enzyme did it appear that the photolabelling was less (40% less, compare lanes 6 and 12 right hand side, figure 3.25).

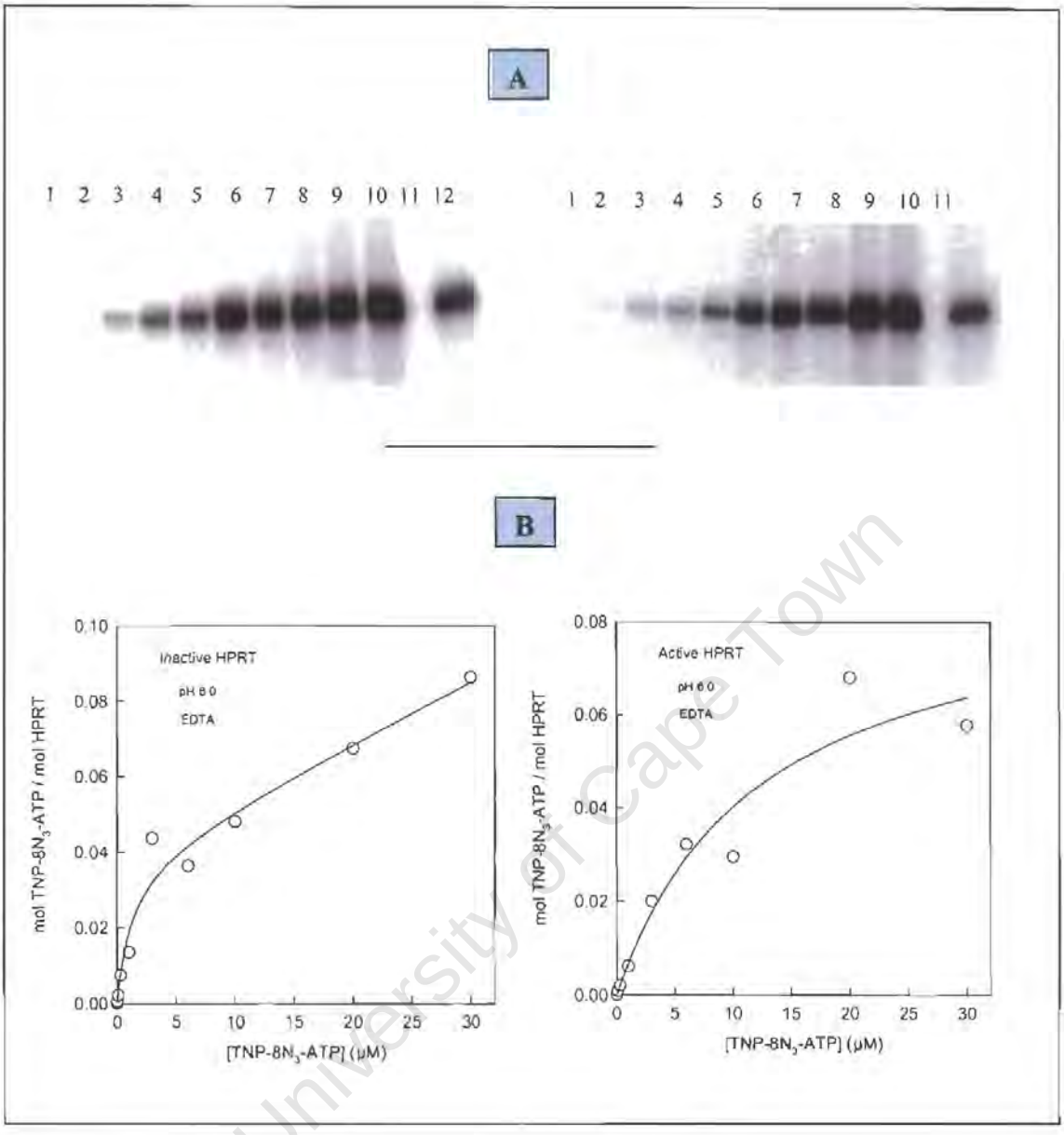

Figure 3.24. Concentration dependence of photolabelling of *Pf*HGXPRT with [γ-^{32}P]TNP-8N$_3$-ATP at pH 6.0 and effect of PRPP. A: Autoradiographs after SDS-PAGE. Photolabelling of isolated (left) and active (right) *Pf*HGXPRT was performed in 25 mM MES·TMAH, pH 6.0, containing 2 mM EDTA, 20% v/v glycerol, 0.01 mg/ml *Pf*HGXPRT, and 0.01 to 30 μM of the photolabel as indicated here: **1**, 0.01 μM; **2**, 0.03 μM; **3**, 0.1μM; **4**, 0.3 μM; **5**,1 μM; **6**, 3 μM; **7**, 6 μM; **8**, 10 μM; **9**, 20 μM; **10**, 30μM; **11**, EMPTY ; **12**, 3 μM + 1 mM PRPP. **B: Quantification.** Concentration data were fitted using Eq. 3.1 (with linear component for isolated *Pf*HGXPRT) to yield the $K_{0.5(TNP\text{-}8N3\text{-}ATP)}$ = 1.24 and 12.24 μM with isolated and active *Pf*HGXPRT respectively and 0.038 and 0.09 mol/mol for isolated and active *Pf*HGXPRT respectively.

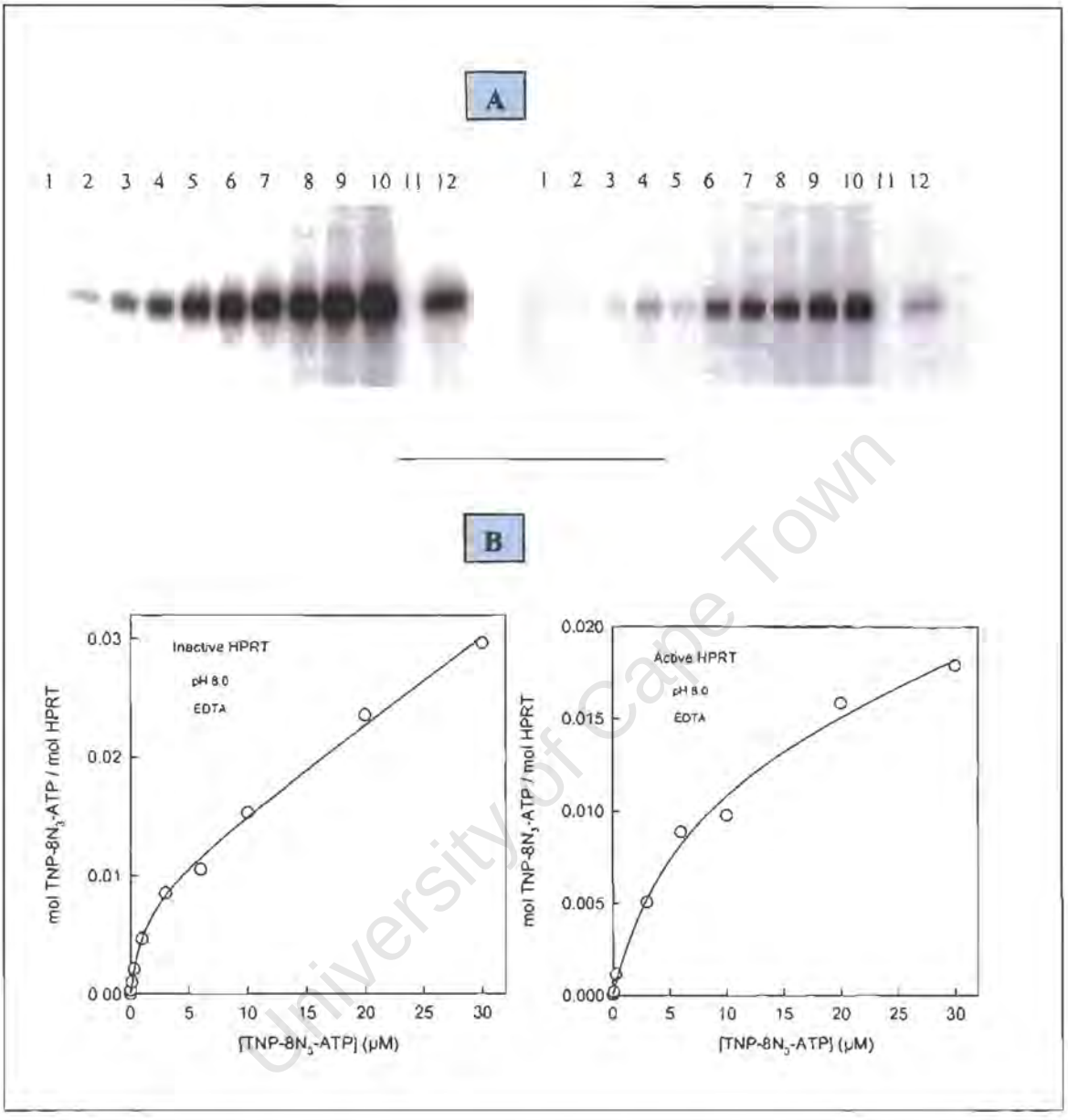

Figure 3.25. Concentration dependence of photolabelling of *Pf*HGXPRT with [γ-^{32}P]TNP-8N$_3$-ATP at pH 8.0 and effect of PRPP. A: Autoradiographs after SDS-PAGE. Photolabelling of isolated (left) and active (right) *Pf*HGXPRT was performed in 25 mM EPPS·TMAH, pH 8.0, containing 2 mM EDTA, 20% v/v glycerol, 0.01 mg/ml *Pf*HGXPRT, and 0.01 to 30 μM of the photolabel as indicated here: **1**, 0.01 μM; **2**, 0.03 μM; **3**, 0.1μM; **4**, 0.3 μM; **5**,1 μM; **6**, 3 μM; **7**, 6 μM; **8**, 10 μM; **9**, 20 μM; **10**, 30μM; **11**, EMPTY ; **12**, 3 μM + 1 mM PRPP. **B: Quantification.** Concentration data were fitted using Eq. 3.1 (with linear component for isolated *Pf*HGXPRT) to yield the $K_{0.5(TNP\text{-}8N3\text{-}ATP)}$ = 1.12 and 6.05 μM with isolated and active *Pf*HGXPRT respectively and 0.008 and 0.014 mol/mol for isolated and active *Pf*HGXPRT respectively.

3.5 Isothermal Titration Calorimetry

We attempted to measure the binding of 4′-iodo-chalcone to *Pf*HGXPRT using ITC microcalorimetry. But first the instrument and our technique was checked using a model binding reaction.

The titration of EDTA with $CaCl_2$ was performed as the model experiment and the results are shown in figure 3.26. The thermodynamic parameters obtained are in the legend to the figure. The titration shows a classical exothermic reaction with the amounts of heat produced starting at large values, diminishing midway, and decreasing at the end on saturation. The K_a, n, ΔH, and ΔS are close to those provided by the manufacturers under these conditions, indicating that the instrument is performing optimally.

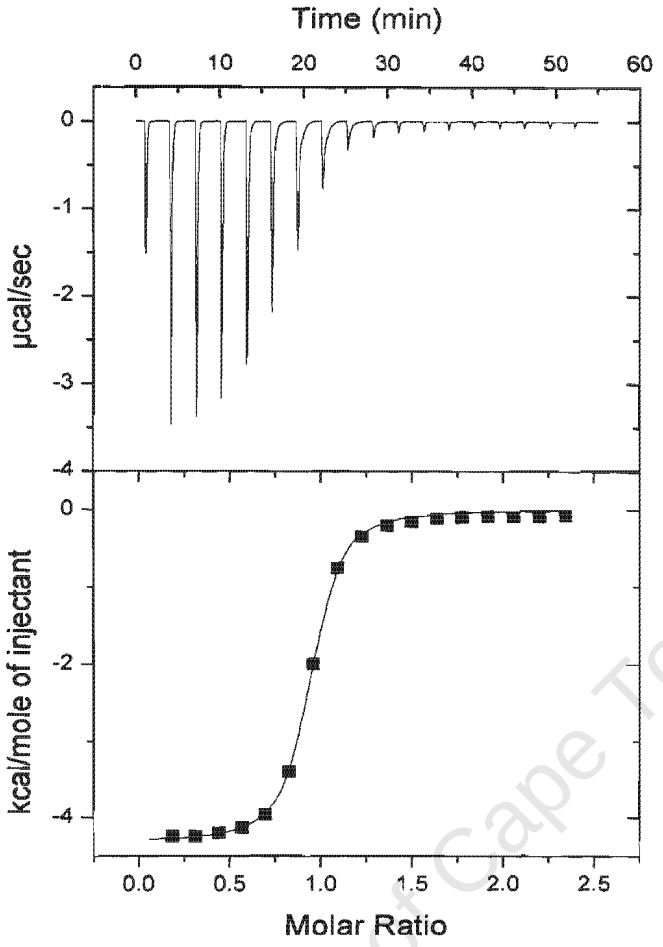

Figure 3.26. ITC data for titration of EDTA with $CaCl_2$: a model exothermic reaction. EDTA, 0.5 mM, in 10 mM MES·TMAH, pH 5.6 (cell) was titrated with 5 mM $CaCl_2$ in the same buffer (syringe). The first injection was 0.5 µl and the subsequent ones 2 µl. The heats produced (µcal/s) for each injection and concentrations of EDTA and $CaCl_2$ were used to calculate the kcal/mole of injectant and molar ratio, and from a fit of the data to Eq 3.3 (see Methods) for a one site binding model. The parameters obtained were: K_a= 3.42 x 10^5 +/- 2.80 x 10^4 M^{-1}, stoichiometry (n) = 0.891 +/- 0.00344, change in enthalpy (ΔH) = -4316 +/- 26.53 cal/mole and change in entropy (ΔS)= 10.8 cal.T^{-1} were calculated. Prior to analysis, heats of dilution were subtracted from the raw data.

It is well know that dilution of DMSO in water produces heat. Our ligand of interest, 4′-iodo-chalcone, needed to be solubilised in concentrated form in DMSO, and we initially considered that we would need to conduct the experiment in 10% DMSO. Since the 10% DMSO was present in both the cell and syringe we thought that the largest error in concentration between cell and syringe may be

in the region of 1%. For this reason, two titrations of 1% and 0.2% DMSO into water were performed and shown in figure 3.27, trace A and B respectively. At the higher concentration there was a slight decrease in amount of heat produced on each injection over the titration period due most probably to the volume of the solution in the cell increasing steadily. This was not so apparent with the 0.2% solution.

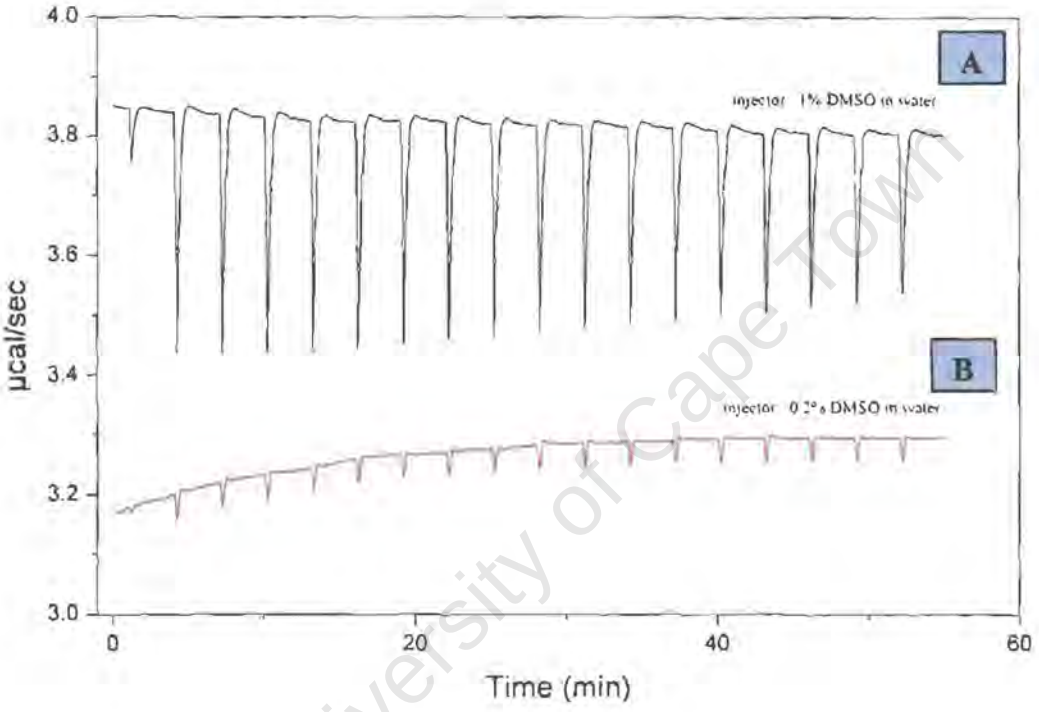

Figure 3.27. Heat effects on dilution of DMSO in water. A: 1% DMSO (in water) injected into degassed distilled water in the cell. **B:** 0.2% DMSO. An initial aliquot of 0.5 µl DMSO was injected, followed by 17 injections of 2 µl each.

In an effort to keep the chalcone in solution and to try to minimize the concentration of DMSO, the solubility of the chalcone in DMSO was investigated at pH 7.0, 8.0, and 9.0 at room temperature and the results obtained are shown in table 3.1. It is evident that the solubility increases at higher pH and that the highest concentration at which the chalcone is soluble at the intermediate pH of 8 is 250 µM. It was decided to use a pH of 8.2 and a concentration of 250 µM in

our experiments. pH 9 was considered rather high to perform the titration experiments.

Table 3.1. Solubility of 4′-iodo-chalcone at pH 7.0, 8.0, and 9.0. The chalcone at the concentrations shown was incubated in 10% DMSO and 100 mM $CaCl_2$ in either 20 mM MOPS·TMAH, pH 7.0, 20 mM EPPS·TMAH, pH 8.0 or CHES·TMAH, pH 9.0. The samples were incubated at 25 °C overnight and examined visually for solubility.

pH	[4′-iodo-chalcone]			
	50 µM	100 µM	250 µM	500 µM
7.0	ppt	yellow ppt	yellow ppt	yellow ppt
8.0	clear	clear	clear	yellow ppt
9.0	clear	clear	clear	clear

In the first protein binding experiment, isolated *Pf*HGXPRT was titrated with 4′-iodo-chalcone in the presence of 1 mM $CaCl_2$. The chalcone is a potent inhibitor of catalytic activity in 1 mM $CaCl_2$, but note that the protein has not been activated. The titration profile (figure 3.28) shows rather similar and small amounts of heat produced after each injection across the entire titration period. Control experiments showed rather analogous results, suggesting that no binding is taking place, no heat is produced during binding, or the protein concentration is too low.

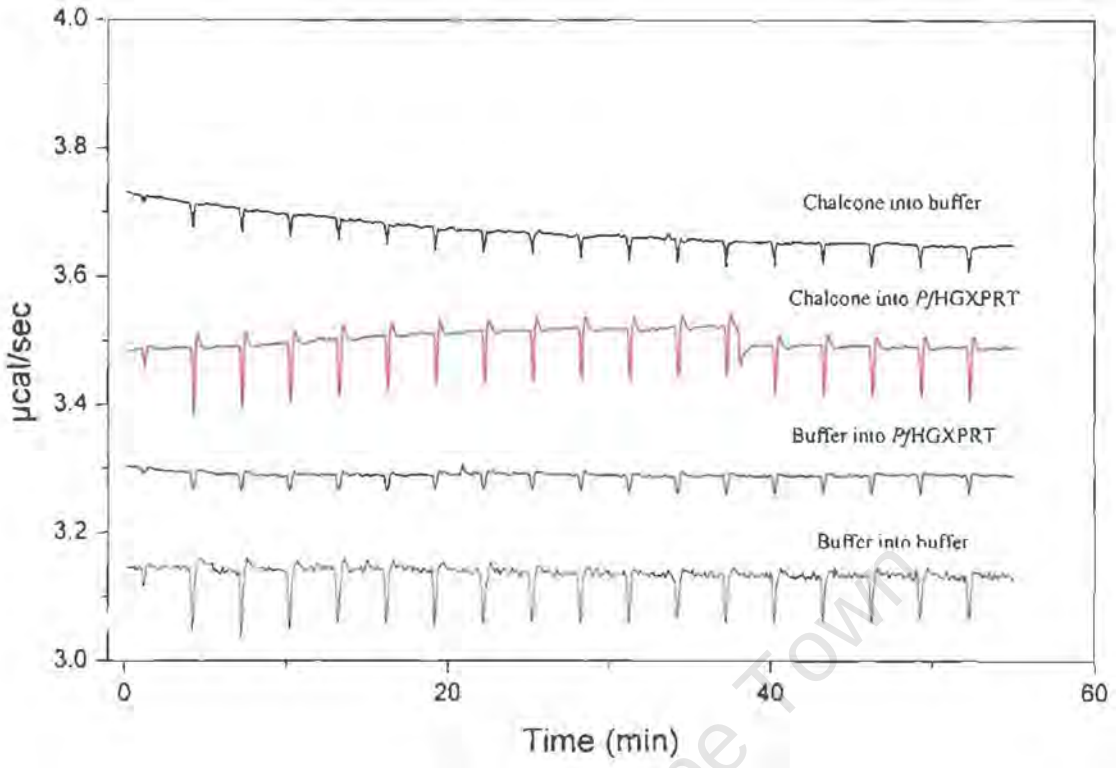

Figure 3.28. Titration of *Pf*HGXPRT with 4′-iodo-chalcone. Binding was studied with 6.0 µM (0 .15 mg/ml) *Pf*HGXPRT (in the cell) and 250 µM chalcone (syringe) and 10 mM EPPS·TMAH, pH 8.2, 1 mM $CaCl_2$ and 10% DMSO in both compartments. Controls were: chalcone into buffer, buffer into *Pf*HGXPRT, and buffer into buffer as indicated. The chalcone was added to DMSO before any of the other constituents as the chalcone precipitates otherwise.

In the next experiment the protein concentration was increased 3-fold and 6-fold, the enzyme activated by prior incubation with 60 µM hypoxanthine and 1 mM PRPP, and the $CaCl_2$ omitted. This necessitated the inclusion of the substrates in the cell and syringe. The results are shown in figure 3.29. Active enzyme at a 3-fold higher concentration (blue trace) gave the same results as before. At 32 µM *Pf*HGXPRT, the heat produced at each injection was higher and there was some semblance of a curved titration effect over the titration period. However, the amount of heat produced that could perhaps be attributable to binding was smaller than the nonspecific component remaining at the end of the titration, which may be due to a DMSO dilution effect. Nonetheless the result seemed encouraging but

the DMSO effect seemed unpredictable and sometimes too large for the small amounts of heat produced by the binding reaction.

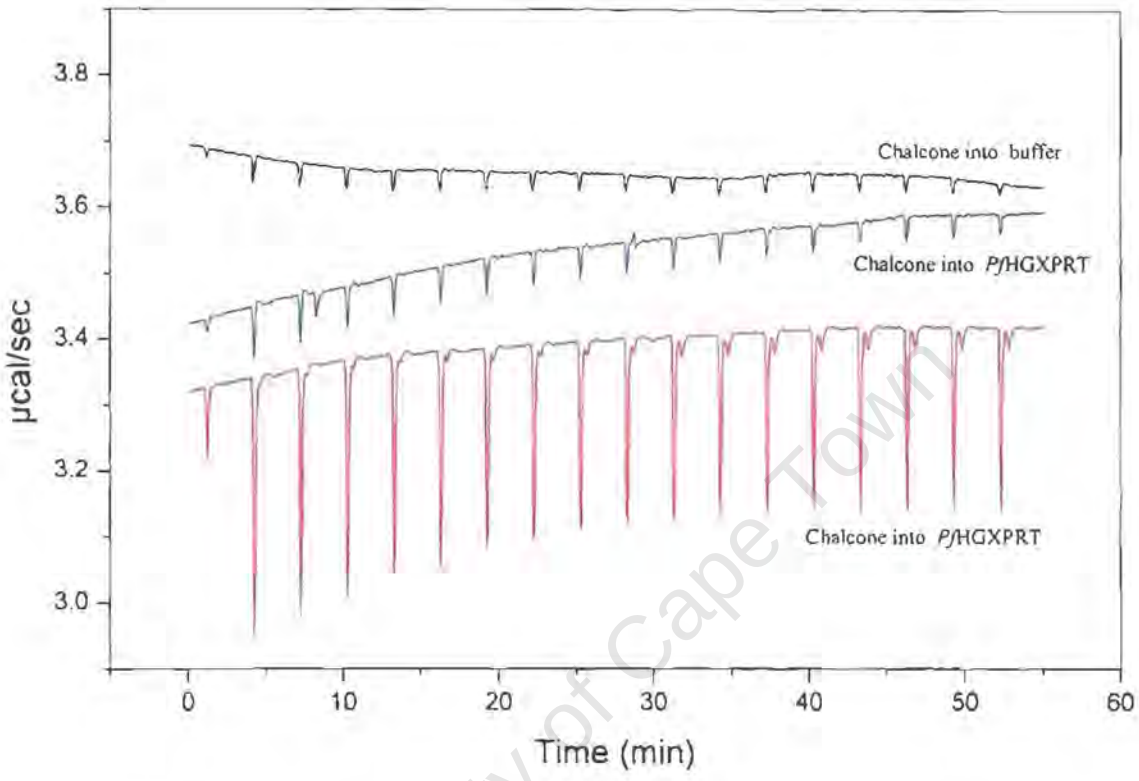

Figure 3.29. Titration of *Pf*HGXPRT with 4′-iodo-chalcone: effect of increasing the amount of protein, using activated enzyme, and removing $CaCl_2$. Binding was studied with either 16 (blue trace) or 32 (red trace) µM *Pf*HGXPRT (in the cell) and 250 µM chalcone (syringe) and 10 (with the lower protein concentration) or 50 (higher protein) mM EPPS·TMAH, pH 8.2, 10% DMSO, 60 µM hypoxanthine and 1 mM PRPP in both compartments. The concentration of buffer coming in with the protein was also compensated for in the syringe compartment by adding 3.2 and 6.5 mM MOPS·TMAH, pH 7.0 at 16 and 32 µM protein, respectively. The control was chalcone into buffer (black trace). The chalcone was added to DMSO before any of the other constituents as the chalcone precipitates otherwise.

We experimented with trying to obtain soluble chalcone in lower concentrations of DMSO, and found that if the stock, concentrated chalcone in neat DMSO was diluted 1000-fold into the syringe buffer and heated at 35°C for a few minutes the

chalcone went into solution. This meant that the concentration of DMSO in the syringe could be 0.1%, instead of the previous 10%.

Accordingly, we devised such an experiment using a new preparation, using the protein as isolated as well as activated (yielding a specific activity of 2.86 μmoles GMP/min/mg of protein) and the results are shown in figure 3.30. Here no DMSO was included in the cell compartment and 0.1% was in the syringe due to diluting the chalcone. Clearly, no heat attributable to chalcone binding can be discerned and the heats of titration are what is expected for diluting 0.1% DMSO into water (compare figures 3.27 and 3.30).

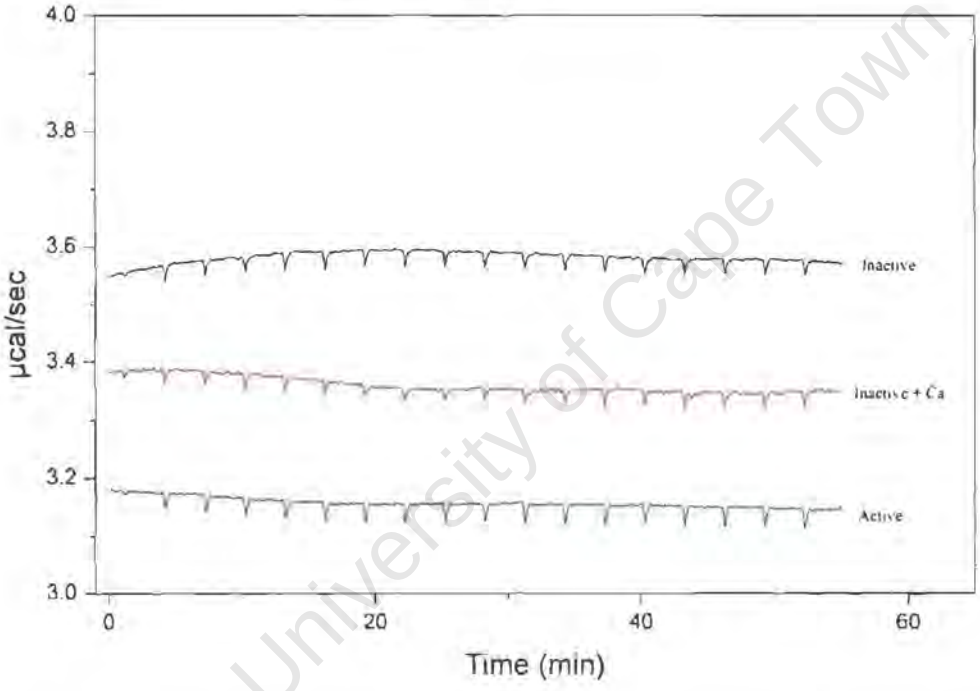

Figure 3.30. Titration of *Pf*HGXPRT with 4'-iodo-chalcone: diminishing the DMSO effect. In these experiments the chalcone was dissolved in buffer by diluting the stock concentrated neat DMSO solution 1000-fold and heating at 35 ^{o}C for a few minutes. In the first titration (black trace), isolated *Pf*HGXPRT (0.92 mg/ml, 36 μM) was titrated with chalcone (100 μM) and both compartments contained 50 mM EPPS·TMAH, pH 8.2 and 0.39 mM MOPS·TMAH, pH 7.0 (the latter because the buffer in which the stock protein was dissolved). In the second titration (red trace), conditions were identical with 1 mM $CaCl_2$ being added to both compartments. In the third titration (blue trace), the *Pf*HGXPRT was activated by prior incubation with both substrates (1 mM hypoxanthine, 2 mM PRPP) and $MgCl_2$ (0.1 mM). Both compartments contained 50 mM EPPS·TMAH, pH 8.35, 0.39 mM MOPS·TMAH, pH 7.0, 1 mM hypoxanthine, 2 mM PRPP and 0.1 mM $MgCl_2$.

CHAPTER 4: Discussion and Conclusions

This research was aimed at developing methodology for ultimately characterising the interaction of an effector chalcone with *Pf*HGXPRT. To date, the interaction had been defined by effects on catalytic activity, e.g. an accelerating effect in $MgCl_2$, an inhibitory effect in $CaCl_2$, and an activating effect through conversion of the isolated enzyme into an active form. What was needed were more direct methods for analysing the interaction. For this, a method for measuring the oligomeric status of the protein was developed; the use of a photoprobe, developed for measuring ATP binding to mutant Ca^{2+}-ATPase, was assessed as an active site probe; and Isothermal Titration Calorimetry was explored as a means of directly measuring chalcone binding.

Expression, purification, and activation of *Pf*HGXPRT

*Pf*HGXPRT was successfully expressed and purified with and without a his-tag using methods developed previously in our laboratory. However, in the present study, we found that induction of both his-tagged and non his-tagged protein expression at 37°C was unfavourable, with very low expression levels and large proportions of protein in the pellet fraction (perhaps insoluble in inclusion bodies). Reducing the temperature of induction to 25° produced higher levels of supernatant (soluble) protein with yields of up to 6 mg and 16 mg for the his-tagged and non his-tagged proteins, respectively. Purification by a single pass through a Nickel-affinity column produced a preparation of approximately 95% purity, as judged visually by SDS-PAGE, whilst purification of the non his-tagged protein by anion-exchange chromatography followed by Reactive Red-120 affinity chromatography provided a preparation which was about 90% pure.

Puzzlingly, the his-tagged *Pf*HGXPRT appeared more soluble than the non his-tagged protein when expressed in *E. coli* (more in the supernatant fraction), but had a much greater tendency to precipitate when isolated in the purified form. It would seem that the his-tag (consisting of six histidine residues at the amino

terminal end) influenced the solubility of the protein. Histidine has a pKa value of 6.1 and so it would be protonated at lower pH values. At pH 7.0, it carries no charge, and the his-tag becomes essentially a hydrophobic tail, which is most likely the reason for the protein coming out of solution. Although the intracellular pH of an *E. coli* cell may be similar, it contains approximately 150 mM KCl and this may be the difference. We eluted the protein from the Ni-chelate column with 1 M imidazole and did not have solubility problems at this high salt concentration, and yet overnight dialysis to remove the imidazole caused precipitation. This prompted us to try removing the imidazole quickly using a small gel filtration column (PD-10), but still the protein tended to aggregate, as revealed after thawing frozen protein, and by the protein failing to elute from the gel filtration HPLC column. The protein stored in high salt could never be activated, but that following passage through the PD-10 column could be. So one has a dilemma, one needs the high salt to keep it soluble, but such conditions favour the dimer (see later) and inactive protein.

While the vast majority of the his-tagged *Pf*HGXPRT appeared in the supernatant fraction, the opposite was true for the non his-tagged form, most appeared in the pellet (insoluble) fraction. Yet, reducing the temperature of induction from 37 to 25°C greatly increased overall yield, both in the supernatant and pellet fractions, and resulted in satisfactory yields of soluble protein, of up to 16 mg/ L culture.

Both forms of the protein were successfully activated by incubation with partial substrates (usually 60 μ hypoxanthine + 1 mM PRPP, without added $MgCl_2$), reaching specific activities of up to 3 μmol/min/mg and 2 μmol/min/mg for the his-tagged and non his-tagged proteins, respectively. These activities were slightly less than the maximal values achieved previously in our laboratory (up to 6 μmol/min/mg of protein; Phehane, 2002; Mbewe, 2005; Mbewe *et al*, 2007).

Gel filtration HPLC

We explored the possibility of using gel filtration HPLC chromatography to analyse the oligomeric status of *Pf*HGXPRT. Sedimentation equilibrium studies by ultracentrifugation have shown that *Pf* HGXPRT is a tetramer and dimer at low and high (up to 1.2 M) salt respectively (Keough *et al*, 1999). Further, the active enzyme is inactivated by dialysis against high salt, and they concluded that the enzyme exists in a salt –dependent, active tetramer↔inactive dimer equilibrium.

Gel filtration HPLC seemed to be an effective technique for separation of the two oligomeric forms of the enzyme and, in addition, it has the advantage of speed and makes direct quantification of the proportions of each species possible. There was a salt-dependent change in proportion of an earlier and later eluting peak. The earlier eluting form was assigned as tetramer and the later eluting form to the dimer. According to the calibration curve obtained using molecular weight standards at 400 mM NaCl, these values were 85 and 55 kDa, respectively.

One problem encountered was that some of the standards changed their elution position depending on the salt concentration, and evidently in these cases there is some interaction with the resin at low salt. The most dramatic is cytochrome c (figure 3.13, peak 6) which failed to elute from the column at 20 mM NaCl. One needs to be aware of this phenomenon when using gel filtration HPLC. Thus molecular weight assignments of an unknown protein need not be accurate depending on what standards you choose, the salt concentration, and how the protein of interest interacts with the resin. In our case, *Pf*HGXPRT did not change its elution position much at concentrations higher than 50 mM NaCl.

Analysis of isolated and active *Pf*HGXPRT produced the same results, in low salt running buffer the protein always appeared as the larger tetrameric species, and in high salt running buffer always the smaller dimeric form. Therefore the tetrameric form need not be active and activation does not appear to convert dimer into tetramer. Rather the activation process probably involves a conformational change in each of the monomers.

Pretreatment of the protein with high salt (1 M NaCl) for 1-20 min made no difference to these characteristics, i.e. if the protein was analysed in a low salt buffer, it eluted as the tetramer rather than the dimer. Either conversion to the dimer at high salt takes a longer time or the equilibrium is very rapid, and readjusts almost immediately when the protein is injected.

For an oligomeric protein such as a tetramer, the following equilibria should apply

$$\text{Tetramer} \overset{K_{eq}}{\longleftrightarrow} \text{Dimer} \overset{K'_{eq}}{\longleftrightarrow} \text{Monomer}$$

and they must necessarily be protein concentration dependent, such that as the concentration is lowered, the equilibrium shifts to the monomer. The concentration range in which the process largely occurs will be dependent on the affinities between subunits and hence the equilibrium constants for each step. Our results show that a 10-fold dilution of *Pf*HGXPRT had no effect on its quarternary structure, suggesting that the association between subunits is very tight.

A surprise, is the low concentrations of divalent cations that alter the tetramer↔dimer equilibrium ($K_{0.5}$~1 mM). This has implications for the nature of the protein in the standard assay, which has 110 mM $MgCl_2$! We have found that the enzyme inactivates irreversibly in the assay medium over the course of a few minutes (the progress curve is curved) and it could reflect a conversion from an active tetramer to inactive dimer. It could be instructive to analyse the protein by gel filtration HPLC after 5 min in the assay medium.

These results lay the foundation for understanding the equilibrium of oligomeric forms of *Pf*HGXPRT and will enable the effects of chalcone binding to be studied in a more meaningful way.

Photolabelling

TNP-$8N_3$-ATP, and later [γ-^{32}P]TNP-$8N_3$-ATP, has been used extensively in our laboratory as a probe of the active site of sarcoplasmic reticulum Ca^{2+}-ATPase. The probe specifically derivatises Lys^{492} at the active site of the enzyme with high efficiency (McIntosh *et al*, 1992). We wanted to examine whether the radiolabelled probe could be used as a probe of the active site of *Pf*HGXPRT, specifically with the aim of establishing whether the chalcone bound here or elsewhere, i.e. is there competitive inhibition of labelling or not.

The usefulness of the technique for measuring active site binding is illustrated using SR Ca^{2+}-ATPase as a model system. The procedure is first to perform a concentration dependence of [γ-^{32}P]TNP-$8N_3$-ATP photolabelling, in order to obtain a $K_{0.5}$ value ($K_{0.5(TNP)}$ = 0.16 μM in our experiment), and then to measure the ATP dependence of inhibition at a fixed [γ-^{32}P]TNP-$8N_3$-ATP concentration. Use of a competitive binding equation provides the true K_d for ATP binding (20 μM in our case). The binding K values we obtained were very similar to those published previously (McIntosh *et al*, 1999).

A novel aspect of the experiments involving *Pf*HGXPRT was an attempt to measure the stoichiometry of derivatisation (see below). When the same procedure (incorporating spots of a known quantity and specific activity of [γ-^{32}P]TNP-$8N_3$-ATP with the gel) was used with SR Ca^{2+}-ATPase a value of 0.04 mol probe/mol Ca^{2+}-ATPase was obtained. This is surprising as we know from other approaches that the extent of derivatisation is actually 10-fold higher (Seebregts and McIntosh, 1989). Thus there appears to be a factor diminishing the real extent of derivatisation, which at present we cannot account for, but needs to be taken into consideration with *Pf*HGXPRT.

It may be thought that [γ-^{32}P]TNP-$8N_3$-ATP might not be an appropriate label of the active site of *Pf*HGXPRT, because the probe is adenine based and a triphosphate species whereas our enzyme binds monophosphates (guanosine,

inosine, or xanthine monophosphate). However, examination of the apo structures of human (figure 4.1) and *Toxoplasma gondii* (figure 1.7F) reveals that the active site is wide open with the flexible catalytic loops pulled back. There is in fact plenty of room for a large probe to be accommodated.

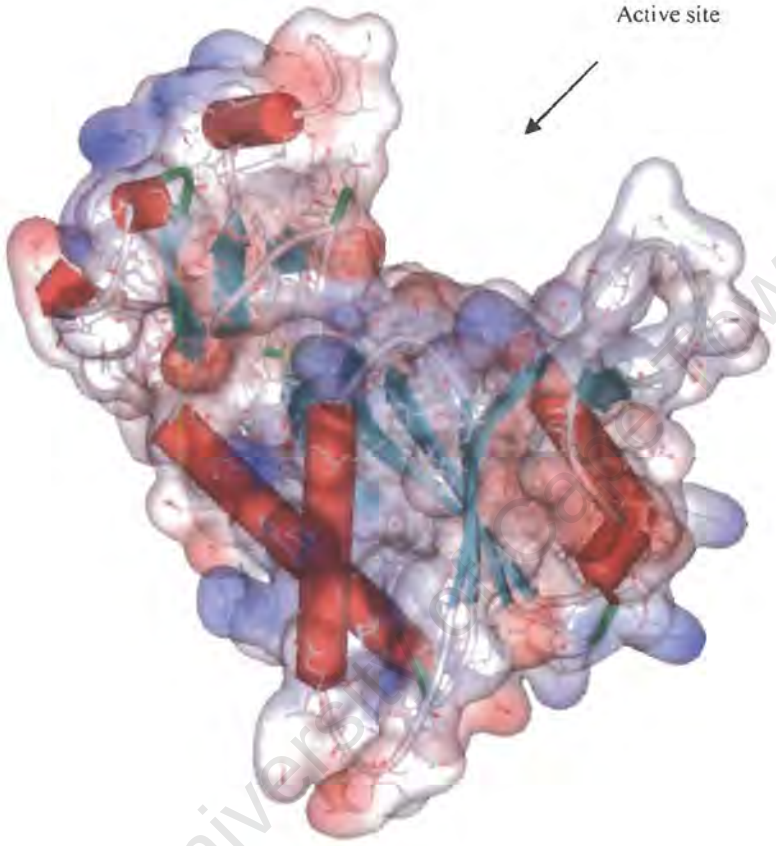

Figure 4.1 Human HGPRT apoenzyme. A semitransparent surface representation of the unliganded form of the enzyme indicating the open active site.

Even the polyphosphate tail may be tolerated by extending out into the medium. An attempt to dock TNP-8N_3-ATP into the active site of the human apoprotein with the phosphates extending from the active site is shown in figure 4.2. The adenine moiety is located under the appropriate phenylalanine residue.

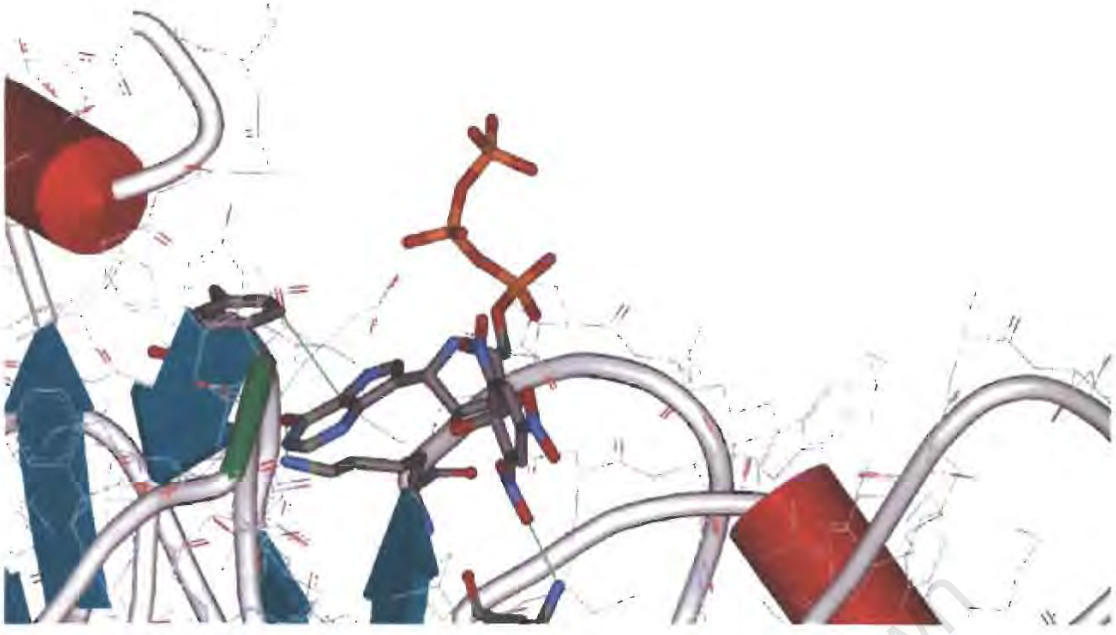

Figure 4.2. Docking of TNPATP into the active site of *Pf*HGXPRT.

Preliminary experiments on the pH dependence of photolabelling of isolated and active *Pf*HGXPRT with [γ-^{32}P]TNP-8N_3-ATP suggested that derivitisation may be more efficient in EDTA, compared to labelling in the presence of the divalent cations (Mg^{2+} and Ca^{2+}). 4′-iodo-chalcone appeared to have little effect on derivatisation, compatible with it binding to an allosteric site (if indeed the probe was derivatising the active site, see below). An allosteric site is suggested from the fact that the chalcone inhibits activity in a non competitive manner with respect to PRPP (Mbewe and McIntosh, unpublished results).

More detailed investigation of derivatisation at pH 6.0 and 8.0 in EDTA (in the absence of the divalent cations) suggested that binding is 5-10 fold tighter for the isolated *Pf*HGXPRT compared with the active enzyme. However, the presence of a relatively large apparently non-specific component with the isolated protein makes the conclusion somewhat uncertain and repeat experiments need to be done.

An important aspect of the results is that the extent of derivatisation varies from 0.04 to 0.09 mol probe/ mol protein at pH 6.0 to 0.001 to 0.01 mol probe/ mol

protein at pH 8.0. The former figures are very close to the 0.04 found for Ca^{2+}-ATPase (actually 0.5 mol/ mol protein), and one must conclude that the efficiency of photolabelling of *Pf*HGXPRT is equally high. Photolabelling with [γ-^{32}P]TNP-$8N_3$-ATP is in fact more efficient than with [γ-^{32}P]TNP-$8N_3$-ITP (Murungi, 2007).

A high extent of derivatisation is useful as it allows determination of the derivatised amino acid residue/s, and was done in the case of SR Ca^{2+}-ATPase (McIntosh *et al*, 1992). The method consists of protease digestion of derivatised protein, separation of fragments by HPLC, purification of the labelled peptides, and sequencing. In this way, with knowledge of the atomic structure, it may be determined whether the derivatised amino acid/s is at the active site.

In the absence of Mg^{2+}, PRPP did not have much of an effect on photolabelling at pH 6.0, but seemed to reduce the level at pH 8.0, although just with active enzyme. Thus, whether the photolabelling is specific for the active site remains equivocal, and further experiments are necessary. The most likely explanation for the poor effect of PRPP is that binding probably requires Mg^{2+}. The atomic structure of the transition state mimic of the active site of *Pf*HGXPRT shows that the pyrophosphate moiety interacts strongly with the two Mg^{2+}, and the latter interact with Asp204 in one case and are in proximity to Glu144 and Asp145 in the other. In the absence of these cations there will be electrostatic repulsion between the pyrophosphate moiety and the acidic residues, which will likely prevent PRPP binding. The experiments need to be repeated with Mg^{2+} in the medium.

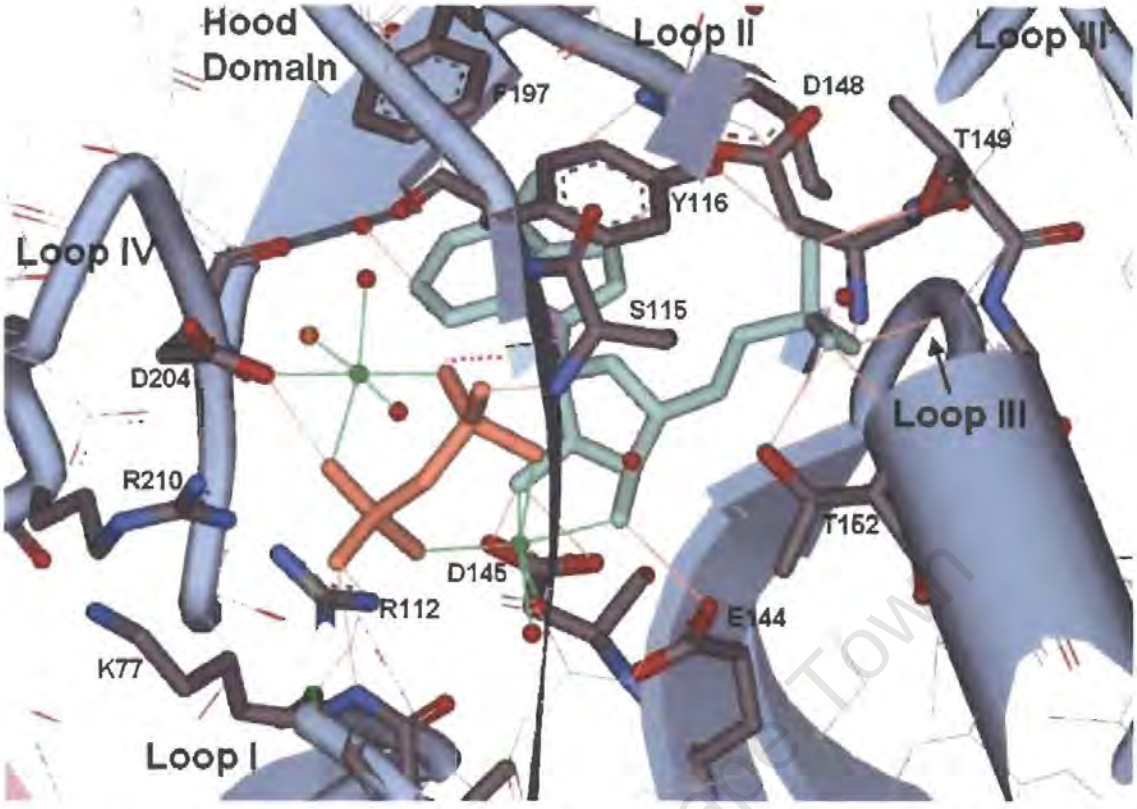

Figure 4.3. *Pf*HGXPRT active site. This diagram illustrates the interactions of immucillinHP (light blue), pyrophosphate (pink), and the two Mg^{2+} (green spheres) in the active site of the transition state mimic. Note how pyrophosphate interacts strongly with the two Mg^{2+}, and the fact that there is only one interaction of the divalent cations with the protein itself (Asp204). (Structure determined by Shi *et al*, 1999*a*).

Isothermal titration calorimetry

ITC is a powerful technique for analysis of binding reactions and provides a profile of useful thermodynamic parameters. We sought to characterise the interaction of 4′-iodo-chalcone with *Pf*HGXPRT.

Initially, we performed a model binding experiment, suggested by the manufacturer, in which EDTA was titrated with $CaCl_2$, and the results indicated that the instrument was working well and that our ability to use the calorimeter was proficient.

4′-iodo-chalcone is fairly insoluble in aqueous medium, and the concentrated stock solutions need to be made up in organic solvents, of which DMSO is the most effective. However, this solvent has the drawback of producing a lot of heat when diluted in water. In retrospect it would seem advantageous to explore the use of other organic solvents like ethanol or methanol. Control experiments with DMSO showed the titration profile obtained with dilution of 1 and 0.2% solutions, and provided the amounts of heat produced if the syringe and cell differed by these concentrations. We attempted to decrease the concentration of DMSO used by testing the solubility of the chalcone at different pH at 10% DMSO. In later experiments, we found that it was possible to reduce the concentration to 0.1% DMSO if the solution was heated.

Our initial experiments were with 10% DMSO in the syringe and cell, and with rather low concentrations of protein (6 μM), and titrations failed to reveal obvious heats of binding. Increasing the concentration of protein to 16 and then 32 μM did not improve the outcome. Also using isolated or active *Pf*HGXPRT seemed to make no difference. Finally, experiments with 0.1% DMSO in the syringe only and 36 μM protein, isolated or active, without or with Ca^{2+} definitively showed that no heats of binding were produced.

We conclude that either the chalcone does not bind under the conditions used or no heat is produced due to a balance of endothermic and exothermic factors. The latter seems more likely. However, it needs to be considered that two of the effects of chalcone, the acceleration (in Mg^{2+}) and inhibition (in Ca^{2+}) are only observed by measuring catalytic activity, and maybe the allosteric site only appears in certain intermediates. Against this idea is the fact that the chalcone alone causes a change from inactive to active enzyme, which must be exerted by binding to the otherwise unliganded protein.

The likelihood of the chalcone binding to an allosteric site is of great significance to us as an allosteric inhibitor of the malarial enzyme has never been found. Due to the high similarity of active site residues in the human and malarial homologues of the enzyme, the possibility of developing a parasite-specific

inhibitor is virtually nil. This observation makes an allosteric inhibitor with *Pf*HGXPRT-specific inhibitory effects all the more interesting.

Concluding remarks

*Pf*HGXPRT was successfully expressed, purified and activated. Gel filtration chromatography was shown to be a useful technique for measuring the proportion of tetrameric and dimeric forms of the enzyme, and confirmed previous findings obtained by ultracentrifugation (Keough *et al*, 1999) that the quarternary structure is sensitive to ionic strength, and further that this sensitivity extends to rather low concentrations of $MgCl_2$ and $CaCl_2$. [γ-^{32}P]TNP-8N_3-ATP could be a useful photoaffinity probe, with extents of derivatization similar to the model system of sarcoplasmic reticulum Ca^{2+}-ATPase, but further work would be needed to establish that it labelled the active site. Preliminary findings suggest that 4′-iodo-chalcone has little effect on photolabelling which is compatible with it binding to an allosteric site. We established that Isothermal Titration Calorimetry (ITC) cannot be used for measuring chalcone binding to *Pf*HGXPRT.

Chen, S-H., Suzuki, C.K., and Wu, S-H. (2008) Thermodynamic characterization of specific interactions between the human Lon protease and G-quartet DNA. *Nucleic Acids Res.* **36**, 1273-1287

Chin, M.S. and Wang, C.C. (1994) Isolation, sequencing and expression of the gene encoding hypoxanthine-guanine-xanthine phosphoribosyltransferase of *Tritrichomonas foetus*. *Mol. Biochem. Parasitol.* **63**, 221-229

Chung, E.W., Henriques, D.A., Renzoni, D., Morton, C.J., Mulhern, T.D., Pitkeathly, M.C., Ladbury, J.E., and Robinson, C.V. (1999) Probing the nature of interactions in SH2 binding interfaces – evidence from electrospray ionization mass spectrometry. *Protein Sci.* **8**, 1962-1970

Cowman, A.F., Morry, M.J., Biggs, B.A., Cross, G.A.M., and Foote, S.J. (1988) Amino acid changes linked to pyrimethamine resistance in the dihydrofolate reductase-thymidylate synthase gene of *Plasmodium falciparum*. *Proc. Natl. Acad. Sci. USA.* **85**, 9109-9113

Cuatrecasas, P., Wilchek, M., and Anfinsen, C.B. (1968) Selective enzyme purification by affinity chromatography. *Proc. Natl. Acad. Sci. USA.* **61**, 636-643

Cutler, P. Affinity chromatography. (2004) p. 139-148. In P. Cutler (ed.), Methods in molecular biology: protein purification protocols, 2nd ed., vol 244. Humana Press Inc, Totowa, N.J.

Cutler, P. Size-exclusion chromatography. (2004) p. 239-252. *In* P. Cutler (ed.) Methods in molecular biology: protein purification protocols, 2nd ed., vol. 244. Humana Press, Inc., Totowa, N.J.

Dahl, E.L. and Rosenthal, P.J. (2007) Multiple antibiotics exert delayed effects against the *Plasmodium falciparum* apicoplast. *Antimicrob. Agents Chemother.* **51**, 3485-3495

Denizli,A, and Piskin, E. (2001) Dye-ligand affinity systems. *J. Biochem. Biophys. Methods.* **49**, 391-416

Dondorp, A.M. and Day, N.P.J. (2007) The treatment of severe malaria. *Trans. R. Soc. Trop. Med. Hyg.* **101**, 633-634

Doonan, S. and Cutler, P. (2004) General strategies, p. 6-8. In P. Cutler (ed.) Methods in molecular biology: protein purification protocols, 2nd ed., vol 244. Humana Press, Inc., Totowa, N.J.

Dormán, G. and Prestwich, G.D. (2000) Using photolabile ligands in drug discover and development. *TIBTECH.* **18**, 64-77

Eads, J.C., Scapin, G., Xu, Y., Grubmeyer, C., and Sacchettini, J.C. (1994) The crystal structure of human hypoxanthine-guanine phosphoribosyltransferase with bound GMP. *Cell.* **78**, 325-334

Eckland, E.H. and Fidock, D.A. (2008) *In vitro* evaluations of antimalarial drugs and their relevance to clinical outcomes. *Int. J. Parasitol.* **38**, 743-747

Eckstein-Ludwig, U., Webb, R.J., Van Goethem, I.D.A., East, J.M., Lee, G., Kimura, M., O'Neill, P.M., Bray, P.G., Ward, S.A., and Krishna, S. (2003) Artemisinins target the SERCA of *Plasmodium falciparum*. *Nature.* **424**, 957-961

Egan, T.J. and Ncokazi, K.K. (2005) Quinoline antimalarials decrease the rate of β-hematin formation. *J. Inorg. Biochem.* **99**, 1532-1539

Fidock, D.A., Nomura, T., Talley, A.K., Cooper, R.A., Dzekunov, S.M., Ferdig, M.T., Ursos L.M., Sidhu, A.B., Naudé B., Deitsch K.W., Su, X.Z., Wootton, J.C., Roepe, P.D., and Wellems, T.E. (2000) Mutations in the *P. falciparum* digestive vacuole transmembrane protein *Pf*CRT and evidence for their role in chloroquine resistance. *Mol. Cell.* **6**, 861-871

Focia, P.J., Craig, S.P., Nieves, Alicea, R., Fletterick, R.J., and Eakin, A.E. (1998) A 1.4 Å crystal structure for the hypoxanthine phosphoribosyltransferase of *Trypanosoma cruzi*. *Biochemistry*. **37**, 15066-15075

Free, M.L., Gordon, R.B., Keough, D.T., Beacham, I.R., Emmerson, B.T., and de Jersey, J. (1990) Expression of active human hypoxanthine-guanine phosphoribosyltransferase in *Escherichia coli* and characterisation of the recombinant enzyme. *Biochim. Biophys. Acta*. **1087**, 205-211

Freedman, D.O. (2008) Malaria prevention in short-term travellers. *N. Engl. J. Med.* **359**, 603-612

Freyer, M.W. and Lewis, E.A. (2008) Isothermal titration calorimetry: experimental design, data analysis, and probing macromolecule/ligand binding and kinetic interactions. *Methods Cell. Biol.* **84**, doi: 10.1016/s0091-679x(07)84004-0

Gayathri, P., Sujay Subbayya, I.N., Ashok, C.S., Selvi, T.S., Balaram, H., and Murthy, M.R. (2008) Crystal structure of a chimera of human and *Plasmodium falciparum* hypoxanthine guanine phosphoribosyltransferase provides insights into oligomerization. *Proteins*. doi: 10.1002/prot.22129

Giacomello, A., and Salerno, C. (1978) Human hypoxanthine-guanine phosphoribosyltransferase: Steady state kinetics of the forward and reverse reactions. *J. Biol. Chem.* **253**, 6038-6044

Gopalakrishnapai, J., Gupta, G., Karthikeyan, T., Sinha, S., Kandiah, E., Gemma, E., Oscarson, S., and Surolia, A. (2006) Isothermal titration calorimetric study defines the substrate binding residues of calreticulin. *Biochem. Biophys. Res. Comm.* **351**, 14-20

Grayer, R.J., Kimmins, F.M., Padgham, D.E., Harborne, J.B., and Ranga Rao, D.V. (1992) Condensed tannin levels and resistance of groundnuts (*Arachis hypogaea*) against *Aphis craccivora*. *Phytochemistry* **31**, 3795-3800

Grayer, R.J. and Harborne, J.B. (1994) A survey of antifungal compounds from higher plants 1982-1993. *Phytochemistry* **37**, 19-42

Guerra, C.A., Gikandi, P.W., Tatem, A.J., Noor, A.M., Smith, D.L., Hay. S.I., and Snow, R.W. (2008) The limits and intensity of *Plasmodium falciparum* transmission: implications for malaria control and elimination worldwide. *PLoS Med*. **5**, 300-311

Hale, V., Keasling, J.D., Renninger, N., and Diagana, T.T. (2007) Microbially derived artemisinin: a biotechnology solution to the global problem of access to affordable antimalarial drugs. *Am. J. Trop. Med. Hyg*. **77**, 198-202

Harborne, J.B. and Williams, C.A. (2000) Advances in flavonoid research since 1992. *Phytochemistry*. **55**, 481-504

Henderson, J.F., Brox, L.W., Kelley, W.N., Rosenbloom, F.M., and Seegmiller, J.E. (1968) Kinetic studies of hypoxanthine-guanine phosphoribosyltransferase. *J. Biol. Chem*. **243**, 2514-2522

Héroux, A., White, E.L., Ross, L.J., and Borhani, D.W. (1999*a*) Crystal structures of the Toxoplasma gondii hypoxanthine-guanine phosphoribosyltransferase-GMP and –IMP complexes: comparison of purine binding interactions with the XMP complex. *Biochemistry*. **38**, 14485-14494

Héroux, A., White, E.L., Ross, L.J., Davis, R.L., and Borhani, D.W. (1999*b*) Crystal structure of *Toxoplasma gondii* hypoxanthine-guanine phosphoribosyltransferase with XMP, pyrophosphate, and two Mg^{2+} ions bound: insights into the catalytic mechanism. *Biochemistry*. **38**, 14495-14506

Horton, H.R., Moran, L.A., Ochs, R.S., Rawn, J.D., and Scrimgeour, K.G. (2002) Principles of biochemistry. 3rd ed., p. 66-69. Prentice-Hall, Inc. Upper Saddle River, N.J.

Keough, D.T., McConachie, L.A., Gordon, R.B., de Jersey, J., and Emmerson, B.T. (1987) Human hypoxanthine-guanine phosphoribosyltransferase. Development of a spectrophotometric assay and its use in detection and characterization of mutant forms. *Clin. Chim. Acta* **163**, 301-308

Keough, D.T., Ng, A-L., Winzor, D.J., Emmerson, B.T., and de Jersey, J. (1999) Purification and characterisation of *Plasmodium falciparum* hypoxanthine-guanine-xanthine phosphoribosyltransferase and comparison with the human enzyme. *Mol. Biochem. Parasitol.* **98**, 29-41

Keough, D.T., Brereton, I.M., de Jersey, J., and Guddat, L.W. (2005) The crystal structure of free human hypoxanthine-guanine phosphoribosyltransferase reveals extensive conformational plasticity throughout the catalytic cycle. *J. Mol. Biol.* **351**, 170-181

Kotzyba-Hibert, F., Kapfer, I., and Goeldner, M. (1995) Recent trends in photoaffinity labelling. *Angew. Chem. Int. Ed. Engl.* **34**, 1296-1312

Krungkrai, S.R., Yuthavong, Y. (1987) The antimalarials action on Plasmodium falciparum of qinghaosu and artesunate in combination with agents which modulate oxidant stress. *Trans. R. Soc. Trop. Med. Hyg.* **81**, 710-714

Ladbury, J.E. and Chowdry, B.Z. (1996) Sensing the heat: the application of isothermal titration calorimetry to thermodynamic studies of biomolecular interactions. *Chem. Biol.* 3, 791-801

Laemmli, U.K. (1970) Cleavage of structural proteins during the assembly of the head of bacteriophage T4. *Nature.* **227**, 680-685.

Leavitt, S. and Freire, E. (2001) Direct measurement of protein binding energetics by isothermal titration calorimetry. *Curr. Opin. Struct. Biol.* **11**, 560--566

Leavitt, S. and Freire, E. (2001) Direct measurement of protein binding energetics by isothermal titration calorimetry. *Curr. Opin. Struct. Biol.* **11**, 560--566

Li, C.M., Tyler, P.C., Furneaux, R.H., Kicska, G., Xu, Y., Grubmeyer, C., Girvin, M.E., and Schramm, V.L. (1999) Transition-state analogs as inhibitors of human and malarial hypoxanthine-guanine phosphoribosyltransferases. *Nat. Struct. Biol.* **6**, 582-587

Lindner, P., Guth, B., Wülfing, C., Krebber, C., Steipe, B., Müller, F., and Plückthun, A. (1992) Purification of native proteins from the cytoplasm and periplasm of *Escherichia coli* using IMAC and histidine tails: a comparison of proteins and protocols. *METHODS: A Companion to Methods in Enzymology* **4**, 41-56

Liu, Y-C., Hsieh, C-W., Wu, C-C., and Wung, B-S. (2007) Chalcone inhibits the activation of NF-κB and STAT3 in endothelial cells via endogenous electrophile. *Life Sciences.* **80**, 1420-1430

Marshall, R.C. and Inglis, A.S. (1986) Protein oligomer composition, preparation of monomers and constituent chains. p. 13-16, 25-27. *In* A. Darbre (ed.), Practical protein chemistry: a handbook. John Wiley & Sons Ltd.

Mbewe, B. (2005) Cloning, expression, purification and drug targeting of *Plasmodium falciparum* hypoxanthine guanine xanthine phosphoribosyltransferase. (HGXPRT). Ph.D. Thesis, University of Cape Town.

Mbewe, B., Chibale, K., and McIntosh, D.B. (2007) Purification of human malaria parasite hypoxanthine guanine xanthine phosphoribosyltransferase (HGXPRT) using immobilized Reactive Red 120. *Protein Expr. Purif.* **52**, 153-158

McConkey, G.A., Rogers, M.J., McCutchan, T.F. (1997) Inhibition of *Plasmodium falciparum* protein synthesis: targeting the plastid-like organelle with thiostrepton. *J. Biol. Chem.* **272**, 2046-2049

McIntosh, D.B., Woolley, D.G., and Berman, M.C. (1992) 2′,3′-O-(2,4,6-trinitrophenyl)-8-azido-AMP and –ATP photolabel Lys-492 at the active site of sarcoplasmic reticulum Ca^{2+}-ATPase. *J. Biol. Chem.* **267**, 5301-5309

McIntosh, D.B., Woolley, D.G., Vilsen, B., and Andersen, J.P. (1996) Mutagenesis of segment ^{487}Phe-Ser-Arg-Asp-Arg-Lys^{492} of sarcoplasmic reticulum Ca^{2+}-ATPase produces pumps defective in ATP binding. *J. Biol. Chem.* **271**, 25778-25789

McIntosh, D.B., Woolley, D.G., MacLennan, D.H., Andersen, J.P., and Vilsen, B. (1999) Interaction of nucleotides with Asp^{351} and the conserved phosphorylation loop of sarcoplasmic reticulum Ca^{2+}-ATPase. *J. Biol. Chem.* **274**, 25227-25236

Miller, L.H., Baruch, D.I., Marsh, K., and Doumbo, O.K. (2002) The pathogenic basis of malaria. *Nature.* **415**, 673-679

Miyase, T., Sano, M., Nakai, H., Muraoka, M., Nakazawa, M., Suzuki, M., Yoshino, K., Nishihara, Y., Tanai, T. (1999*a*) Antioxidants from *Lespedeza homoloba* (I). *Phytochemistry* **52**, 303-310

Miyase, T., Sano, M., Yoshino, K., Nonaka, K. (1999*b*) Antioxidants from *Lespedeza homoloba* (II). *Phytochemistry* **52**, 311-319

Murungi, E.K. (2007) Purification and characterisation of *Plasmodium falciparum* HGPRT. MSc Thesis. University of the Western Cape.

Nabarro, D.N. and Tayler, E.M. (1998) The "Roll Back Malaria" campaign. *Science.* **280**, 2067-2068

Nzila, A. (2006) Inhibitors of *de novo* folate enzymes in *Plasmodium falciparum*. *Drug Discov. Today*. **11**, 939-944

Peterson, D.S., Walliker, D., and Wellems, T.E. (1988) Evidence that a point mutation in dihydrofolate reductase-thymidylate synthase confers resistance to pyrimethamine in falciparum malaria. *Proc. Natl. Acad. Sci. USA*. **85**, 9114-9118

Phehane, V.N. (2002) Expression and drug targeting of parasitic hypoxanthine-guanine phosphoribosyltransferase (HGPRT). Ph.D. Thesis, University of Cape Town, South Africa.

Porath, J., Carlsson, J., Olsson, I., and Belfrage, G. (1975) Metal chelate affinity chromatography: a new approach to protein fractionation. *Nature*. **268**, 598-599

PrayGod, G., de Frey, A., and Eisenhut, M. (2008) Artemisinin derivatives versus quinine in treating severe malaria in children: a systematic review. *Malaria J.* **7**, 210-218

Price, R.N., Nosten, F., Luxemburger, C., ter Kuile, F.O., Paiphun, L., Chongsuphajaisiddhi, T., and White, N.J. (1996) Effects of artemisinin derivatives on malaria transmissibility. *Lancet*. **347**, 1654-1658

Queen, S.A., Vander Jagt, D., and Reyes, P. (1988) Properties and substrate specificity of a purine phosphoribosyltransferase from the human malaria parasite, *Plasmodium falciparum*. *Mol. Biochem. Parasitol.* **30**, 123-133

Rao, M.V., and Ormrod, D.P. (1995) Ozone exposure decreases UVB-sensitive flavonoid mutant of *Arabidopsis*. *Photochem. Photobiol.* **61**, 71-78

Ralph, S.A., D'Ombrain, M.C., and McFadden, G.I. (2001) The apicoplast as an antimalarial drug target. *Drug. Resist. Updat.* **4**, 145-151

Raman, C.S., Allen, M.J., and Nall, B.T. (1995) Enthalpy of antibody – cytochrome c binding. *Biochemistry*. **34**, 5831-5838

Saeki, T., Hayakawa, S., Isemura, M., and Miyase, T. (2000) Importance of a pyrogallol-type structure in catechin compounds for apoptosis-inducing activity. *Phytochemistry* **53**, 391-394

Schumacher, M.A., Carter, D., Ross, D.S., Ullman, B., and Brennan, R.G. (1996) Crystal structures of *Toxoplasma gondii* HGXPRTase reveal the catalytic role of a long flexible loop. *Nat. Struct. Biol.* **3**, 881-887

Scopes, R. (1994) Protein purification: principles and practice, 3rd ed., p.17-21, 26-38, 126-132, 135-136, 238-250, 270-277, 296-298. Springer-Verlag New York, Inc.

Seebregts, C.J. and McIntosh, D.B. (1989) 2′,3′-*O*-(2,4,6-trinitrophenyl)-8-azido-adenosine mono-, di-, and triphosphates as photoaffinity probes of the Ca^{2+}-ATPase of sarcoplasmic reticulum. *J. Biol. Chem.* **264**, 2043-2052

Selkirk, C. (2004) Ion-exchange chromatography. p. 125-130. *In* P. Cutler (ed.) Methods in molecular biology: protein purification protocols, 2nd ed., vol. 244. Humana Press Inc., Totowa, N.J.

Shahabuddin, M. and Scaife, J. (1990) The gene for hypoxanthine phosphoribosyl transferase of *Plasmodium falciparum* complements a bacterial HPT mutation. *Mol. Biochem. Parasitol.* **41**, 281-288

Shi, W., Li, C.M., Tyler, P.C., Furneaux, R.H., Cahill, S.M., Girvin, M.E., Grubmeyer, C., Schramm, V.L., and Almo, S.C. (1999*a*) The 2.0 Å structure of malarial purine phosphoribosyltransferase in complex with a transition-state analogue inhibitor. *Biochemistry*. **38**, 9872-9880

Shi, W., Li, C.M., Tyler, P.C., Furneaux, R.H., Grubmeyer, C., Schramm, V.L., and Almo, S.C. (1999*b*) The 2.0 Å structure of human hypoxanthine-guanine phosphoribosyltransferase in complex with a transition-state analog inhibitor. *Nat. Struct. Biol.* **6**, 588-593

Singh, A., Thornton, E.R., Westheimer, F.H. (1962) The photolysis of diazoacetylchymotrypsin. *J. Biol. Chem.* **237**, 3006-3008

Singh, S.K. and Kishore, N. (2008) Calorimetric and spectroscopic studies on the interaction of methimazole with bovine serum albumin. *J. Pharm. Sci.* **97**, 2362-2372

Sinha, S.C. and Smith, J.L. (1999) The PRT protein family. *Curr. Opin. Struct. Biol.* **11**, 733-739

Studier, F.W. (2005) Protein production by auto-induction in high-density shaking cultures. *Protein Expr. Purif.* **41**, 207-234

Surolia, N. and Surolia, A. (2001) Triclosan offers protection against blood stages of malaria by inhibiting enoyl-ACP reductase of *Plasmodium falciparum*. *Nat. Med.* **7**, 167-173

ter Kuile, F., White, N.J., Holloway, P., Pasvol, G., and Krishna, S. (1993) *Plasmodium falciparum*: in vitro studies of the pharmacodynamic properties of drugs used for the treatment of severe malaria. *Exp. Parasitol.* **76**, 85-95

Tournaire, C, Croux, S., and Maurette, M. (1993) Antioxidant activity of flavonoids: efficiency of singlet oxygen ($^1\Delta_g$) quenching. *J. Photochem. Photobiol. B.* **19**, 205-215

Triglia, T., Menting, J.G.T., Wilson, C., and Cowman, A.F. (1997) Mutations in dihydropteroate synthase are responsible for sulfone and sulphonamide resistance in *Plasmodium falciparum*. *Proc. Natl. Acad. Sci. USA.* **94**, 13944-13949

Watt, G., Loesuttivibool, L., Shanks, G.D., Boudreau, E.F., Brown, A.E., Pavanand, K., Webster, H.K., and Wechgritaya, S. (1992) Quinine with tetracycline for the treatment of drug-resistant falciparum malaria in Thailand. *Am. J. Trop. Med. Hyg.* **47**, 108-111

Webster, H.K., Wiesmann, W.P., Walker, M.D., Bean, T., and Whaun, J.M. (1984) Hypoxanthine metabolism by human malaria infected erythrocytes: focus for the design of new antimalarials drugs. *Adv. Exp. Med. Biol.* **265A**, 219-223

White, N.J. (2008) Qinghaosu (Artemisinin): the price of success. *Science*. **320**, 330-334

WHO Malaria Fact Sheet No 94 (2007) Available online at http://www.who.int/mediacentre/factsheets/fs094/en/, Accessed 5 May 2008

WHO World Malaria Report (2005) Available online at http://www.rbm.who.int/wmr2005/index.html, Accessed 5 May 2008

Winzerling, J.J., Berna, P., and Porath, J. (1992) How to use immobilized metal ion affinity chromatography. *METHODS: a companion to methods in enzymology* **4**, 4-13

Xu, Y., Eads, J., Sacchettini, J.C., and Grubmeyer, C. (1997) Kinetic mechanism of human hypoxanthine-guanine phosphoribosyltransferase: rapid phosphoribosyl transfer chemistry. *Biochemistry*. **36**, 3700-3712

Yamey, G. (2004) Roll Back Malaria: a failing global health campaign. *BMJ.* **328**, 1086-1087